2022

Skeletal ontogeny of the Plainfin Midshipman, Porichthys notatus (Percomorphacea: Batrachoidiformes

Diego F. B. Vaz

Eric J. Hilton
Virginia Institute of Marine Science

Recommended Citation

Vaz, Diego F. B. and Hilton, Eric J., Skeletal ontogeny of the Plainfin Midshipman, Porichthys notatus (Percomorphacea: Batrachoidiformes (2022). *Journal of Anatomy*.
DOI: 10.1111/joa.13794

Received: 29 May 2022 | Revised: 8 November 2022 | Accepted: 9 November 2022

DOI: 10.1111/joa.13794

Journal of Anatomy ANATOMICAL SOCIETY WILEY

ORIGINAL ARTICLE

Skeletal ontogeny of the Plainfin Midshipman, *Porichthys notatus* (Percomorphacea: Batrachoidiformes)

Diego F. B. Vaz[1,2] | **Eric J. Hilton**[3]

[1]Museum of Comparative Zoology, Harvard University, Cambridge, Massachusetts, USA

[2]Guam Ecosystems Collaboratorium Biorepository, Guam EPSCoR, Marine Laboratory, University of Guam, Mangilao, Guam, USA

[3]Department of Fisheries Science, Virginia Institute of Marine Science, William & Mary, Gloucester Point, Virginia, USA

Correspondence
Diego F. B. Vaz, Museum of Comparative Zoology, Harvard University, 26 Oxford St, Cambridge, MA 02138 USA.
Email: dbistonvaz@fas.harvard.edu

Funding information
Virginia Insitute of Marine Science, William and Mary; National Science Foundation; Museum of Comparative Zoology, Harvard University

Abstract

Batrachoidiformes are benthic fishes that utilize the undersides of rocks as spawning nests. Their larvae are attached to the nest and nourished by a large yolk sac. The evolutionary shift from feeding, free-swimming larvae to sedentary larvae that are reliant on their yolk sac for nutrition can lead to changes in skeletal development. Batrachoidiformes also have many morphological specializations, such as five pectoral-fin radials (versus four in other acanthomorphs) that are of uncertain homology, the determination of which may have phylogenetic implications. A larval series of *Porichthys notatus* was collected and its skeletal ontogeny is described. In *P. notatus* the ossification of the pharyngeal toothplates occurs relatively later than in percomorphs with free-swimming larvae. The posterior basibranchial copula cartilage (= fourth basibranchial) in *Porichthys notatus* has a unique development among fishes: it initially develops as a paired element at 6.8–7.1 mm NL before fusing posteriorly and forming single median cartilage at 7.4 mm SL. Cartilages of hypobranchial four are transitory, being observed in two specimens of 6.8 and 7.3 mm NL before fusing with ceratobranchial four. The previously identified dorsalmost pectoral radial is a bone formed by a hypertrophied propterygium that ossifies later in development. The earliest stages of *P. notatus* have three dorsal spines, but during late larval development, the growth of the third dorsal spine is interrupted. The development of *P. notatus* is compared and discussed in context to that of other acanthomorph.

KEYWORDS
development, early-life history, larva, variation

1 | INTRODUCTION

Ontogenetic variation represents a fundamental source of morphological variation, together with individual and phylogenetic variations (Grande, 2004; Hilton & Bemis, 2012). Early ontogeny in particular is often useful in comparative anatomical studies of fishes and other organisms to inform hypotheses of homology for unique anatomical structures. For example, Johnson and Britz (2005) demonstrated that the clavus of Molidae (Tetraodontiformes) is formed by elements of the posterior ends of both dorsal and anal fins, refuting previous hypothesis that the clavus was a highly modified caudal skeleton. Ontogenetic variation is also informative in systematic analysis. Hilton et al. (2019) demonstrated that the pattern of ossification of the vertebral column within species of Bathymasteridae (Zoarcoidei) is variable and suggests that the distinct pattern observed in *Ronquilus* and *Bathymaster* could be

a synapomorphy grouping these taxa. As for any morphological feature, the systematic information of ontogenetic studies of a particular group of organisms requires broadly comparative data. However, obtaining complete developmental series is difficult and to date, there are relatively few studies characterizing the early skeletal ontogeny (Bird & Mabee, 2003; Britz & Conway, 2009; Britz & Johnson, 2005; Cubbage & Mabee, 1996; Johnson & Britz, 2005; Kubicek & Conway, 2016; Mattox et al., 2014; Potthoff, 1974, 1975, 1980; Potthoff et al., 1980, 1984, 1988; Potthoff & Kelley, 1982; Potthoff & Tellock, 1993; Warth et al., 2017). Therefore, providing ontogenetic descriptions is important to grow the body of knowledge on the ontogeny of fishes, particularly for relatively closely related taxa (e.g., species within a family). The more information that becomes available, the more robust ontogenetic characters will become for systematic analyses. Herein, we describe the early skeletal ontogeny of *Porichthys notatus*, as an exemplar for the teleostean order Batrachoidiformes.

Batrachoidiformes is a relatively small order of percomorph fishes comprising a single family, Batrachoididae, with 23 genera and 82 species (Greenfield, 2014; Greenfield et al., 2008). These fishes are commonly known as toadfishes and midshipman. These are small to medium-sized fishes (total length, TL, ranging from 20 to 50 cm), and have a wide, stocky body with a dorsoventrally compressed head that bears fleshy supraorbital and oral cirri (Greenfield et al., 2008). Despite the relatively small size of this order, Batrachoidiformes are distributed worldwide, inhabiting mostly benthic habitats of coastal regions (Collette, 2005; Greenfield et al., 2008). Reproductive behavior and early life history are unknown for most species of Batrachoidiformes. Collette (2005) summarized most of the information known for the order, and the most detailed accounts comes from *Poricthys notatus* (Arora, 1948), *Aphos porosus* (Balbontín et al., 2018), *Opsanus tau* (Dovel, 1960), and, a lesser extent, *Halobratrachus didactylus* (Felix et al., 2016). Male toadfishes are nest builders and vocalize to attract females during the spawning season (Arora, 1948; Balbontín et al., 2018; Dovel, 1960; Felix et al., 2016; Rice & Bass, 2009). Females lay large eggs (>5 mm diameter) on the roof of nests that are formed by rocks or other hard substrates (Arora, 1948; Britz & Toledo-Piza, 2012; Dovel, 1960). After hatching from the egg, larvae remain attached to the nest while gradually absorbing their yolk sac. The time that larvae are attached to the nest is dependent on water temperature and it may take up to 60 days for a larva to detach from the nest and become a free-swimming juvenile (Balbontín et al., 2018).

Despite extensive descriptions of the external morphology in early development of *Opsanus tau* and *Porichthys notatus* (Arora, 1948; Dovel, 1960; Watson, 1996), studies and descriptions of the development of the internal morphology from early-life to adult stages are lacking for Batrachoidiformes. Balbontín et al. (2018) offered a generalized skeletal description of larval specimens of *Aphos porosus*, however, they did not provide accounts of individual bones and cartilages. Felix et al. (2016) focused their ontogenetic descriptions on the stato-acoustic organs and swimbladder of larval stages of *Halobatrachus didactylus*.

The goal of this manuscript is to describe the ontogeny of the skeleton in *Porichthys notatus*, the Plainfin Midshipman. This species is endemic to the northeast Pacific Ocean, occurring in coastal areas from British Columbia (Canada) to Bahia Magdalena (Mexico; Walker & Rosenblatt, 1988). These descriptions are then used as the basis for the assessment of homology for specializations of the batrachoidiforms, which contributes to a better understanding of the diversity and evolution of highly modified morphological structures of the order.

2 | MATERIALS AND METHODS

Larvae of *Porichthys notatus* were collected in Brinnon, WA, USA, in June 2017 and 2018, during full or new moons at low tides when the nests were exposed (Figure 1) and fixed on the same day. Fixation and preservation of specimens follow Kubicek and Conway (2016). Larval (56) and post-larval (5) specimens were cleared and double stained with alizarin red S and alcian blue following protocols adapted from Dingerkus and Uhler (1977) and Taylor and Van Dyke (1985). An important modification made to prevent damage of small specimens (up to 25 mm TL) caused by the acidity of the Alcian Blue 8GX solution was to leave small specimens immersed in the stain for no longer than 2 h. Specimens between 5 and 10 mm TL were usually stained after 30 min. A subsample of specimens (16) was cleared and single-stained only with alizarin red S to confirm the time of appearance of bones (Kubicek & Conway, 2016). Results from both approaches were congruent and subsequently combined.

Cleared and stained specimens were examined and dissected with binocular dissecting microscopes. Images were captured with a Zeiss Axiocam camera attached to a Zeiss Discovery V20 stereomicroscope. Z-stacked images were rendered to increase the depth of field using AxioVision software. A compound microscope with transmitted light, Leica 2500P with a Nikon 7000 camera attached, was used to examine early stages of branchial cartilages. Images were adjusted for color balance and contrast, and figures were prepared using Adobe Photoshop©.

After specimens were cleared and stained, 19 cartilages and 108 bones were scored as present (indicated by uptake of stain) or absent (no trace of a stained structure) for each individual examined. All fin rays, fin spines, pterygiophores of both dorsal and anal fins, branchiostegal rays, gill rakers, pharyngeal teeth, intermuscular bones (except epineural one), and vertebrae (except ural centra) were scored as a single element instead of scoring each individual bone or cartilage.

All data were compiled in Microsoft Excel© to identify the smallest specimen in which an element was present. Tables organizing the sequence of development were constructed in Rstudio© according to the protocols of Cubbage and Mabee (1996), Bird and Mabee (2003), Mattox et al. (2014), and Kubicek and Conway (2016). Throughout this manuscript, the term "fixed length" refers to the size at which a structure was always present; i.e., all specimens longer than the fixed length will have a

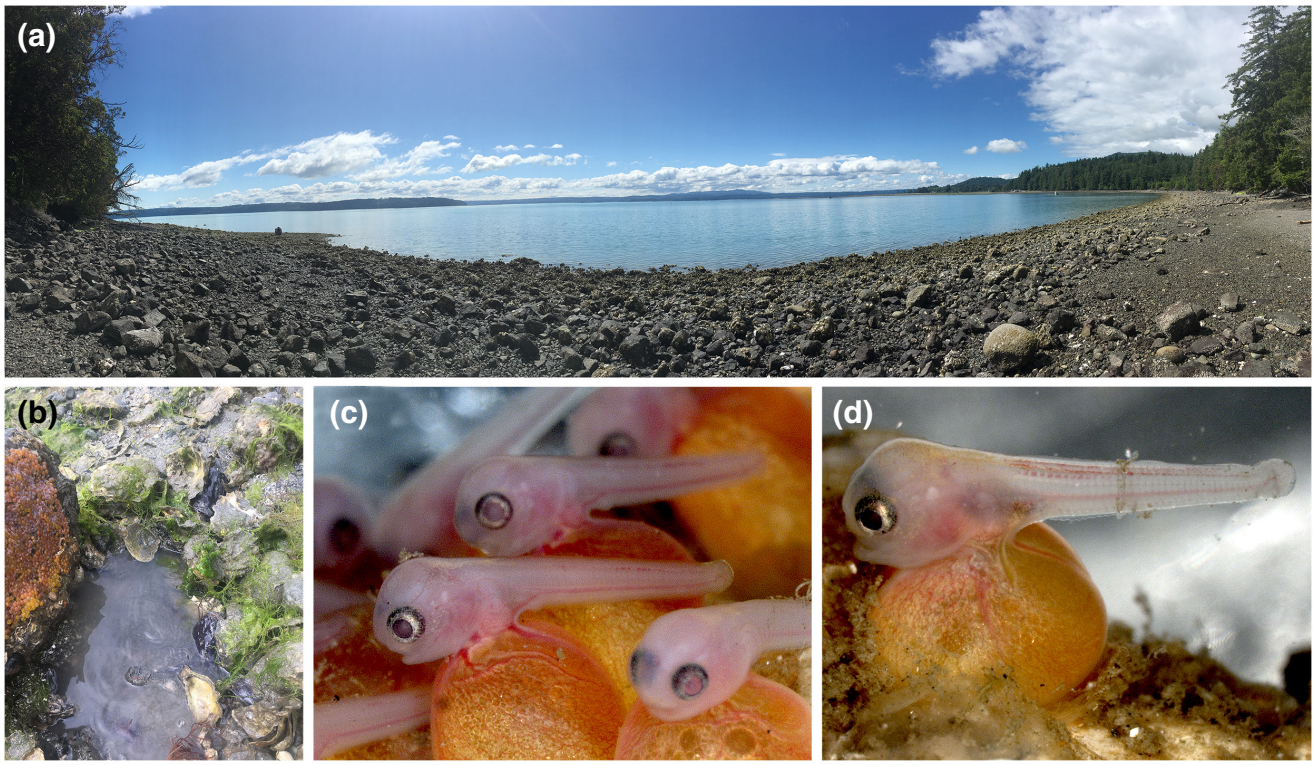

FIGURE 1 Field site. (a) Panoramic image of Seal Rock Campground, Brinnon, WA, USA at low tide. (b) Boulder covering the nest moved to expose egg masses and specimens. (c, d) Underwater image took from live specimens kept at Friday Harbor Laboratories in the summer of 2017.

given structure present. The terms "minimum length or size" or "earliest occurrence" refer to the smallest size at which a cartilage or a bone was found. Lengths are indicated as notochord length (NL) for specimens without caudal-fin rays or standard length (SL) when caudal-fin rays are developed. Terminology of skeletal elements follows Hilton (2011) and (for the caudal skeleton) Vaz and Hilton (2020). Terminology of early cartilages of the neurocranium follows de Beer (1937). *Porichthys notatus* (as do Batrachoidiformes in general; Collette, 2005) has an extended yolk-sac larval stage and lacks a free-swimming larval stage. The term larva as used here follows Richards (2005) and was used for specimens that hatched from the egg but remained attached to the rock in the nest, whether or not the yolk-sac was externally visible or internalized (although still present; Figure 2). The term juvenile was used for specimens that were detached from the rock, but were free-swimming in their nests. Among the specimens examined, the smallest free-swimming specimens of *Porichthys notatus* were 24 mm SL.

2.1 | Material examined

Institutional abbreviations follow Sabaj (2019). The ontogenetic series of *Porichthys notatus* includes 72 cleared-and-stained larval specimens, with sizes ranging from 5.4 to 25 mm SL, and five juveniles.

Double-stained specimens (n = 56): Larvae—VIMS 40257, 6.5 mm NL; VIMS 40258, 14.3 mm SL; VIMS 40259, 13.1 mm SL; VIMS 40260, 16.1 mm SL; VIMS 40261, 16.3 mm SL; VIMS 40262, 7.11 mm NL; VIMS 40263, 6.8 mm NL; VIMS 40264, 18.6 mm SL; VIMS 40265, 15.4 mm SL; VIMS 40266, 11.9 SL; VIMS 40267, 10.6 mm SL; VIMS 40268, 10 mm SL; VIMS 20269, 11.8 mm SL; VIMS 40270, 14.3 mm SL; VIMS 40271, 13.7 mm SL; VIMS 40272, 10.9 mm SL; VIMS 40273, 9.7 mm SL; VIMS 40274, 6.8 mm NL; VIMS 40275, 7.9 mm SL; VIMS 40276, 11.5 mm SL; VIMS 40277, 9.0 mm SL; VIMS 40278, 8.2 mm SL; VIMS 40279, 7.9 mm SL; VIMS 40280, 8.4 mm SL; VIMS 40281, 7.8 mm NL; VIMS 40282, 6.2 mm NL; VIMS 40283, 7.3 mm NL; VIMS 40284, 7.9 mm NL; VIMS 40285, 6.0 mm NL; VIMS 40286, 6.4 mm NL; VIMS 40287, 5.4 mm NL; VIMS 40856, 24.3 mm SL; VIMS 40858, 6.7 mm NL; VIMS 40859, 7.4 mm SL; VIMS 42844, 6.4 mm NL; VIMS 42845, 7.4 mm NL; VIMS 42846, 8.8 mm SL; VIMS 42847, 6.0 mm NL; VIMS 42848, 6.5 mm NL; VIMS 42849, 6.6 mm NL; VIMS 42850, 8.6 mm SL; VIMS 42851, 13.9 mm SL; VIMS 42852, 11.4 mm SL; VIMS 42853, 8.5 mm SL; VIMS 42854, 8.7 mm SL; VIMS 42855, 6.5 mm SL; VIMS 42856, 6.9 mm NL; VIMS 42857, 7.5 mm SL; VIMS 42858, 7.1 mm NL; VIMS 42859, 7.1 mm NL; VIMS 42860, 7.6 mm NL; VIMS 42861, 8.8 mm SL; VIMS 42862, 23.3 mm SL; VIMS 42863, 24.5 mm SL; VIMS 42864, 24.3 mm SL. Juveniles—FMNH 122401, 120.24 mm SL; USNM 104530 (2), 98.2 mm SL, 98.3 mm SL; VIMS 38017, 84.0 mm SL; VIMS 38018, 84.8 mm SL.

Single-stained specimens (n = 16): VIMS 42826, 5 specimens, 16.6 mm SL, 15.2 mm SL, 15.3 mm SL, 12.8 mm SL, 11.8 mm SL; VIMS

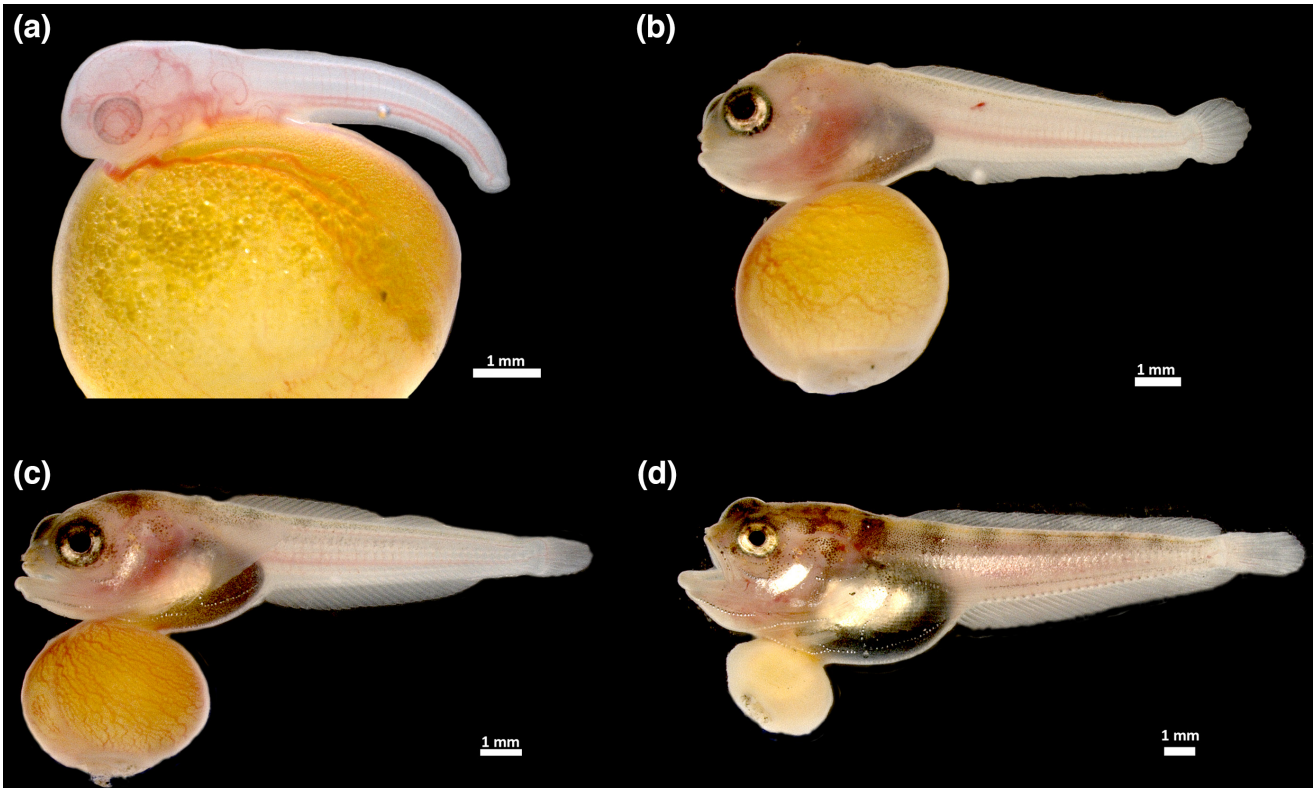

FIGURE 2 External morphological changes during early life history observed in live specimens of *Porichthys notatus*. (a) Specimen approximately 6.5 mm NL. (b) 11 mm SL specimen. (c) 13 mm SL specimen. (d) 18 mm SL specimen.

42825, 7 specimens, 6.3 mm NL, 6.11 mm NL, 7.8 mm SL, 6.2 mm NL, 6.6 mm NL, 6.7 mm NL, 6.2 mm NL.; VIMS 42815, 4 specimens, 10.3 mm SL, 12.1 mm SL, 9.5 mm SL, 8.3 mm SL (tail partially severed).

3 | RESULTS

3.1 | Neurocranium

The sequence of ossification of the neurocranium is: parasphenoid (fixed length observed at 7.5 mm SL; minimum size observed 6.0 mm NL); exoccipital (fixed, 7.9 mm SL; minimum, 7 mm SL), basioccipital (fixed, 8.2 mm SL; minimum, 7 mm SL); frontal (fixed, 8.7 mm SL; minimum, 7.1 mm NL); autosphenotic (fixed, 9.7 mm SL, minimum, 8.7 mm SL) and epioccipital (minimum and fixed at 9.7 mm SL); pterotic (fixed, 10 mm SL; minimum, 8.7 mm SL); vomer (fixed, 11.5 mm SL; minimum, 8.7 mm SL); supraoccipital (fixed, 11.8 mm SL; minimum, 11.5 mm SL); basisphenoid and prootic (minimum and fixed at 11.8 mm SL); nasal and lateral ethmoid (minimum and fixed at 13.1 mm SL); and pterosphenoid (minimum and fixed at 18.6 mm SL) (Figures 3, 4).

The neurocranium of *Porichthys notatus* gradually becomes more dorsoventrally flattened during ontogeny. The width-to-depth ratio is approximately 1:1 to from 6 to 10 mm SL. At larger sizes this ratio increases to approximately 1.5:1 at 13.1 mm SL, and to 2:1 when larvae are free swimming (24.3 mm SL).

3.1.1 | Ethmoid region

At 6.2 mm NL, the anterior tips of the *trabecula cranii* expand laterally to form the early stages of the ethmoid plate (Figures 3a,b). At 6.8 mm NL the lateral margins of the ethmoid plate project dorsally to form the *lamina orbitonasalis* cartilages (as seen in Figure 3b); these reach the dorsal margin of the head at 7.9 mm SL, extending dorsally to reach the level of the *taenia marginalis*. At 7.9 mm SL the anterior tips of the *trabecula cranii* connect through a cartilaginous outgrowth to fully form the ethmoid plate (Figure 3c).

Lateral ethmoid

At 13.1 mm SL, the lateral portions of the *lamina orbitonasalis* cartilage begin to ossify perichondrally to form the lateral ethmoid bones (Figure 3f). Endochondral ossification of the lateral ethmoid is present at 16.1 mm SL (Figure 3g) and is expanded medially around the foramen for the olfactory nerve. This ossification entirely replaces the *lamina orbitonasalis* cartilages and dorsally contacts the frontals at 24.3 mm SL (Figure 3i).

Vomer

The vomer is first present as a small, triangular, laminar bone ventral to the ethmoid plate at 8.7 mm SL (fixed at 11.4 mm SL; Figure 3e). By 13.1 mm SL, the vomer has expanded and covers most of the anterior part of the ventral surface of the ethmoid plate, having its posterior margin contacting the parasphenoid at an interdigitating

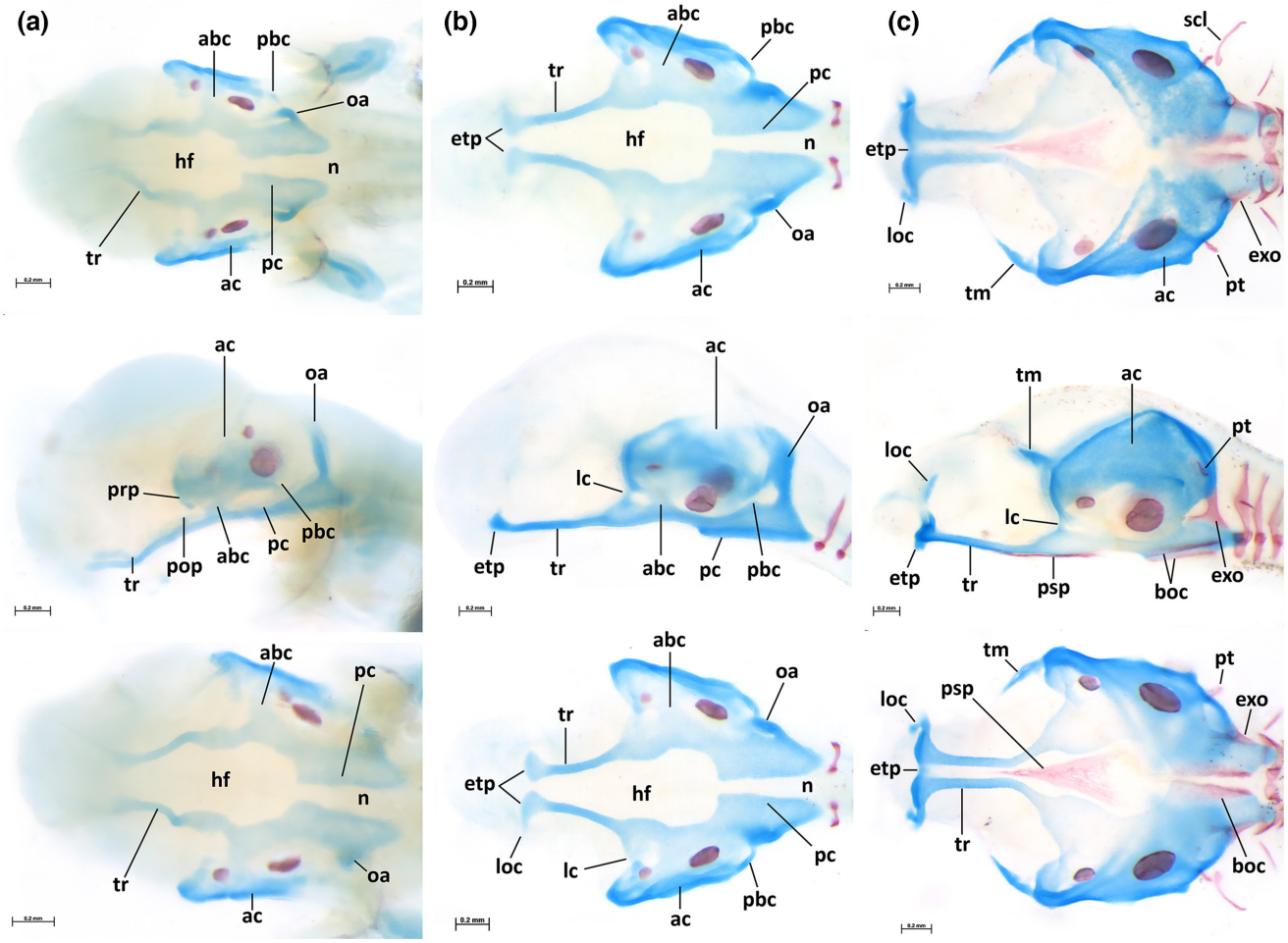

FIGURE 3 Ontogeny of the neurocranium of *Porichthys notatus* in dorsal, lateral, and ventral view. (a) VIMS 40285, 6.0 mm NL. (b) VIMS 40283, 7.28 mm NL. (c) VIMS 40275, 7.9 mm SL. (d) VIMS 40277, 9 mm SL. (e) VIMS 40272, 10.9 mm SL. (f) VIMS 40259, 13.1 mm SL. (g) VIMS 40260, 16.1 mm SL. (h) VIMS 40264, 18.6 mm SL. (i) VIMS 40856, 24.3 mm SL (j) VIMS 38018, 84.5 mm SL. (k) Illustration of neurocranium of VIMS 38018. Abbreviations: abc, anterior basicapsular commissure; ac, auditory capsule; apr, autopterotic; asp, autosphenotic; boc, basioccipital; bsp, basisphenoid; epi, epioccipital; exo, exoccipital; etp, ethmoid plate; fr, frontal; hf, hypophyisial fenestra; le, lateral ethmoid; loc, *lamina orbitonasalis* cartilage; n, nasal; oa, occipital arch; pbc, posterior basicapsular commissure; pc, parachordal cartilage; pop, postpalatine process; pro, prootic; prp, prootic process; psp, parasphenoid; pt, posttemporal; pts, pterosphenoid; tm, taenia marginalis; tr, *trabecula cranii*; ts, tectum synoticum; v, vomer.

suture (Figure 3f). From 16.1 mm SL, the anterodorsal margin of the vomer projects posterodorsally over the dorsal surface ethmoid plate and a pair of teeth appear on its lateral edges (Figure 3g). In the 24.3 mm SL (Figure 3i), the ventral margin of the vomer is triangular, with a slightly concave posterior margin; its posterior edge extends over the anterior edge of the parasphenoid, similar to the condition in juvenile specimens. The dorsal margin of the vomer is convex, extending over the anterior region of the ethmoid plate cartilage, not contacting any adjacent bones. In larger juveniles (VIMS 38018), the dorsal margin of the vomer extends posterodorsally over the anterior margins of the lateral ethmoid, with an elongate posterior projection, forming a suture with the frontals (Figures 3j,k).

Nasal

The nasal bones are first present at 13.1 mm SL (Figure 3f) as two concave laminae anterior to the anterodorsal edges of the lateral portions of the *lamina orbitonasalis* cartilages. These bones remain similar shape in larger larvae and juveniles (Figures 3g–k).

3.1.2 | Orbital region

The smallest specimen examined (VIMS 40287, 5.4 mm NL) has a pair of elongate cartilages, the *trabecula cranii*, that extend the length of the anteromedial ventral surface of the head (Figure 3a). Distinct *trabecula cranii* cartilages with a similar arrangement are observed to 18.6 mm SL (Figure 3h). Although most of *the trabecula cranii* cartilages are replaced by the basisphenoid in larger larval specimens, remains of these cartilages can be observed in both larva (Figure 3i) and juveniles (VIMS 38018). The *taenia marginalis* cartilage is first observed in the posterodorsal region of the orbital region at 6.0 mm NL and is fixed at 7.7 mm SL (Figure 3c).

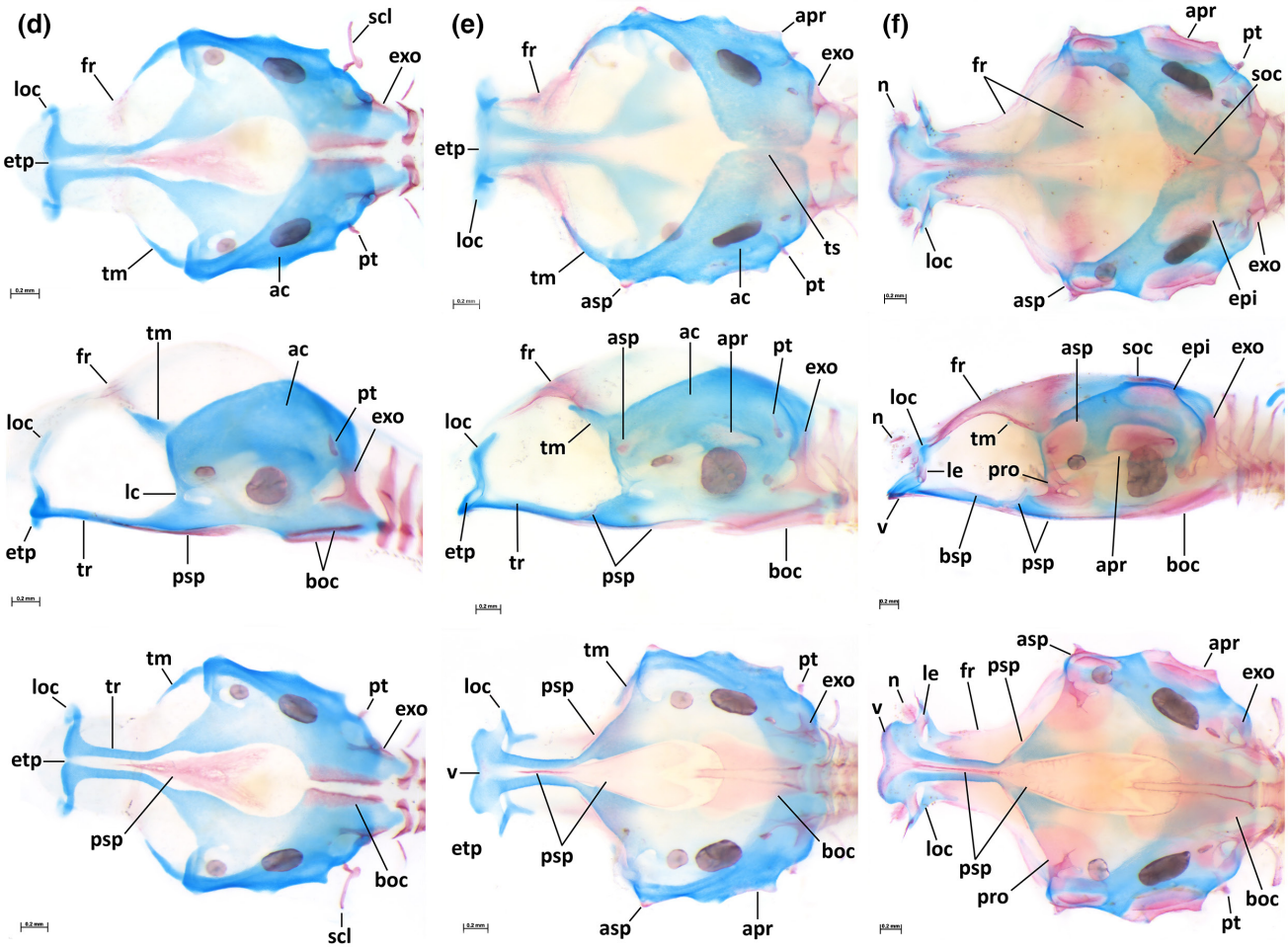

FIGURE 3 (Continued)

At 16.1 mm SL, a cartilaginous *taenia marginalis* is still present (Figure 3g).

Frontals

Frontals are first observed at 7.1 mm NL, fixed at 8.7 mm SL, and are located along the lateral margin of the dorsal surface of the head, dorsomedial to the anterior edge of the *taenia marginalis* (Figure 3d). From 9.7 mm SL to 10.9 mm SL, frontals expand anterior to the *lamina orbitonasalis* cartilages, forming a triangular bone (Figure 3e). The frontals expand to meet in the midline and cover the anterior region of the dorsal roof by 11.8 mm SL. At 13.1 mm SL, the anteromedial margins of the frontals are first seen to be fused (Figure 3f). The frontals extend into the posterior half of the skull roof at 16.1 mm SL and they are almost completely fused along the midline (only the posterior portion remains separate; Figure 3g). At 24.3 mm SL, the fused frontals project over the anterior margin of the supraoccipital and the medial margins of the frontals project ventrally, forming acute processes that contact the dorsal tip of the basisphenoid (Figure 3i). The groove for the supraorbital canal on the dorsal surface of the frontals develops at the juvenile stage (i.e., > 30 mm SL; Figures 3j,k).

Parasphenoid

The parasphenoid is first observed at 6.0 mm NL, fixed at 7.5 mm SL, as a triangular, laminar dermal bone. It is positioned in the middle of the hypophysial fenestra (i.e., the space between the cartilages of *trabecula cranii*). At 7.9 mm SL, the parasphenoid extends from the anterior third to the middle of the ventral surface of the neurocranium and extends posteriorly to the level of the anterior margin of the sagitta, acquiring an arrow shape (Figure 3c). At 9.7 mm SL, the parasphenoid develops a slender ascending process, extending posterodorsally from its posterior third (Figure 3e). At 11.8 mm SL, the parasphenoid extends posteriorly, nearly contacting the anterior margin of the basioccipital. The ascending process of the parasphenoid is rectangular and contacts the prootic at 18.6 mm SL (Figure 3h), and covers its anteroventral edge at 24.3 mm SL (Figure 3i). At this size the tip of the anterodorsal process of the autosphenotic becomes rounded and forms an acute angle with the lateral margin of the frontal, similar to that observed in larger juveniles (Figures 3j,k).

Basisphenoid

The earliest stages of ossification of the basisphenoid occur in the posterodorsal margin of the *trabecula cranii* at 11.8 mm SL and are

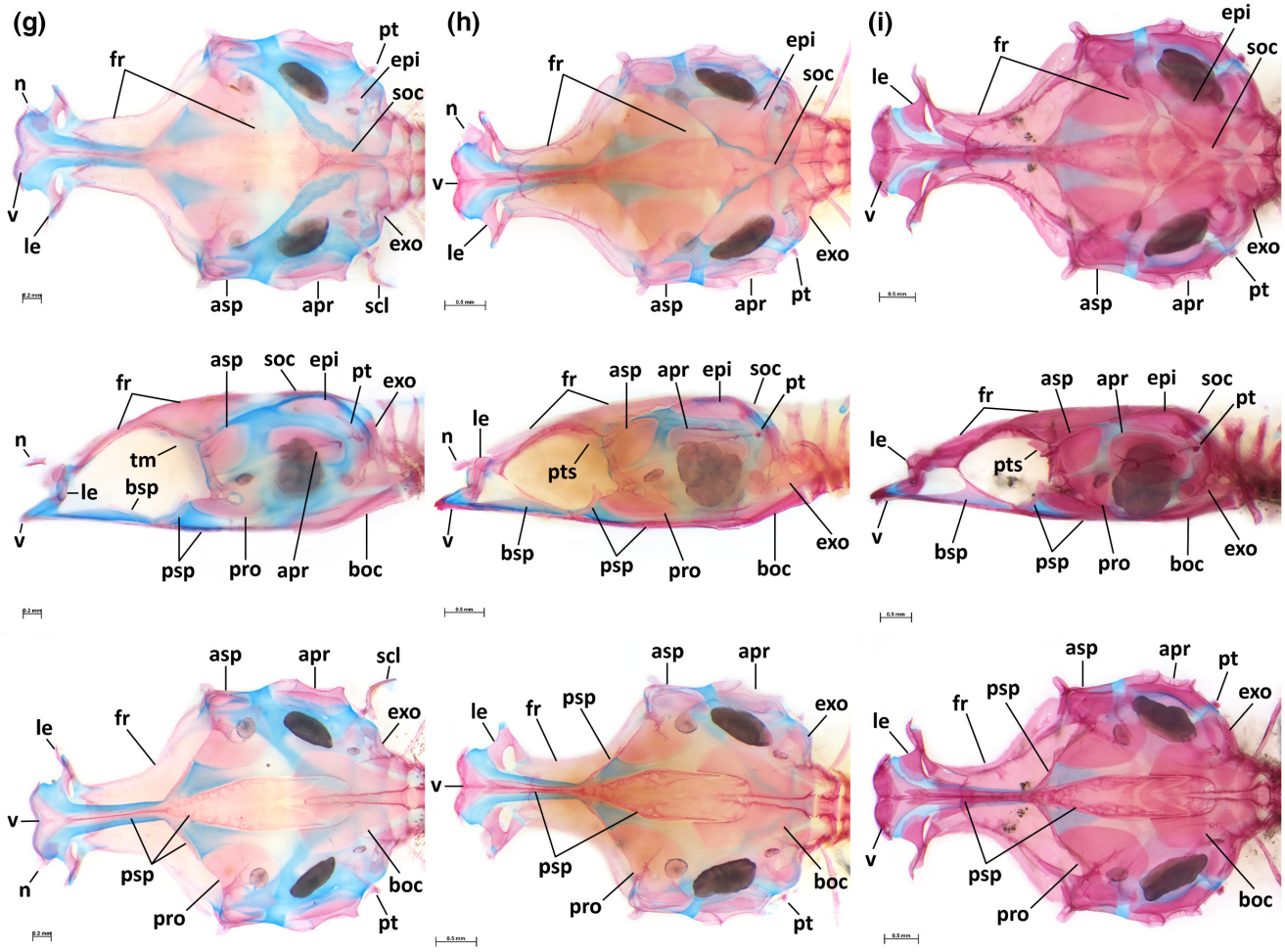

FIGURE 3 (Continued)

represented by thin and elongate bone (Figure 3f). Ossification of the basisphenoid continues at 16.1 mm SL, replacing the *trabecula cranii* ventrally (Figure 3g). The basisphenoid also expands dorsally, forming a wide triangular bone that extends from the lateral ethmoid to the posterior process of the parasphenoid (Figure 3h). Its dorsal edge projects anterodorsally, and contacts the ventral process of the frontals at 24.3 mm SL (Figure 3i). The shape of the basisphenoid at this size is similar to that observed in larger juveniles (Figures 3j,k).

Pterosphenoid

The *taenia marginalis* cartilages are entirely replaced by bone at 18.6 mm SL, forming a triangular pterosphenoid (Figure 3h). The dorsal margin of the pterosphenoid is straight and attaches to the ventral margin of the frontals, with its posterodorsal edge contacting the dorsal region of the prootic (Figure 3i). The triangular outline of the pterosphenoid remains in juveniles, but in those specimens the ventral edge of the pterosphenoid extends farther ventrally, contacting the dorsal margin of the ascending process of the parasphenoid.

3.1.3 | Otic region

The anterior basicapsular commissure is visible at 6.0 mm NL (Figure 3a). This commissure is located in the posterior extremity of the *trabecula cranii* and projects dorsolaterally, continuous with the auditory capsule. Anterior to the commissure there is a small triangular postpalatine process. At 6.2 mm NL, the postpalatine and prootic processes meet to form the lateral commissure, enclosing the foramen for passage of the trigeminal nerve (as seen in Figure 3b). The auditory capsule is a rectangular cartilage that extends laterally at the level of the sagitta. The anteroventral edge of the auditory capsule bears the prootic process. The posteroventral edge of the auditory capsule also has a small projection that represents the early stages of the posterior basicapsular commissure (Figure 3a,b). From the ventral edge of the anterior basicapsular commissure, the parachordal cartilages extend posteriorly lateral to the notochord. At 6.2 mm NL, the posterior basicapsular commissure extends ventrally to reach the parachordal cartilage, delimiting the foramen for the vagus nerve (Figure 3b). The auditory capsule extends beyond the dorsal margin of the occipital arch. The auditory capsule covers the

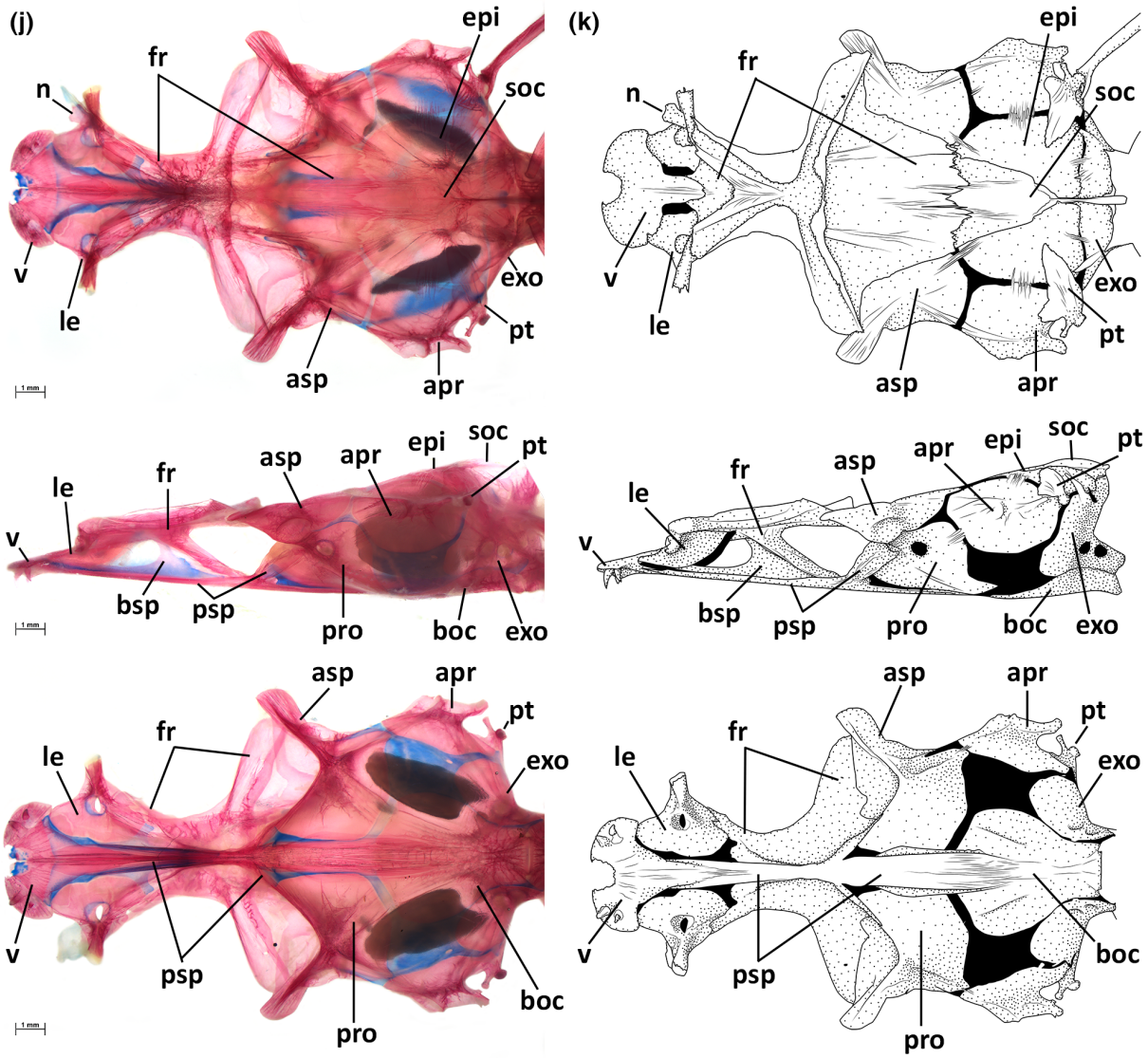

FIGURE 3 (Continued)

entire posterodorsal region of the neurocranium at 6.8 mm NL and is continuous with the occipital arch (Figure 3c). The *tectum synoticum* is first observed at 9.7 mm SL as a small, elongate cartilage connecting the narrow space between the posterior regions of the medial margins of the auditory capsule. The anterior notch that is formed between the anterior regions of the medial margins (Figure 3e) remains open until 11.8 mm SL, at which size the supraoccipital starts ossifying.

Autosphenotic

The earliest stages of the ossification of the autosphenotic are first observed at 8.7 mm SL and fixed at 9.7 mm SL, in the anterodorsal edge of the auditory capsule, posterior to the *taenia marginalis* (Figure 3e). At 11.8 mm SL, the autosphenotic expands to replace most of the anterolateral surface of the cartilage of the otic capsule and the anterolaterally directed process of the autosphenotic appears along its dorsolateral edge (Figures 3f–h). At 24.3 mm SL, both dorsal and lateral surfaces of the autosphenotic are rectangular. The tip of the anterodorsal process of the autosphenotic is rounded and forms an acute angle with the lateral margin of the frontal (Figure 3i). The medial region of the dorsal surface of the autosphenotic is covered by posterolateral region of the frontals. This condition of the autosphenotic described for the 24.3 mm SL specimen is similar to that observed in juveniles (Figures 3j,k).

Epioccipital

The first trace of the epioccipital appears at 9.7 mm SL, along the posterodorsal edge of the auditory capsule, ventral to the posttemporal bone. At 13.1 mm SL, endochondral ossification of the epioccipital replaces most of the dorsal region of the cartilaginous *tectum synoticum* and is shaped as a rounded triangle (Figure 3f). At 16.1 mm SL, the medial edge of the epioccipital projects over the lateral margin of the supraoccipital. The epioccipital remains as a rounded triangle bone in larger larval specimens and juveniles.

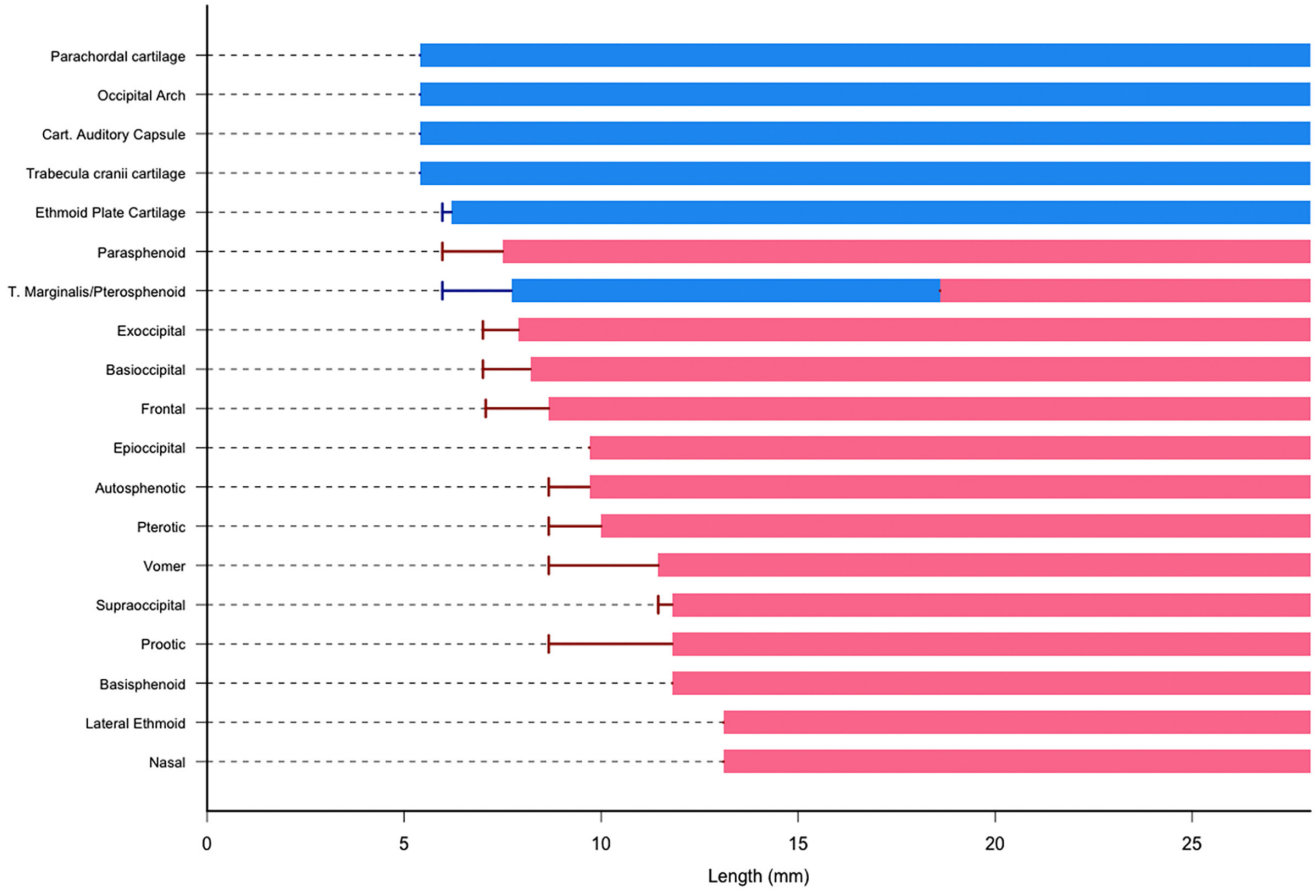

FIGURE 4 Diagram of sequence of development of cartilages and bones of the neurocranium of *Porichthys notatus*. Bars correspond to fixed length. Error bars correspond to the smallest size that a structure was found. Bars in blue correspond to cartilage, red to bone. Lengths presented in mm NL/SL.

In juvenile specimens there are interdigitating sutures between the epioccipital and surrounding bones. The anterolateral edge of the epioccipital has two or three interdigitations with the posteromedial edge of the dorsal surface of the autosphenotic. The lateral margin of the epioccipital has four or five interdigitations with the medial margin of the pterotic. The posterior margin of the epioccipital also forms five or six interdigitations with the dorsal edge of the exoccipital (Figures 3j,k).

Pterotic

In the smallest specimen observed with an ossified pterotic (8.7 mm SL), endochondral ossification of the autopterotic is already present and is located in the dorsolateral edge of the posterior region of the auditory capsule (Figure 3e). The autopterotics expand to replace most of the posterolateral surface of the otic capsule cartilage at 11.8 mm SL. At 13.1 mm SL, the groove in the autosphenotic and autopterotic that forms the articulation surfaces for the anterior and posterior heads of the hyomandibula begin to form at this size (Figure 3f). At 16.1 mm SL, the autopterotic has replaced most of the posterodorsal region of the optic capsule; the region ventral to the pterotic remains cartilaginous (even in juveniles). The dermopterotics first develop as a membranous ridge on dorsolateral margin of the autopterotic, and forms the compound pterotic at 18.6 mm SL (Figure 3h). At 24.3 mm SL, the compound pterotic has rectangular both dorsal and lateral surfaces; the anterodorsal margin has a single interdigitating suture with the posterior margin of the autosphenotic (similar to that observed in juveniles). The lateral edge of the pterotic has a small, triangular lateral process projecting posterolaterally (Figure 3i). In juveniles, this process is robust, trapezoidal, and posteriorly projected, with its tip extending close to the lateral process of the posttemporal (Figures 3j,k).

Prootic

The prootic first appears at 8.7 mm SL and fixes at 11.8 mm SL. The ossification of the prootic first occurs around the foramina for passage of the trigeminal nerve. At 13.1 mm SL, the endochondral ossification of the prootic extends posterior to the autosphenotic and almost completely covers the cartilaginous anterior basicapsular commissure (Figure 3f). At 16.1 mm SL, the anterodorsal edge of the prootic contacts the anteroventral edge of the autosphenotic and the posterior margin of the prootic extends posteriorly to the level of the anterior margin of the pterotic (Figure 3g). At 18.6 mm SL, the anteroventral edge of the prootic contacts the ascending process of the parasphenoid. At 24.3 mm SL, the prootic has a trapezoidal outline, with the dorsal margin slightly posterodorsally oriented. Its anterior edge contacts the ventrolateral edge of the autosphenotic

(forming the only contact with other otic bones at this size). The anterior margin of the prootic is straight, with the anteroventral region covered by the ascending process of the parasphenoid. The posterior margin is straight dorsally and convex ventrally; the ventromedial margin is slightly convex. In juveniles, the posterodorsal edge of the prootic has interdigitating sutures with the anteroventral margin of the pterotic. The middle of the ventromedial margin of the prootic is covered by the lateral margins of the parasphenoid (Figures 3j,k).

3.1.4 | Occipital region

The cartilaginous occipital arch extends dorsally from the posterior edge of the parachordal cartilages to reach the level of the dorsal margin of the sagitta at 5.4 mm NL. A *tectum posterius* (the connection between the occipital arches) is not present or is continuous with the *tectum synoticus*, as a distinct cartilage in this position was not recognized at any stage of development. Additional evidence supporting the absence of the *tectum posterius* is that the notch separating the dorsal edges of the occipital arches is present in large larval specimens (Figures 3e–g).

Supraoccipital

Perichondral ossification of the supraoccipital first occurs at 11.4 mm SL, fixes at 11.8 mm SL, filling most of the anterior concavity anterior to the *tectum synoticum*. At 13.1 mm SL endochondral ossification of the supraoccipital is present at the dorsal midline of the *tectum synoticum* (Figure 3f). The supraoccipital extends posteriorly, reaching the dorsal edge of the foramen magnum at 16.1 mm SL (Figure 3g). At 18.6 mm SL, the supraoccipital is triangular (similar to that observed in larger larva and juveniles), extending anteriorly to contact the posterior margin of the frontals (Figure 3h). At 24.3 mm SL, the posterior margin of frontals extend over the anterior margin of supraoccipital and the medial edges of epioccipitals extend partially over the lateral margins of supraoccipital, similar to that observed in juveniles (Figures 3i–k).

Exoccipital

The exoccipital first appears at 7 mm SL (fixed at 7.9 mm SL) within the cartilaginous region of the occipital arch where it posteriorly encloses the foramen for passage of the vagus nerve. The exoccipital expands ventrally and reaches the anteroventral margin of the foramen for the vagus nerve (Figure 3c). At 11.8 mm SL, ossification of the exoccipital further expands ventrally, replacing most of the occipital arch cartilage (Figure 3f). At 16.1 mm SL endochondral ossification of the exoccipitals meet the posterior tip of the supraoccipital, fully enclosing the foramen magnum (Figure 3g). The exoccipital acquires the juvenile outline at 18.6 mm SL, with a triangular anterolateral surface and a rectangular posteromedial surface (Figure 3h). In juveniles, the ventral margin of the exoccipital has two interdigitations with the lateral margin of the basioccipital and the dorsomedial region of the exoccipital has other five-interdigitating sutures with the posterior margin of the epioccipital (Figures 3j,k).

Basioccipital

The earliest indication of the basioccipital occurs at 7 mm SL (fixed at 8.2 mm SL) as endochondral ossifications of the medial margins of the parachordal cartilages (Figure 3c,d). At 10.9 mm SL, the anterior tip of the notochord ossifies and fuses with the basioccipital through a membranous lamina that grows between the tip of the ossified notochord and the basioccipital, forming a hexagonal-shaped bone (Figure 3e). The anterior margin of the basioccipital is convex medially, with its lateral edges expanding anterolaterally to the posterior edge of parasphenoid at 13.1 mm SL (Figure 3f) At this size, the width of basioccipital increases, being twice the width of the parasphenoid. At 16.1 mm SL, the anterolateral region of the basioccipital expands laterally to the level of the ventral margin of the prootic (Figure 3g). The middle of the anterior margin extends anteriorly, forming two triangular extensions, which, at 18.6 mm SL, develops into a single triangular process, extending beyond the anterolateral edges of the basioccipital and contacts the posterior notch of the parasphenoid (Figure 3h). The triangular process in the middle of the anterior margin of the basioccipital projects anteriorly to meet the dorsal surface of the parasphenoid at 24.3 mm SL (Figure 3i). The anterolateral region of the basioccipital is semi-rectangular, extending laterally to the level of the ventral region of the posterior margin of the prootic. The lateral margins of the basioccipital are convex anteriorly, concave posteriorly, and posteromedially oriented, narrowing the breadth of the posterior region of the basioccipital to about half of the anterior width. In juveniles, the middle of the lateral margin of the basioccipital has two interdigitating sutures with the ventral margin of the exoccipital (Figures 3j,k).

3.2 | Jaws and hyopalatine arch

The sequence of ossification of jaws and hyopalatine arch is: dentary (fixed length at 6.8 mm NL; minimum length observed is 6.0 mm NL), angular and maxilla (fixed, 6.9 mm NL; minimum, 6.0 mm NL), premaxilla (fixed, 7.7 mm SL; minimum, 7 mm SL), retroarticular (fixed, 8.2 mm SL; minimum, 7 mm SL), hyomandibular (fixed, 8.2 mm SL; minimum, 7.1 mm SL), sympletic (fixed, 8.2 mm SL; minimum, 7.9 mm SL); articular (minimum and fixed at 8.2 mm SL); ectopterygoid (fixed, 9.7 mm SL; minimum, 8.2 mm SL); quadrate (fixed, 9.7 mm SL; minimum, 8.7 mm SL), mentomeckelian (fixed, 10.9 mm SL; minimum, 8.7 mm SL); metapterygoid (fixed, 10.9 mm SL; minimum, 8.7 mm SL); dermopalatine (fixed, 10.9 mm SL; minimum, 8.7 mm SL); autopalatine (fixed, 11.8 mm SL; minimum, 10.9 mm SL); and endopterygoid (minimum and fixed at 16.1 mm SL) (Figures 5–7).

In the smallest specimen observed, 5.4 mm NL, three distinct cartilages are present: the palatoquadrate, Meckel's cartilage, and the hyosymplectic. Meckel's cartilage is elongate, with the posterodorsal tip bearing a concave articulatory surface that receives the ventral point of the palatoquadrate (Figures 5a,b). From 5.4 mm NL to 6.0 mm NL, the palatoquadrate cartilage is rectangular with slightly convex margin; its posteroventral edge articulates with the Meckel's cartilage (Figure 5a). The anterodorsal portion of the palatoquadrate

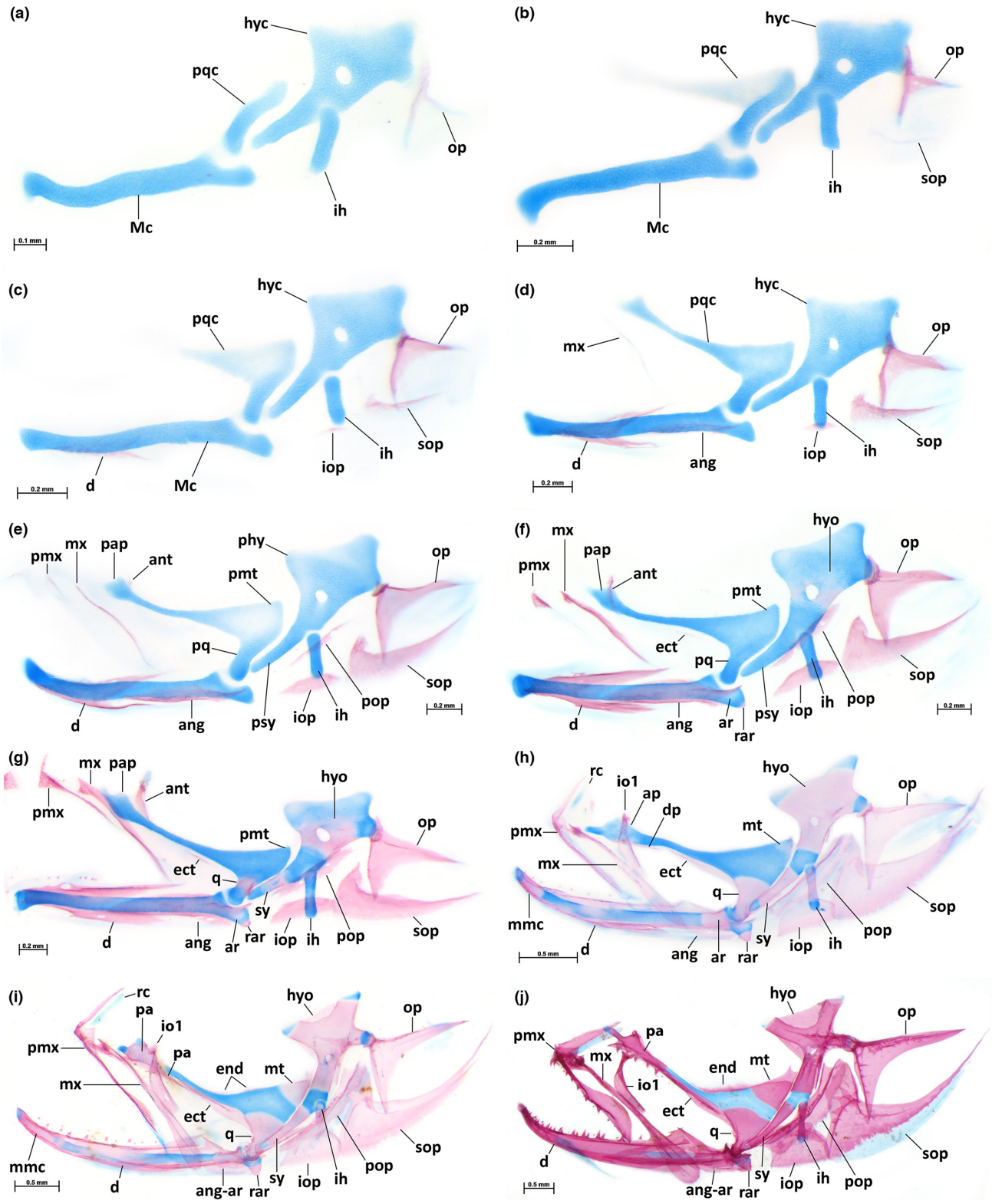

FIGURE 5 Ontogeny of jaws, hyopalatine arch, infraorbital, and opercular series of *Porichthys notatus*, in lateral view. (a) VIMS 40285, 6.0 mm NL. (b) VIMS 40282, 6.2 mm NL. (c) VIMS 40274, 6.8 mm NL. (d) VIMS 40859, 7.4 mm SL. (e) VIMS 40279, 7.9 mm SL. (f) VIMS 40278, 8.2 mm SL. (g) VIMS 40273, 9.7 mm SL. (h) VIMS 40269, 11.8 mm SL. (i) VIMS 40260, 16.1 mm SL. (j) VIMS 40856, 24.3 mm SL. Abbreviations: ap, autopalatine; ang, angular; ar, articular; d, dentary; dp, dermopalatine; ect, ectopterygoid; end, endopterygoid; hyc, hyosympletic cartilage; hyo, hyomandibula; ih, interhyal; io1, infraorbital one; iop, interopercle; mc, Meckel's cartilage; mmc, mentomeckelian; mt, metapterygoid; mx, maxilla; op, opercle; pa, palatine; pap, *pars autopalatina*; pop, preopercle; phy, *pars hyomandibularis*; pmt, *pars metapterygoidea*; pmx, premaxilla; pq, *pars quadrata*; pqc, palatoquadrate cartilage; psy, *pars symplectica*; q, quadrate; rar, retroarticular; rc, rostral cartilage; sop, subopercle; sy, symplectic.

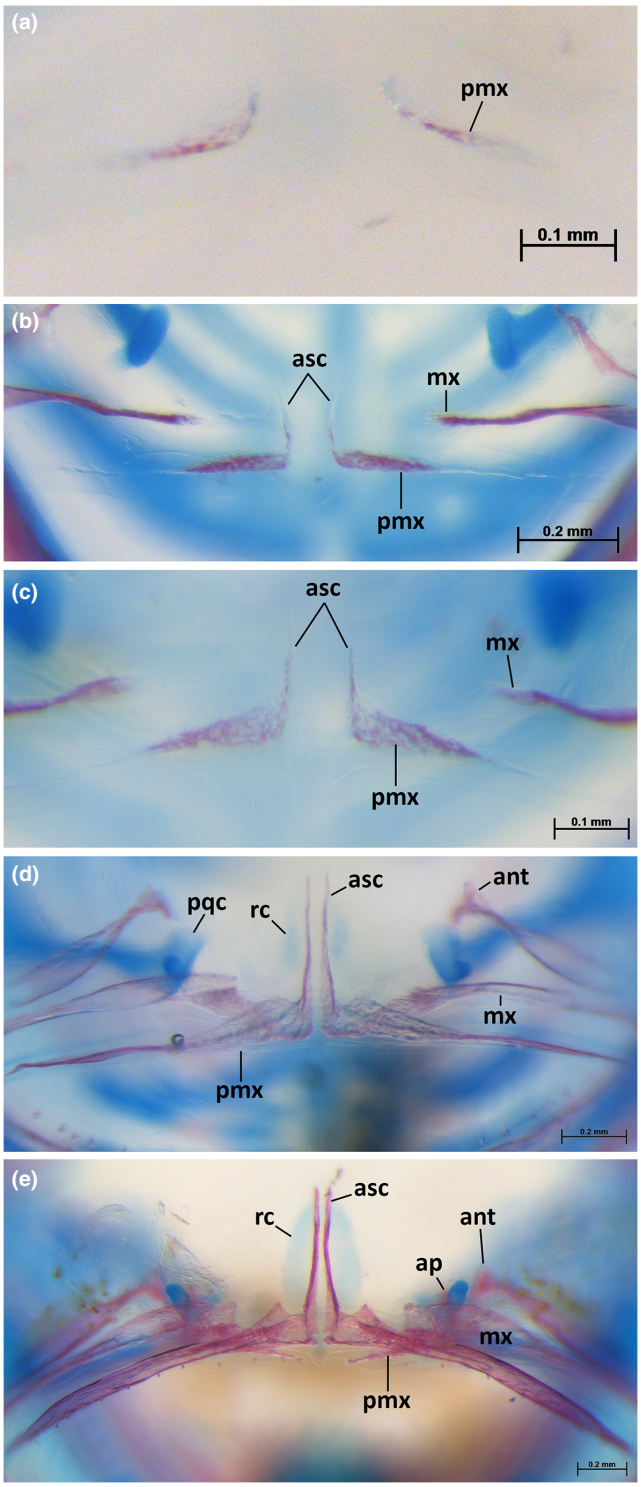

FIGURE 6 Ontogeny of the ascending process of the premaxilla of *Porichthys notatus* in frontal view. (a) VIMS 40275, 7.9 mm SL. (b) VIMS 40278, 8.2 mm SL. (c) VIMS 40277, 9 mm SL. (d) VIMS 40269, 11.8 mm SL. (e) VIMS 40260, 16.1 mm SL. Abbreviations: Ap, autopalatine; asc, ascending process of the premaxilla; io1, infraorbital one; mx, maxilla; pmx, premaxilla; pqc, palatoquadrate cartilage; rc, rostral cartilage.

is a triangular lamina at 6.2 mm NL (Figure 5b) but by 7.1 mm NL the palatoquadrate projects substantially anteriorly and the anteriormost point (i.e., the *pars autopalatina*) is slightly expanded. At 7.4 mm SL (Figure 5d), the *pars autopalatina* projects slightly dorsally, and at 7.5 mm SL, the anterior tip of the *pars autopalatina* start projecting anteriorly; this projection forms a distinct cartilaginous process at 9.7 mm SL (Figure 5g). The hyosympletic cartilage is present and already has a distinct foramen for passage of the hyomandibular branch of the fascialis nerve in the smallest specimen observed (5.4 mm NL). The *pars hyomandibularis* is trapezoidal and bears a posterior process for articulating with the opercle (Figures 5a–e). The *pars symplectica* is rod-shaped, tapering anteroventrally, extending close to the jaw joint (Figures 5a–f).

Dentary

The dentary first develops at 6.0 mm NL and is fixed at 6.8 mm NL. This bone is an arrow-shaped laminar bone positioned in the middle of the lateral surface of Meckel's cartilage (Figure 5c). At this first appearance, it is narrower than and about half the length of Meckel's cartilage. At 7.1 mm NL, the dentary projects posteriorly, extending beyond the dorsal and ventral margins of Meckel's cartilage. In larger specimens, the dentary gradually grows, reaching the symphysis of the Meckel's cartilage at 10.9 mm SL (Figures 5d–h). At this size, the dentary covers almost two-thirds of the Meckel's cartilage and the groove on the ventral margin of the dentary for the mandibular canal is distinct. At 16.1 mm SL (Figure 5i), the dorsal edge of posterior margin of the dentary projects posterodorsally, forming the anterior component of the coronoid process. At this size, the mentomeckelian bone is fused to the anterior region of the dentary. At 24.3 mm SL, the dentary is similar to that observed in juveniles: a robust, elongate bone that tapers and projects medially, reaching its antimere at the symphysis. The posterior margin of the dentary has a deep notch that contacts the anterior region of the anguloarticular. The posterodorsal edge of the dentary projects dorsally, forming a triangular projection that corresponds anterior half of the coronoid process. A groove is present on the posterior region of the lingual surface, where sits the anterior part of the remains of the Meckel's cartilage. Another groove is present on the anterior region of the labial surface of the dentary for attachment of the infralabial ligament (Figure 5j). Teeth associated with the dentary first appear in soft tissue at 9.7 mm SL (Figure 5g) and become ankylosed to the dentary at 16.1 mm SL (Figure 5i).

Mentomeckelian

Ossification of the mentomeckelian first appears at 8.7 mm SL and is fixed at 10.9 mm SL as an endochondral ossification near the anterior tip of Meckel's cartilage (as seen in Figure 5h). The mentomeckelian fuses to the dentary by 16.1 mm SL (Figure 5i).

Anguloarticular

The angular first appears at 6.0 mm NL and is fixed at 6.9 mm SL. In its earliest stages, the angular is a slender elongated laminar bone that extends along the posterolateral surface of Meckel's cartilage (Figure 5d). The angular grows ventral to the margin of Meckel's cartilage by 7.5 mm SL (Figure 5e) and beyond its dorsal margin by 8.2 mm SL (Figure 5f), at which size it forms part of the jaw joint.

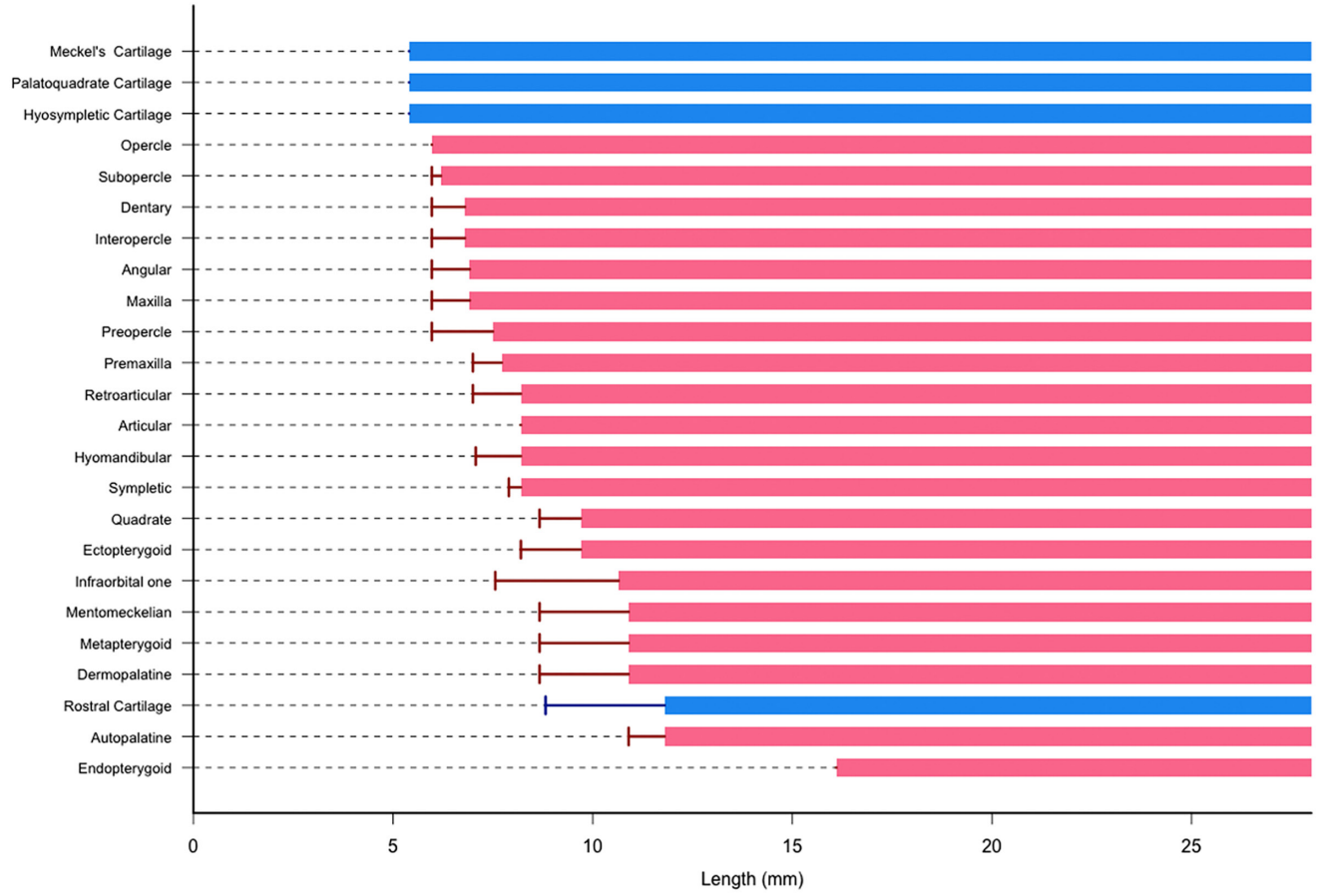

FIGURE 7 Diagram of sequence of development of cartilages and bones of jaws, hyopalalatine, infraorbital, and opercular series of *Porichthys notatus*. Bars correspond to fixed length. Error bars correspond to the smallest size that a structure was found. Bars in blue correspond to cartilage, red to bone. Lengths presented in mm NL/SL.

At 10.9 mm SL, the angular grows dorsally to form the posterior half of the coronoid process; this process is fully developed at 16.1 mm SL (Figure 5i). The earliest trace of the articular is a small endochondral ossification that forms at 8.2 mm SL in the posterior part of the socket of articulation of the jaw joint (Figure 5f). The endochondral ossification of the articular extends anterior to the socket of articulation of Meckel's cartilage at 10.9 mm SL. At 16.1 mm SL, the articular has replaced most of the posterior region of the Meckel's cartilage and is fused to the angular, forming the anguloarticular. At 24.3 mm SL, the anguloarticular has a rectangular base, with the socket for articulation with quadrate positioned in its posterodorsal margin (Figure 5j). The anterodorsal margin is expanded dorsally, forming an anterodorsally projected triangular lamina that corresponds to the posterior half of the coronoid process. The anterior margin is angular, with its lateral surface contacting the medial surface of the posterior region of the dentary. The medial surface of the anguloarticular has a groove in its anterior region for the posterior portion of the remnant of the Meckel's cartilage. The posterior margin of the anguloarticular is straight and posterodorsally oriented, closely attached to the retroarticular. This condition described at 24.3 mm SL is similar to that observed in juveniles.

Retroarticular

The retroarticular is first observed at the posterior tip of Meckel's cartilage at 7 mm SL and fixed at 8.2 mm SL. This bone becomes triangular by 16.2 mm SL, reflecting the condition observed in juveniles. At 24.3 mm SL, this triangular-shaped bone is tightly attached to the posterior margin of the anguloarticular bone.

Quadrate

The quadrate is first present at 8.7 mm SL, fixed at 9.7 mm SL (Figure 5g), and in those sizes endochondral ossification of the *pars quadrata* is already present. Ossification of the quadrate progresses gradually both dorsally and ventrally, with the articular region being completely ossified by 11.8 mm SL (Figure 5h). The posteroventral process of the quadrate (sensu Arratia & Schultze, 1991) was first observed at 9.7 mm SL as an angular projection from the posterolateral edge of the base of the quadrate, extending slightly over the lateral surface of the ventral edge of the hyosympletic cartilage (Figure 5g). This process is as long as the depth of the quadrate at 11.8 mm SL (Figure 5h) and extends over the ventrolateral surface of the sympletic; at this size, the ventral edge of the sympletic contacts the base of the posteroventral process of the quadrate. The relationship between the posteroventral process of the quadrate and the

sympletic observed at this size remains similar in later larval stages and juveniles. At 16.1 mm SL, the posteroventral process remains angular and is longer than the quadrate (Figure 5i). The shape of the quadrate and its posteroventral process at 16.1 mm SL is similar to that of later larval stages (Figure 5j) and in juveniles.

Metapterygoid

In the earliest stages with an ossified metapterygoid it could not be determined if the bone consisted only of perichondral ossification or if endochondral ossification had already started. The bone was first observed along the posterodorsal edge of the palatoquadrate cartilage at 8.7 mm SL (fixed at 10.9 mm SL), with complete endochondral and perichondral ossifications at 11.8 mm SL (Figure 5h). By 16.1 mm SL, the entire posterodorsal edge of the palatoquadrate is replaced by the metapterygoid (Figure 5i). At the posterior tip of the metapterygoid there is a membranous outgrowth (i.e., without apparent cartilaginous precursor) that forms a dorsal projection with two spikes. The posterior spike widens and contacts the hyomandibula at 24.3 mm SL (Figure 5j). At this size, the anteroventral edge of the metapterygoid contacts the posterior edge of the endopterygoid. In juveniles, the posterior tip of the metapterygoid extends over and attaches to the posteroventral region of the metapterygoid.

Palatine

The dermopalatine first appears at 8.7 mm SL and fixes at 10.9 mm SL. At the earliest stages, the dermopalatine is shaped as a small, thin laminar bone, positioned slightly posterior to the expanded anterior region of the palatoquadrate cartilage. The autopalatine first appears at 10.9 mm SL and is fixed at 11.8 mm SL (Figure 5h) in the expanded region of the anterior part of the palatoquadrate cartilage. At this size, the dermopalatine extends from the anteroventral portion of the ventral margin of the autopalatine to almost the middle of the palatoquadrate cartilage. The dermopalatine also expands dorsoventrally, acquiring a triangular shape. At 16.1 mm SL (Figure 5i) the autopalatine and dermopalatine fuse along the longitudinal axis to form the palatine. The anterior tip of the palatine projects anteriorly, extending beyond the base of the maxillary process. The posterior region of the palatine extends beyond the anterior region of the ectopterygoid, forming a weak overlapping suture. At this size, teeth on the palatine are first observed. The anterior region of the palatine is almost entirely ossified, with exception of the anterodorsal process for articulation with the lateral ethmoid and the maxilla. At 24.3 mm SL, the palatine is elongated with a cylindrical posterior region and an angular posteroventral edge that forms a tight overlapping suture with the anterior region of the ectopterygoid. The anterior region of the palatine is twice deeper than the posterior region, with a triangular dorsal margin that articulates with the ventral region of the lateral ethmoid. The anterodorsal process of the palatine projects anterolaterally and articulates with the anteroventral region of the lateral ethmoid and the posterior surface of the maxillary process of the maxilla. The posteroventral edge of the palatine is angular and is anteroventrally directed and extends beyond the dorsal edge of the palatine (Figure 5j). The ventral surface of the palatine bears five conical, fang-like teeth. The shape of the palatine observed at this size is similar to that observed in adults.

Ectopterygoid

The ectopterygoid first occurs at 8.2 mm SL and fixes at 9.7 mm SL (Figure 5g). In its earliest stages, the ectopterygoid is shaped as a thin laminar bone ventral to the palatoquadrate cartilage and anterior to the jaw joint. By 10.9 mm SL, this lamina extends anteriorly to reach the middle of the palatoquadrate and posteriorly to reach the developing quadrate. The ectopterygoid is expanded dorsoventrally at 11.8 mm SL to tightly contact the quadrate (Figure 5h). At 16.1 mm SL, the ectopterygoid is elongated and angular anteriorly, with its anterior tip contacting the posterior region of the palatine (Figure 5i). The posterior region of the ectopterygoid is trapezoidal and twice deeper than the anterior region. The shape of the ectopterygoid observed at 16.1 mm SL is similar to that observed in larger larvae (Figure 5j) and juveniles.

Endopterygoid

The endopterygoid first appears as two thread-like bones at 16.1 mm SL (Figure 5i) over the dorsal margin of the palatoquadrate cartilage, one at the level of the quadrate and the other at the level of the posterior tip of the ectopterygoid. There appears to be connective tissue uniting the two ossifications (this condition was observed on multiple specimens). At 18.6 mm SL, the two parts of the ectopterygoid fuse into a single elongated element. At 24.3 mm SL (Figure 5j), the depth of the endopterygoid is almost two-thirds of the depth of the ectopterygoid, extending from the middle of the ectopterygoid to the anteroventral edge of the metapterygoid. The endopterygoid in juveniles displays dorsal projections, but the development of these features occurs in later sizes. Larval specimens up to 24.5 mm SL lack such endopterygoid projections.

Maxilla

The maxilla was first present in a specimen of 6.0 mm NL but is fixed only at 6.9 mm NL. At its earliest occurrence, the maxilla is a small, thin, and laminar bone and is smaller than the interhyal. By 7.4 mm SL (Figure 5d), the length of the maxilla has doubled and by 7.5 mm SL the maxilla expands dorsoventrally (Figure 5e). At 8.2 mm SL (Figure 5f) the anterior tip of the maxilla forms a rudimentary articulatory head for contact with the premaxilla and the vomer. At 9.7 mm SL (Figure 5g) the anterodorsal tip of the maxilla is projected anteriorly, and the ventral edge is expanded into a triangular process. The body of the maxilla thickens, especially anteriorly. By 11.8 mm SL, the anterodorsal projection of the maxilla is a distinct anterolaterally directed process, although it is shorter than the more ventral process (Figure 5h). At this size the posterior portion of the maxilla expands dorsoventrally, forming a wide and flattened lamina that receives the external face of the coronomaxillary ligament (i.e., maxillary process). At 16.1 mm SL (Figure 5i) the posterior region of the maxilla is almost twice as deep as the anterior part, similar to the adult condition.

Premaxilla

The premaxilla first appears at 7 mm SL, fixed at 7.7 mm SL as a small yet elongate bone (less than one third the length of the maxilla), with a slightly enlarged anterior tip (Figure 5e). It is transversely oriented anterior to the maxilla. At 7.9 mm SL (Figure 6a), there is a slight dorsal projection at its and anterior tip, and at 8.2 mm SL (Figures 5f, 6b) this projection becomes a thin ascending process of the premaxilla that is approximately one-third the length of the main body of the premaxilla. The posterior tip of the premaxilla is continuous with a membranous thread that extends laterally to the level of the mid-portion of the maxilla (Figure 6b). At 9.7 mm SL, the membranous part of the premaxilla ossifies into an elongate, rod-like bone (Figure 5g). The anterior part of the premaxilla ventral to the ascending process is triangular and relatively thick, as tall as the ascending process (Figures 5g, 6c). The ascending process grows substantially by 10.9 mm SL and is as wide as the anterior tip and approximately half the length of the main portion of the premaxilla. At 11.8 mm SL (Figures 5h, 6d), the articular process of the premaxilla is present, positioned posterior to the ascending process on the dorsal margin of anterior region of the premaxilla. The articular process of premaxilla at 16.1 mm SL (Figure 6e), acquires a triangular shape and articulates with the anterior tip of the maxilla, as observed in adults. The posterodorsal tip of the premaxilla develops a semi-elliptical laminar projection at 16.1 mm SL (Figure 5i). This projection is more than two times as deep as the anterior region of the premaxilla by 18.6 mm SL. At 24.3 mm SL (Figure 5j), the premaxilla has a triangular, robust ascending process at its anteromedial edge; at this size the width of the base of the ascending process of the premaxilla is as long as the depth of the posterior region of the premaxilla. The posterior surface of the ascending process articulates with the anterior surface of the rostral cartilage. Laterally adjacent to the ascending process, a triangular articular process of the premaxilla is present, its depth approximately one-quarter of the length of the ascending process of the premaxilla. The posterior surface of the articular process of the premaxilla articulates with the anterior surface of the maxillary process. Posterior to both the ascending and articular processes, the premaxilla is sub-cylindrical and thin. The posterior region of the premaxilla, however, is laminar and shaped as a semi-circle; the depth of the posterior region of the premaxilla is three times the depth of the anterior region. The shape described for this larval size is similar to that observed in adults.

Rostral cartilage

The rostral cartilage is first observed at 8.8 mm SL and is fixed only at 11.8 mm SL. In its earliest stages, the rostral cartilage is approximately one-half the length of the ascending process. At 16.1 mm SL (Figure 6e), the rostral cartilage is elongated, semi-rectangular, slightly concave in its anterior surface, and anteroposteriorly flattened. The length of the rostral cartilage is as long as the ascending process of the premaxilla, as seen in larger larvae (Figure 5j) and adults.

Hyomandibular

Ossification of the *pars hyomandibularis* is first observed at 7.1 mm SL and is fixed at 8.2 mm SL. The earliest stages of ossification of the hyomandibular (both perichondrally and endochondrally) are observed around the foramen for the hyomandibular branch (Figure 5f). The ossification develops gradually both dorsally and ventrally (Figure 5g), with the *pars hyomandibularis* almost entirely ossified at 11.8 mm SL (Figure 5h); the tips of anterior and posterior dorsal heads and the posterior opercular process remain cartilaginous throughout ontogeny. By 16.1 mm SL (Figure 5i) the anterior, posterior, and dorsal margins of the hyomandibular develop membranous flanges, acquiring a Y-shaped outline. The shape of the hyomandibular observed at 16.1 mm SL is similar to that observed in larger larvae (Figure 5j) and juveniles.

Sympletic

Ossification of the *pars symplectica* is first observed at 7.9 mm SL, fixed at 8.2 mm SL, with both endochondral and perichondral bone present at the midpoint of the *pars symplectica* (Figure 5g). At 10.9 mm SL, the ventral edge of the sympletic contacts the posteroventral region of the quadrate. At 11.8 mm SL, the ventral portion of the sympletic is laterally covered by the posteroventral process of the quadrate (Figure 5h). Ossification proceeds both dorsal and ventrally, with the symplectic ossified almost entirely (with exception of its extremities) by 16.1 mm SL (Figure 5i). The sequence of development of jaws, hyopalatine, infraorbital, and opercular series is summarized in Figure 7)

3.3 | Infraorbital bones

The only infraorbital bone present in *Porichthys notatus* is infraorbital one (=lachrymal of Greenfield et al., 2008) (Figures 5, 7). Infraorbital one is first present at 7.5 mm SL (Figure 5e) as a small (less than one-half the depth of the *pars autopalatina*), elliptical bone that is dorsolateral to the anterior tip of the palatoquadrate cartilage. At a larger size, 7.9 mm SL, infraorbital one is longer than the greatest depth of the *pars autopalatina* and at 8.2 mm SL (Figure 5f) the anterior tip of infraorbital one develops a socket for articulation with the *lamina orbitonasalis* (and in later stages, with the lateral ethmoid bone). The posterior region of infraorbital one widens at 9.7 mm SL (Figure 5g), representing the early stages of the groove for the infraorbital canal. At 11.8 mm SL (Figure 5h), the infraorbital one projects posteroventrally beyond the dorsal margin of the maxilla at 16.1 mm SL (Figure 5i), as observed in larger larvae (Figure 5j) and adults.

3.4 | Opercular series

The sequence of ossification of bones of the opercular series is: opercle (minimum and fixed length observed at 6.0 mm NL), subopercle (fixed length at 6.2 mm NL; minimum length observed at 6.0 mm NL), interopercle (fixed, 6.8 mm NL; minimum, 6.0 mm NL), and preopercle (fixed, 7.5 mm SL; minimum, 6.0 mm NL) (Figures 5, 7).

Opercle

The opercle first appears at 6.0 mm NL as an inverted L-shaped bone with a small socket at its anterodorsal corner to meet the opercular process of the hyosymplectic cartilage (Figure 5a). At 6.2 mm NL, a concave flange is present between the base of the posterior and vertical limbs of the opercle (Figure 5b). This outline persists through development, although the limbs of the opercle become gradually more robust in larger sizes. The vertical limb of the opercle contacts the ventral margin of the subopercle at 6.8 mm SL. By 16.1 mm SL (Figure 5i), the posterior limb is a thickened spine and the vertical limb is laminar. At this size, the vertical limb articulates with the anterodorsal process of the subopercle, as in larger larvae (Figure 5j) and juveniles.

Subopercle

The subopercle first appears at 6.0 mm NL and fixes at 6.2 mm NL; (Figure 5b). In the earliest sizes, this bone is concave, narrow, and as long as the opercle, and begins to expand anteriorly at 6.8 mm NL (Figure 5c). At 7.1 mm NL, it acquires a comma shape, with its anterior edge as wide as the opercle and its posterior region tapered (Figure 5d). At 7.5 mm SL, the anterior edge of the subopercle forms a distinct angular projection that articulates with the ventral limb of the opercle (Figure 5e). At 8.2 mm SL (Figure 5f), the subopercle is larger than the opercle and its posterior tip extends beyond the posterior margin of the opercle. The posterior edge of the subopercle branches into a dorsal filament at 11.8 mm SL (Figure 5h). The indentation between the dorsal filament and the posterior edge of the subopercle gradually increases at larger sizes, reaching the anterior region of the subopercle in juveniles. At 24.3 mm SL and juveniles, the subopercle is comma-shaped, with a deep concave dorsal margin and convex ventral margin. The posterior tip has a dorsal filament that is one-quarter the length of the subopercle. The anterior margin of the subopercle is concave and shallow. The anterodorsal edge has a large semi-elliptical process that extends dorsally to the dorsal edge of the preopercle. The lateral surface of this anterodorsal process of the subopercle articulates with the medial surface of the vertical limb of the opercle. The anteroventral edge is rounded and contacts the posterior margin of the interopercle.

Interopercle

The first occurrence of the interopercle is at 6.0 mm NL, but it is only fixed at 6.8 mm NL. When it first appears the interopercle is a short thin bone (approximately one-third of subopercular length) that is positioned laterally to the ventral tip of the interhyal (Figure 5c). At 7.1 mm NL, the interopercle expands dorsoventrally and is approximately one-third of the length of the interhyal. It continues to elongate, and at 7.5 mm SL it is more than one-half the length of the subopercle. At larger sizes, most of the growth of the interopercle occurs in the dorsoventral direction, and by 11.8 mm SL (Figure 5h) the interopercle is as long as the interhyal and has the trapezoidal shape that is seen in larger larvae and juveniles (Figures 5i,j).

Preopercle

The preopercle is the last bone of the opercular series to become fixed, 7.5 mm SL, although its first occurrence is also at 6.0 mm NL (like the other bones from the opercular series). It first ossifies as a thin bone positioned posterior and parallel to the posterior margin of the hyosymplectic cartilage. The preopercle expands laterally at 7.9 mm SL (Figure 5e), with a distinct foramen close to its dorsal edge for innervation of neuromasts of the preoperculomandibular lateral-line sensory canal; at 8.2 mm SL (Figure 5f), a second more ventral foramen is present. By 11.8 mm SL (Figure 5h), the preopercle is much larger than smaller specimens, extending from the level of the foramen for the hyomandibular branch of the fascialis nerve at the hyomandibula to the ventral margin of the symplectic. The anterior margin of the preopercle projects laterally forming the groove that houses the sensory canal. At 16.1 mm SL (Figure 5i) this groove becomes deeper, acquiring the shape observed in larger larvae (Figure 5j) and juveniles.

3.5 | Ventral hyoid arch

The sequence of ossification in the ventral hyoid arch is: branchiostegal rays (smallest size observed and fixed length at 5.4 mm NL), anterior ceratohyal (fixed length at 7.7 mm SL; minimum size observed at 7.1 mm NL), ventral hypohyal (fixed, 8.2 mm SL; minimum, 7.1 mm NL), posterior ceratohyal (fixed, 9.7 mm SL; minimum, 8.7 mm SL), interhyal (fixed, 10 mm SL; minimum, 8.7 mm SL), urohyal (fixed, 11.8 mm SL; minimum, 8.7 mm SL), dorsal hypohyal (minimum and fixed at 11.8 mm SL), and basihyal (minimum and fixed at 18.6 mm SL) (Figures 5, 8–10).

The interhyal, ceratohyal, and hypohyal cartilages, and the posteriormost branchiostegal are present in the smallest specimen observed (5.4 mm NL). The interhyal is short and rod-like throughout its development, contacting the medial surface of the hyosymplectic cartilage dorsally and the posterior edge of the ceratohyal cartilage ventrally (Figures 5a–f). At 6.0 mm NL, the hypohyal cartilage is trapezoidal in shape and approximately 25% the length of the ceratohyal cartilage (Figure 8a). The foramen for the hyoid artery is present at 6.0 mm NL and at 7.4 mm SL the posterodorsal edge of the hypohyal cartilage projects posteriorly over the ceratohyal cartilage. At 8.2 mm SL (Figure 8b), the posterodorsal projection of the hypohyal extends to the anterior third of the ceratohyal cartilage. The ceratohyal cartilage is rectangular anteriorly at 6.4 mm NL, but its posterior half is broad and trapezoidal in shape, tapering to the posterior edge (Figure 8a). In larger larvae, the posterodorsal edge of the ceratohyal cartilage forms a distinct depression for articulation with the ventral edge of the interhyal cartilage (Figures 8b,c). The basihyal cartilage is first seen at 7.1 mm NL. This element has a rod-like shape and contacts the medial edge of the hypohyal cartilages and the anterior edge of the *copula communis* cartilage (Figures 8c, 10c–g).

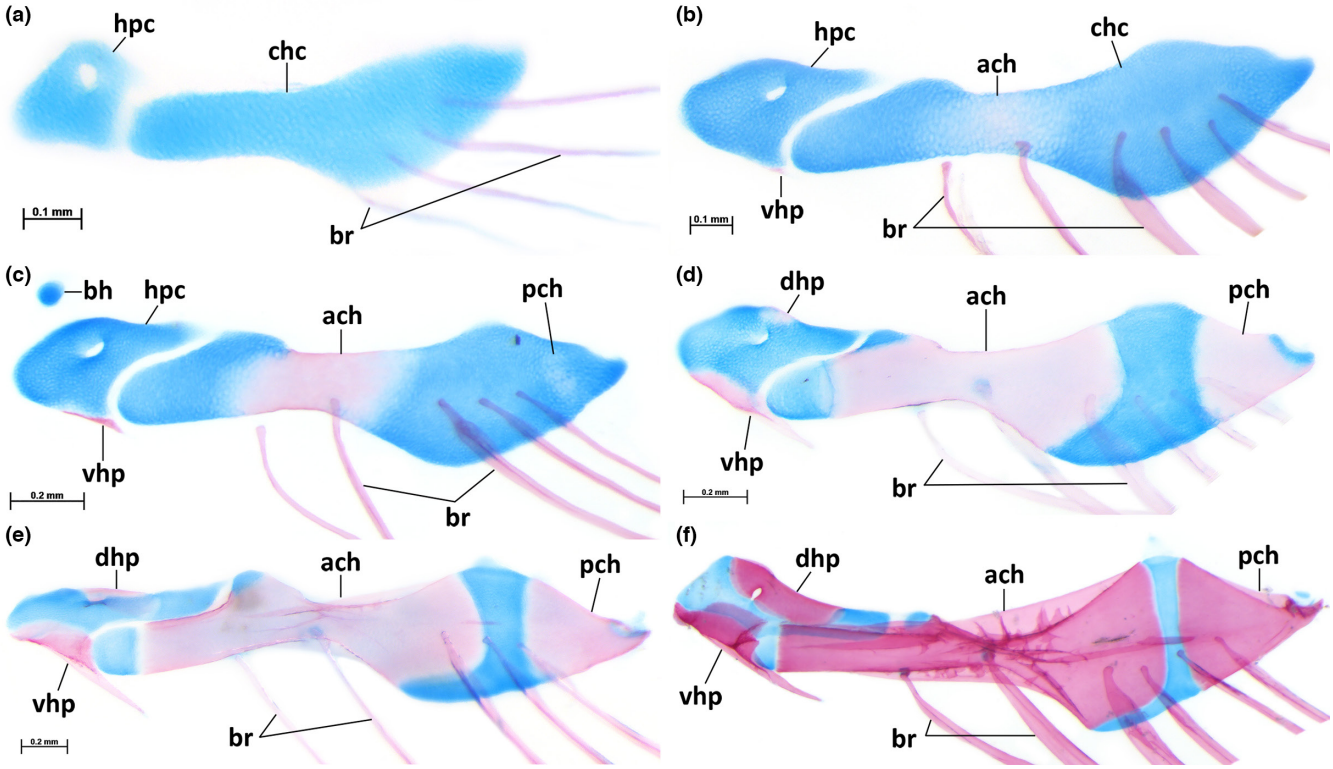

FIGURE 8 Ontogeny of the ventral hyoid arch of *Porichthys notatus* in lateral view. (a) VIMS 40286, 6.4 mm TL. (b) VIMS 40278, 8.2 mm SL. (c) VIMS 40273, 9.7 mm SL. (d) VIMS 40269, 11.8 mm SL. (e) VIMS 40260, 16.1 mm SL. (f) VIMS 40856, 24.3 mm SL. Abbreviations: ach, anterior ceratohyal; bh, basihyal; br, branchiostegal rays; chc, ceratohyal cartilage; dhp, dorsal hypohyal; hpc, hypophyal cartilage; pch, posterior ceratohyal; vhp, ventral hypohyal.

Interhyal

The smallest specimen with the earliest stages of ossification of the interhyal has 8.7 mm SL, but ossification of this bone fixes only at 10 mm SL. The interhyal becomes fully ossified (except the dorsal and ventral tips) at 11.8 mm SL (Figure 5h). At this size, the interhyal already has the shape seen in larger larvae and juveniles: a small, rod-like element (approximately two-thirds the length of the sympletic) with a dorsal cartilaginous head for articulating with the ventral edge of the hyomandibular and dorsal edge of sympletic (i.e., the remains of the hyosympletic cartilage) and a ventral cartilaginous head that sits in the articular socket on the posterior edge of the posterior ceratohyal (Figures 5i,h).

Anterior ceratohyal

Ossification of the anterior ceratohyal first occurs near the midpoint of the ceratohyal cartilage at 7.1 mm SL and is fixed at 7.7 mm SL (Figure 8b). The ossification continues gradually in both anterior and posterior directions (Figure 8c). At 7.9 mm SL, a rounded bulge develops anteriorly on its dorsal margin; this will become the point of contact with the dorsal hypohyal (Figures 8b–f). At 9.7 mm SL (Figure 8c), about half of the ceratohyal cartilage is ossified anteriorly. The anterior ceratohyal is almost entirely ossified at 16.1 mm SL (Figure 8e), with exception of its posterior tip and where it contacts the posterior ceratohyal. This bone is elongated anteriorly, with a dorsal process that articulates with the hypohyal cartilage (and in larger sizes, the dorsal hypohyal). The posterior region of the anterior ceratohyal is approximately 1.5 times wider than the anterior region. The posterior margin of the anterior ceratohyal is straight, with a rounded posteroventral edge. There are thin projections of bone that make initial contact between the anterior and posterior ceratohyals at this size; this interdigitation becomes more extensive in juveniles. The groove for articulation with the second branchiostegal is fully formed at 16.1 mm SL. The shape of the anterior ceratohyal at 24.3 mm SL is similar to that of 16.1 mm SL specimens, except it is more robust and having both dorsal and ventral margins relatively less concave (Figure 8f).

Posterior ceratohyal

The first trace of bone of the posterior ceratohyal appears at 9.7 mm SL and is located slightly anterior to its articulation with the interhyal (Figure 8c). At 10.9 mm SL, the posterior ceratohyal is trapezoidal-shaped, with a convex anterior margin and concave posterior margin and extending anteriorly to the origin of the posteriormost branchiostegal (as seen in Figure 8d). At 16.1 mm SL, the posterior ceratohyal is triangular, with the posterior edge having a shallow concavity for articulation with the interhyal (Figure 8e). At 24.3 mm SL, the posterior ceratohyal remains triangular (as observed in larger juveniles), with the anterior region of the posterior ceratohyal extending anteriorly to the level of the base of the fifth branchiostegal ray and contacting the interdigitation projecting

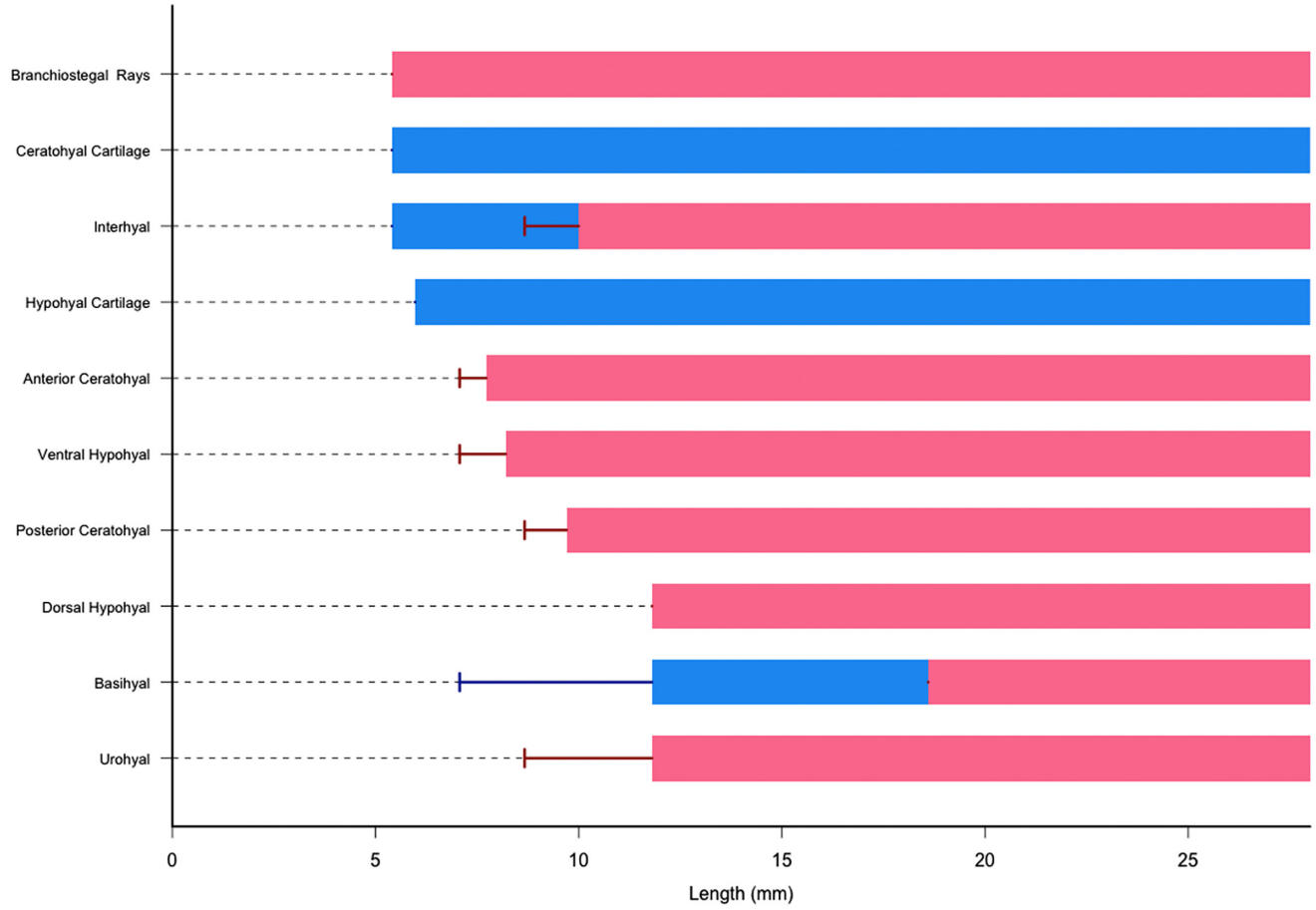

FIGURE 9 Diagram of sequence of development of ventral hyoid arches of *Porichthys notatus*. Bars correspond to fixed length. Error bars correspond to the smallest size that a structure was found. Bars in blue correspond to cartilage, red to bone. Lengths presented in mm NL/SL.

from the anterior ceratohyal. The posterior edge of the posterior ceratohyal at 24.3 mm SL has a deeper concavity for articulating with the interhyal.

Branchiostegals

Each individual branchiostegal ossifies in a proximal-to-distal direction, but as a series they develop in a posterior to anterior direction. The two most posterior branchiostegals are present at 6.0 mm NL, and by 6.4 mm NL, the two central branchiostegals appear (Figure 8a). At 7.1 mm NL, the second branchiostegal is present and traces of the anteriormost branchiostegal are visible. The second branchiostegal develops a distinct head of articulation at 7.9 mm SL, contacting the medial surface of the ceratohyal cartilage. As noted above, this region of the anterior ceratohyal will form a groove that serves as a point of articulation for the second branchiostegal. At 7.4 mm SL, the anteriormost branchiostegal contacts the ventral margin of the ceratohyal cartilage, and its proximal head is formed at 7.9 mm SL (Figure 8b).

From their first appearance until 24.3 mm SL (Figures 8c–f), the bases of the four posterior branchiostegals gradually widen, becoming the widest region of each element. The anterior edge tapers dorsally, resulting in a semi-circular projection (similar to that observed in juveniles). The second branchiostegal also widens through development, although its widest area is on the anterior third of the length of the element, at the level of the posterodorsal edge of the anterior ceratohyal. The anterior edge of the second branchiostegal is elongated and tapers anterodorsally to reach the groove of articulation with the anterior ceratohyal. The anteriormost branchiostegal is slightly narrower than the second, with thin anterior edge that projects dorsally with a semi-circular proximal head that articulates with the ventral margin of the anterior ceratohyal (Figure 8f).

Ventral hypohyal

Perichondrondral ossification of the ventral hypohyal is first present at 7.1 mm NL, fixed at 8.2 mm SL, located along the ventral margin of the hypohyal cartilage, forming a thin bony ridge that is loosely associated with the underlying cartilage. This ridge gradually develops into a triangular, posteroventrally directed process that extends past the tip of the anterior ceratohyal. Chondral ossification of the ventral hypohyal is first observed in the region of contact between the posteroventral process and the hypohyal cartilage at 9.7 mm SL. The ventral hypohyal gradually ossifies dorsally, reaching the middle of the hypohyal cartilage by 16.1 mm SL (Figure 8e). The condition at this size is similar to that present in larger larvae (Figure 8f). In juveniles, the anterdorsal margin of the ventral hypohyal expands

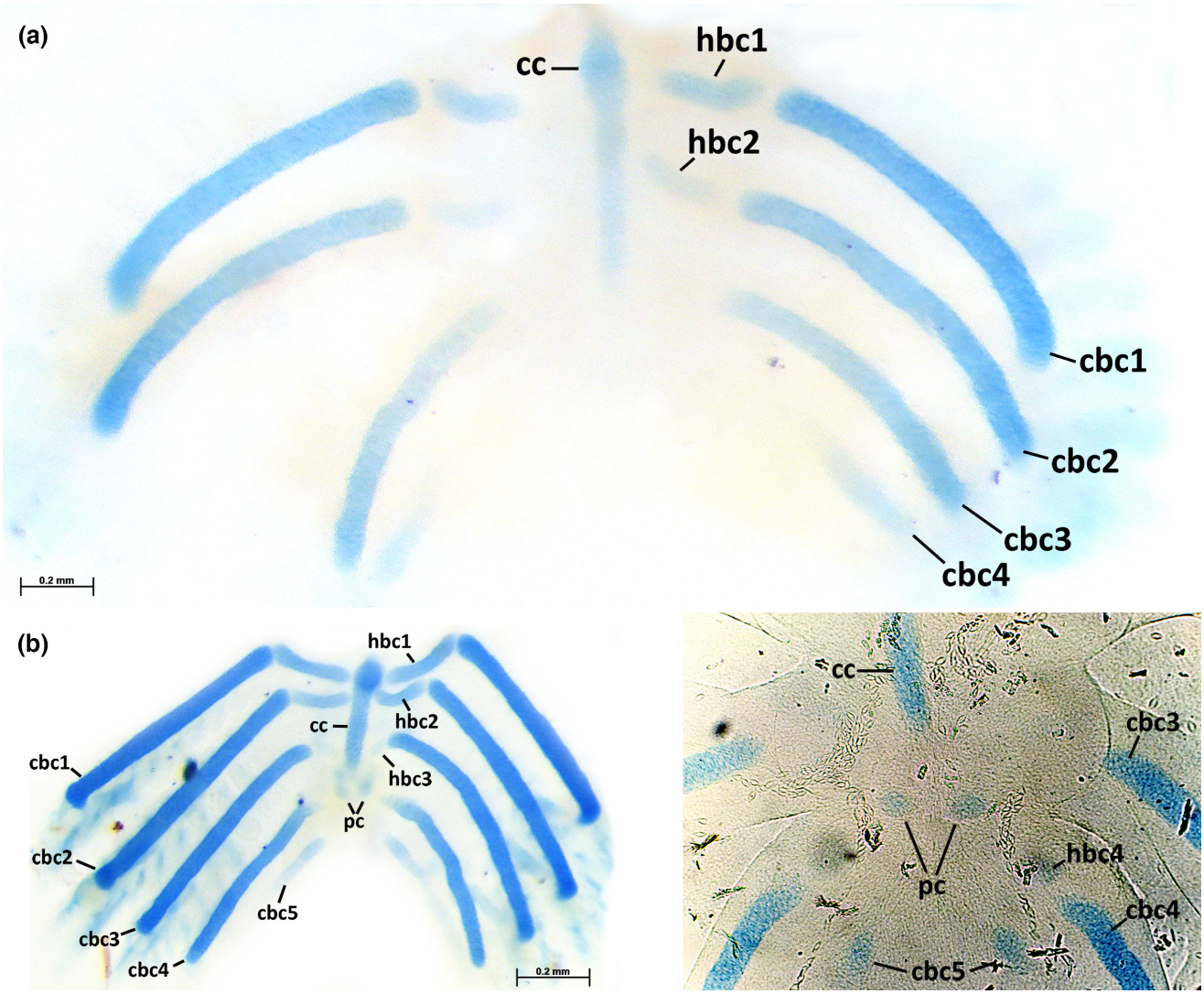

FIGURE 10 Ontogeny of the branchial arches of *Porichthys notatus*. (a) Ventral gill-arch elements of VIMS 40285 (6.0 mm NL) in dorsal view. (b) on left, ventral gill-arch elements of VIMS 40262 (7.1 mm NL) in dorsal view. On right, posterior region of cleared-and-stained gill arches of VIMS 40274 (6.8 mm NL) on compound microscope (100× magnification). Note the absence of cells between right and left posterior copula. (c) Ventral (top left) and dorsal (right) gill arches of VIMS 40284 (7.5 mm SL) in dorsal view. On bottom left, posterior region of ventral gill arches of VIMS 40858 (6.7 mm SL) under compound microscope (100× magnification) showing the earliest stages of fusion of right and left posterior copula. (d) Ventral (left) and dorsal (right) gill arches of VIMS 40277 (9 mm SL) in dorsal view. (e) Ventral (top left) and dorsal (right) gill arches of VIMS 40272 (10.9 mm SL) in dorsal view. Bottom-left shows a close-up of anterior branchial elements in ventral view. (f) Ventral (top left) and dorsal (right) gill arches of VIMS 40269 (11.8 mm SL) in dorsal view. Bottom-left shows a close-up of anterior branchial elements in ventral view. (g) Ventral (top left) and dorsal (right) gill arches of VIMS 40260 (16.1 mm SL) in dorsal view. (h) Ventral (top left) and dorsal (right) gill arches of VIMS 40264 (18.6 mm SL) in dorsal view. Bottom-left shows a close-up of anterior branchial elements in ventral view. Abbreviations: Bb, basibranchial; bh, basihyal; cb, ceratobranchial bone; cbc, ceratobranchial cartilage; cc, copula communis; eb, epibranchial bone; ebc, epibranchial cartilage; pb, pharyngobranchial bone; pbc, pharyngobranchial cartilage; hb, hypobranchial bone; hbc, hypobranchial cartilage; pc, posterior copula; tp, tooth plate; uh, urohyal; up, uncinate process.

dorsally, replacing the anterior edge of the remaining of the precursor hypohyal cartilage.

Dorsal hypohyal

Ossification of the dorsal hypohyal is first seen in much larger individuals (11.8 mm SL; Figure 8d) than the ventral hypohyal. The ossification of the dorsal hypohyal first occurs dorsal to the foramen for the hyoid artery; by 16.2 mm SL the dorsal hypohyal has fully replaced the area of the hypohyal cartilage dorsal to the foramen for the hyoid artery (Figure 8e). At 24.3 mm SL (Figure 8f), the dorsal hypohyal bone extends from the anterodorsal edge to the distal third of the hypohyal cartilage. Ossification of the dorsal hypohyal then proceeds ventrally from the region around the foramen for the hyoid artery and in juveniles, it almost contacts the ventral hypohyal.

Basihyal

Ossification of the basihyal is seen in 18.6 mm SL (Figure 10h) and larger specimens, although at this size the basihyal is almost fully

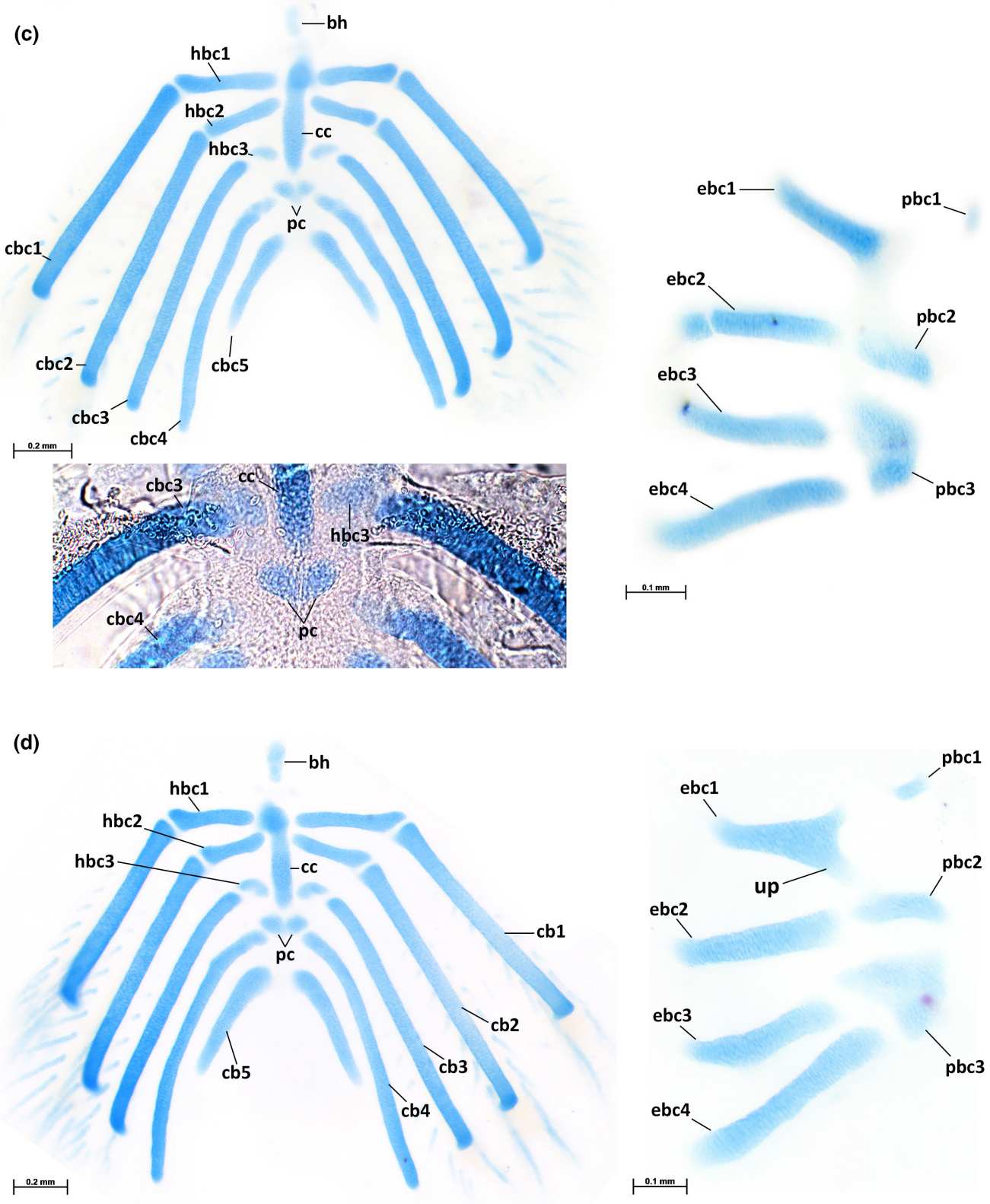

FIGURE 10 (Continued)

ossified. The basihyal is a small rod-shaped bone, its length is less than half of the length of hypobranchial one. The posterior edge of the basihyal contacts the anterior edge of the *copula communis*, and the lateral surfaces of the basihyal contact the dorsomedial surfaces of the dorsal hypohyal at 24.3 mm SL and juveniles.

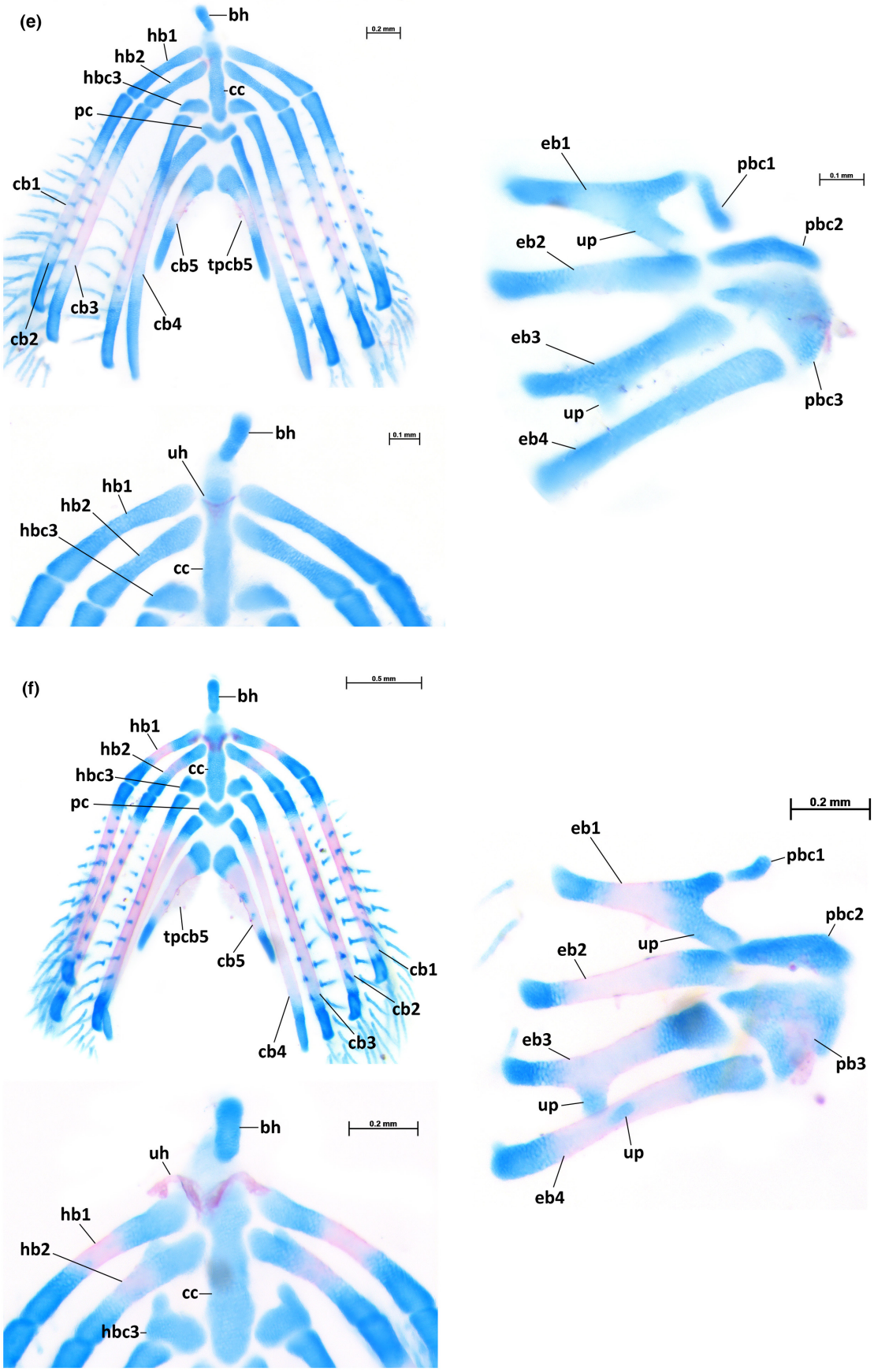

FIGURE 10 (Continued)

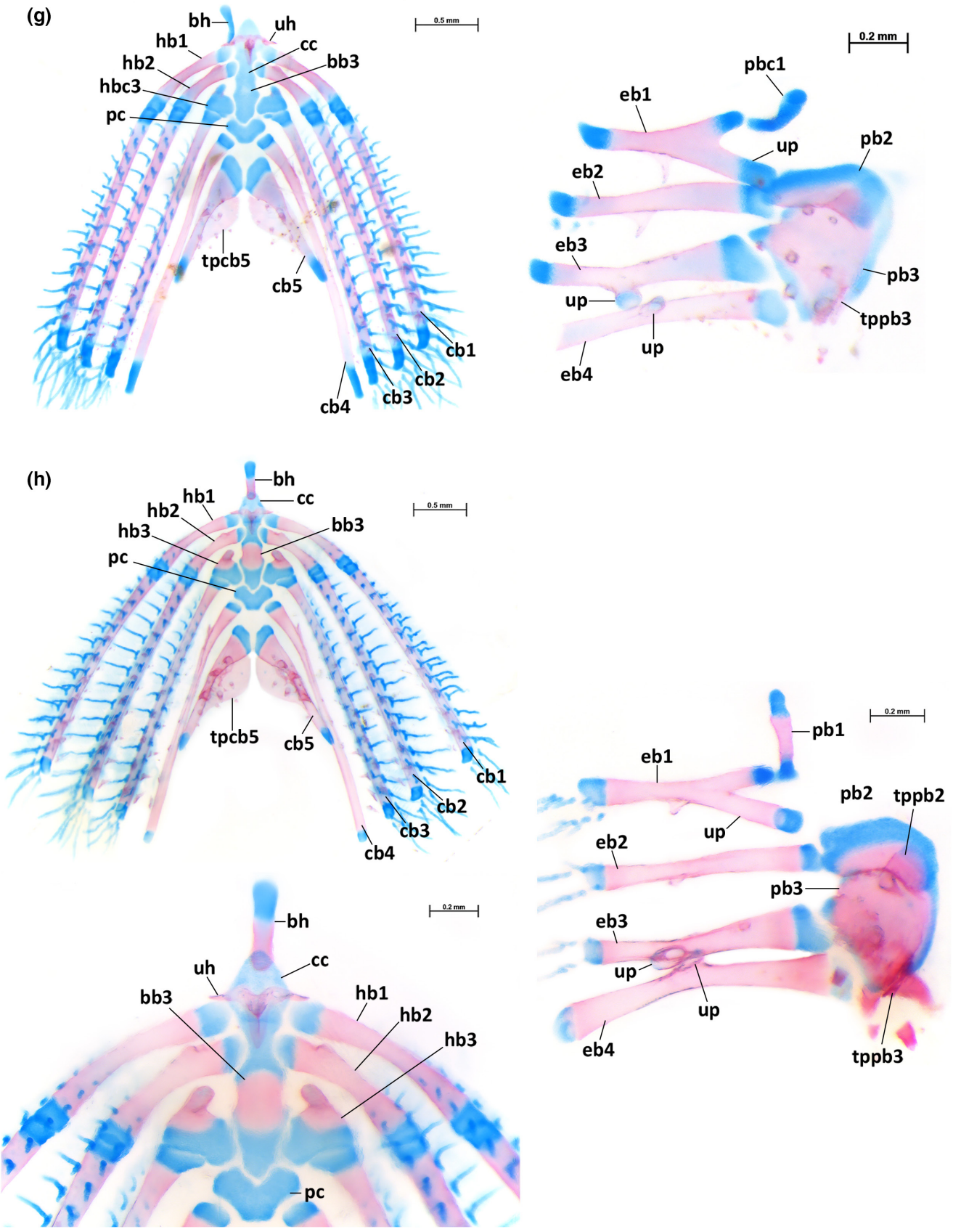

FIGURE 10 (Continued)

Urohyal

The urohyal first appears at 8.7 mm SL and is fixed at 11.8 mm SL. In the smallest sizes, the urohyal is a small, pyramid-shaped bone with its base directed anteriorly and in close contact with the ventral surface of the *copula communis* (Figure 10e). The urohyal expands laterally and resembles two half-moons fused medially at 11.8 mm SL (Figure 10f). By 16.1 mm SL, the medial portion of the urohyal thickens and projects ventrally, forming a T-shaped bone that is similar in form to that of juveniles and adults (Figure 10g,h). The sequence of development of the ventral hyoid arch is summarized in Figure 9.

3.6 | Gill arches

The sequence of ossification of gill arches develops in the following order: ceratobranchial 1–5 and epibranchial 1–4 (fixed length at 10.9 mm SL, minimum size observed at 8.7 mm SL), tooth patch of ceratobranchial five (minimum and fixed length at 10.9 mm SL); hypobranchial 1–2 (fixed, 11.4 mm SL; minimum, 8.7 mm SL); tooth plate of pharyngobranchial three (minimum and fixed at 11.4 mm SL); pharyngobranchial 2–3 (minimum and fixed at 11.8 mm SL); gill rakers (fixed, 16.1 mm SL; 13.1 mm SL); basibranchial three and tooth plate of pharyngobranchial two (fixed, 16.1 mm SL; minimum, 13.9 mm SL); hypobranchial 3 (fixed 18.6 mm SL, minimum, 13.9 mm SL); pharyngobranchial one and tooth plate of epibranchial three (minimum and fixed at 18.6 mm SL) (Figures 10, 11).

3.6.1 | Ceratobranchial series

A 6.0 mm NL specimen has the four anterior ceratobranchial cartilages (Figure 10a). At this size, the three anterior cartilages are elongate and similar in size; ceratobranchial 4 is approximately one-half the length of ceratobranchial 3; by 6.2 mm NL it is approximately three-fourths the length of ceratobranchial 3 and by 7.9 mm SL it is similar in length to the other ceratobranchials, as seen in adults. The fifth ceratobranchial cartilage has a fixed occurrence in specimens larger than 6.6 mm NL (Figure 10b), but this cartilage is present in one specimen with 6.0 mm NL (VIMS 42847). In the smallest sizes, the ceratobranchial 5 is a small circular cartilage that grows to approximately one-fourth the length of ceratobranchial cartilage 4 by 7.1 mm NL (Figure 10b) and about half its length at 7.5 mm SL (Figure 10c); this is the relative size difference of ceratobranchials

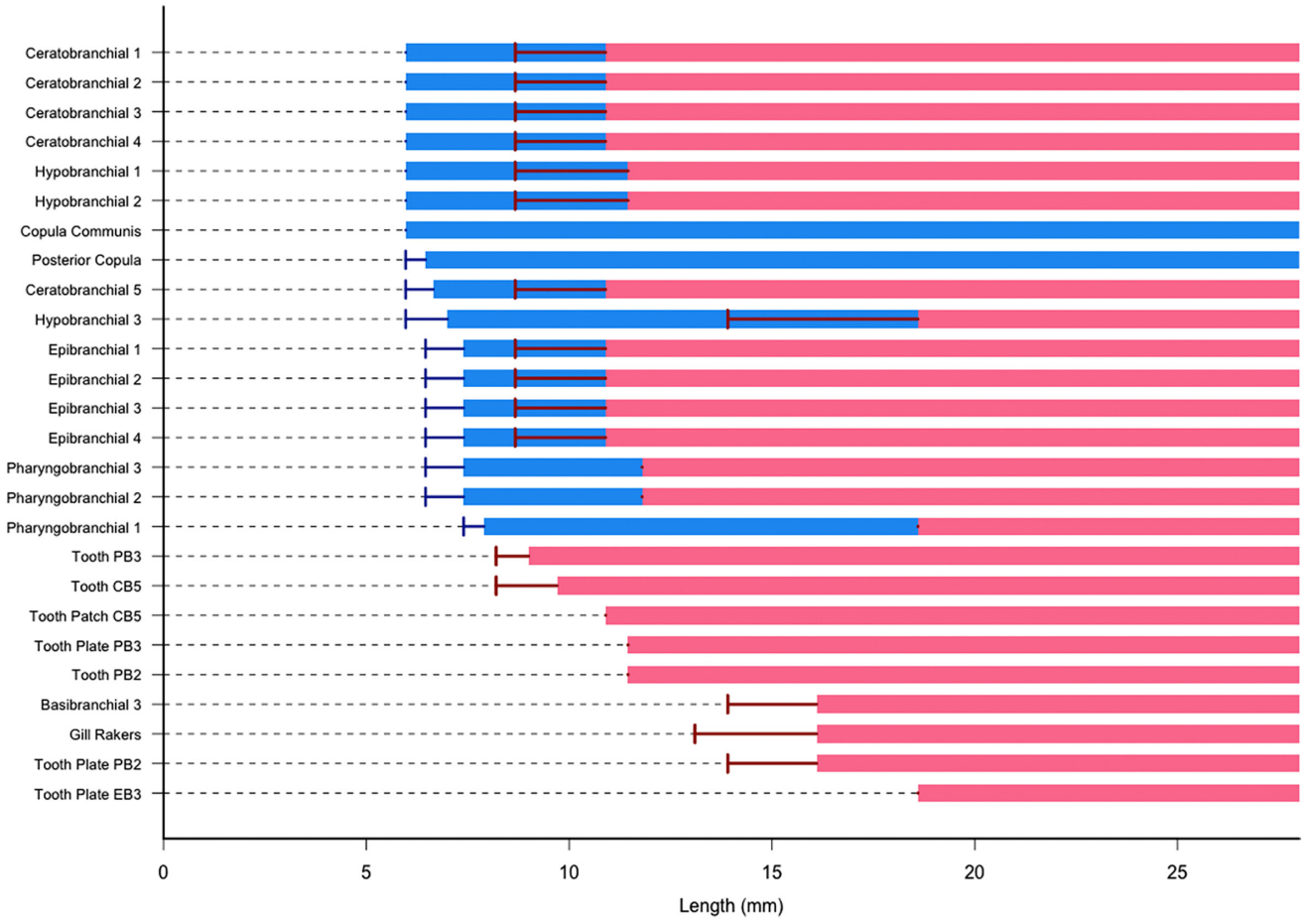

FIGURE 11 Diagram of sequence of development of gill arches of *Porichthys notatus*. Bars correspond to fixed length. Error bars correspond to the smallest size that a structure was found. Bars in blue correspond to cartilage, red to bone. Lengths presented in mm NL/SL.

4 and 5 in juveniles and adults. At this size, the proximal tip of ceratobranchial 5 cartilage is slightly expanded, but by 16.1 mm SL (Figure 10g) it is almost three times wider than the posterior tip (similar to the condition in adults).

Ceratobranchials

The first ossification of the ceratobranchials occurs at 8.7 mm SL, at which point the initial stages of perichondral ossification are present in the middle of each cartilage. At 10.9 mm SL (Figure 10e), approximately half of the length of ceratobranchial cartilages are replaced by bone, and by 11.8 mm SL (Figure 10f), ceratobranchials are almost entirely ossified. At 16.1 mm SL (Figure 10g), ceratobranchials one to four are rod-shaped bones having only their extremities filled with cartilage, with their posterior surface covered by gill filaments, similar to the condition in larger larvae and juveniles (Figure 10h). A pair of small pharyngeal teeth is present at 8.2 mm SL and positioned on the dorsal surface of the fifth ceratobranchial cartilage (the presence of the first pair of teeth is fixed only at 9.7 mm SL). The fifth ceratobranchial tooth patch first develops at 10.9 mm SL (Figure 10e) as a small medial expansion from the medial margins of ceratobranchial 5. At this size, another pair of pharyngeal teeth is present. The tooth patch broadens to become as wide as the posterior part of the fifth ceratobranchial by 11.8 mm SL (Figure 10f); it becomes about two times as wide as the more posterior portion of the main portion bone by 16.1 mm SL (Figure 10g), similar to that observed in larger larvae (Figure 10h). Additional teeth populate the tooth patch of ceratobranchial five during development, until it supports nine small, sparsely distributed conical teeth. Gill rakers on ceratobranchials are first observed at 16.1 mm SL as small pyramidal structures on the posterior region of the trailing edges of the first three ceratobranchials (Figure 10g); by 18.6 mm SL there are gill rakers on the trailing edge of ceratobranchials 1 to 4 (Figure 10h). At 24.3 mm SL, ceratobranchials 1–3 have nine pairs of gill rakers organized in two longitudinal rows. Ceratobranchial 4 has a single row of six gill rakers. Although more distinctly formed in larger larval sizes, their shape remains pyramidal and unicuspid, lacking the multiple cusps that are observed on the gill rakers of juveniles and adults.

3.6.2 | Hypobranchial series

Hypobranchial cartilages 1 and 2 are already present at 6.0 mm NL (Figure 10a), and until 6.4 mm NL, they are concave. From 6.8 mm NL to 9.7 mm SL (Figures 10b–d), these cartilages are straight, and from 10.9 mm SL (Figure 10e), they are slightly convex, as seen in adults. Hypobranchials 3 appear to be present in a 6.0 mm NL specimen, but their presence is only fixed at 7 mm NL (Figure 10b). In the earliest stages, hypobranchials 3 are two pairs of circular cartilages that are in series with hypobranchials 1 and 2 (Figure 10b). Hypobranchial 3 acquires a semi-circular shape by 7.4 mm SL (Figure 10c), and by 9.7 mm SL it develops an anteroventrally directed process. A pair of cartilages between the anteromedial edge of ceratobranchial four and posterior copula was observed in two specimens (VIMS 40274, 6.8 mm NL; VIMS 40283, 7.3 mm NL; Figure 10b). Considering their position, these cartilages are tentatively identified as hypobranchial four. In other teleosts hypobranchial four cartilages are transitory and fuse to ceratobranchial cartilages during development (e.g., *Salmo*, de Beer, 1937; *Salminus brasiliensis*, Mattox et al., 2014; in the latter, inferred by their Figure 10, although this element was not labeled). Additional specimens are needed to confirm whether the observed pair of cartilages are indeed hypobranchial four that fuse to cerabranchials during development or if they are malformations in these two specimens.

Hypobranchials

The earliest perichondral ossification of hypobranchials 1 and 2 is = at 8.7 mm SL, but it becomes fixed at 10.9 mm SL. By 11.8 mm SL (Figure 10f), about half of the cartilage components of hypobranchials 1 and 2 are replaced by bone (both peri- and endochondrally), and by 16.2 mm SL (Figure 10g), these elements are almost entirely ossified. An anteroventrally directed process on the anterior margin of hypobranchial two starts developing at this size. At 18.6 mm SL, hypobranchials one and two are morphologically similar to the condition observed in juveniles: rod-shaped bones and curved posteriorly. At this size, the anteroventral process on the anterior margin of hypobranchial two is still a broad, trapezoidal process. At 24.3 mm SL, the anteroventral process of hypobranchial two acquires the juvenile outline, having an acute and angular edge. At this size, the anterior margin of hypobranchial one develops a shallow triangular process, similar to that observed in juveniles. Ossification of hypobranchial three is first observed at 13.9 mm SL, but only fixed at 18.6 mm SL (Figure 10h). Ossification of hypobranchial three proceeds in an anterior-to-posterior direction. At 18.6 mm SL, only the anterior half of hypobranchial three cartilage is replaced by bone. At 24.3 mm SL, ossification of hypobranchial three has replaced all of the cartilage except for the medial edges. Hypobranchial three is a broad, rectangular cartilage with rounded edges and a large anteroventral process on its anterolateral edge. The anteroventral process of hypobranchial three has a rounded edge (Figure 10h), and at 24.3 mm SL, the edges of the processes have a small triangular process that project medially.

3.6.3 | Basibranchial series

The *copula communis* is a rod-like cartilage that extends from the hypohyals to the level of the third ceratobranchials in the smallest size observed (6.0 mm NL) to 16.2 mm SL (Figures 10a–g). The posterior copula cartilage (Mattox et al., 2014; = basibranchial four cartilage in Kubicek & Conway, 2016) is first observed at 6.0 mm NL (VIMS 42847). Initially, from 6.0 to 7.3 mm NL (e.g., VIMS 40262, 40,283), the posterior copula is represented by a pair of cartilages (Figure 10b). At 6.7 mm SL, the left and right posterior copula cartilages begin to fuse across the midline. Fusion of the paired posterior copula cartilages is fixed at 7.4 mm SL (Figures 10c,d). The resulting

median element is heart-shaped at 7.4 mm SL to 8.2 mm SL, before becoming V-shaped at larger sizes. The posterior copula (=basibranchial four) remains cartilaginous in juveniles and adults.

Basibranchials

Two ossifications of the *copula communis* (basibranchials 1 and 3) are found in juveniles and adults. The earliest trace of ossification of basibranchial 3 appears at 13.9 mm SL and is fixed at 16.1 mm SL (Figure 10g). At 18.6 mm SL (Figure 10h) the basibranchial three has replaced most of the posterior region of the *copula communis* cartilage, forming a rectangular bone that is similar to the shape observed in larger larvae and juveniles. An ossified basibranchial 1 was not found in any larval specimens, but in juveniles (VIMS 38018, 84.5 mm SL) it is formed by a small circular bone that is close to the anterior tip of the *copula communis*.

3.6.4 | Epibranchial series

The earliest stages of epibranchials 1–4 are rectangular cartilages that are first observed at 6.4 mm NL and fixed at 7.4 mm NL (Figure 10c). At 7.5 mm SL (Figure 10c), the anteromedial edge of epibranchial 1 is projected medially and extends ventromedially to contact pharyngobranchial 1 at 10.9 mm SL. The anteromedial edge of epibranchial 1 cartilage projects dorsally as an uncinate process that contacts pharyngobranchial 2 at 10.9 mm SL (Figure 10e). Epibranchials 2–4 have a rectangular shape during their entire development. At 9.0 mm SL (Figure 10d), the dorsal margin of the cartilages of epibranchials 3 and 4 start to develop a cartilaginous uncinate process.

Epibranchials

Ossification of all epibranchial cartilages is first observed at 8.7 mm SL and fixed at 10.9 mm SL. In specimen VIMS 40272 (10.9 mm SL; Figure 10e), the ossification appeared to comprise endochondral bone in the middle portion of the epibranchial cartilages. A second site of endochondral ossification is present in the uncinate process of epibranchial 1. At 11.8 mm SL (Figure 10f), more than two-thirds of the epibranchial cartilages are replaced by bone. At the middle of the dorsal margin of bone of epibranchials 1 and 2, a triangular bony process develops, which develops into secondary uncinate process on these epibranchials. At 18.6 mm SL, epibranchials are entirely ossified except for their extremities and resemble the condition observed in juveniles (Figure 10h). Epibranchial one is Y-shaped, having its medial region projecting anteromedially with its medial edge articulating with phrayngobranchial one. A large uncinate process (approximately half the length of epibranchial one) projects from the medial region of epibranchial one to articulate with pharyngobranchial two. The dorsal margin of epibranchial one has secondary uncinate process that is triangular-shaped. Epibranchials 2–4 are rod-shaped. The medial edge of epibranchial three is slightly larger than those of epibranchials two and four. The dorsal margin of epibranchial two has a triangular uncinate process, similar to the secondary uncinate process of epibranchial one. Epibranchials three and four have a cylindrical uncinate processes on their dorsal margins that are capped with cartilage. The uncinate process of epibranchial three is projected posteriorly and its medial surface contacts the lateral margin of the uncinate process of epibranchial four. Epibranchials 1–3 have a single gill raker on each element at 24.3 mm SL.

3.6.5 | Pharyngobranchial series

The cartilages of pharyngobranchials 2–3 are rectangular and first observed at 6.4 mm NL and fixed at 7.4 mm NL. Pharyngobranchial one is first observed at 7.4 mm SL as a small circular cartilage (and fixed in development at 7.9 mm SL; Figure 10c), which gradually extends into a cylinder (Figure 10d) and articulate with epibranchial one at 10.9 mm SL (Figure 10e). In its earliest stages, pharyngobranchial 2 is comma-shaped, though it gradually acquires a trapezoidal shape during ontogeny. Pharyngobranchial 2 first contacts pharyngobranchial 3 at 9.7 mm SL. Pharyngobranchial 3 is expanded posteriorly to the level of epibranchial 4 by 7.4 mm NL. At 7.5 mm SL (Figure 10c) it becomes trapezoidal before attaining its triangular shape by 8.2 mm SL.

Pharyngobranchials

Pharyngobranchial one is a rod-shaped bone that ossifies at a relatively large size (18.6 mm SL; Figure 10h). At 24.3 mm SL, its ossification is similar to that observed in juveniles. The earliest stages of ossification of pharyngobranchial 2 and 3 are first observed at 10.9 mm SL (Figure 10e), with endochondral ossification clearly occurring at 11.8 mm SL. By 16.1 mm SL (Figure 10g) both pharyngobranchial 2 and 3 are almost entirely ossified. At 18.6 mm SL (and larger larvae and juveniles), pharyngobranchial two is trapezoidal (twice wider than long) with a slightly concave anterior margin and convex posterior margin (Figure 10h). The lateral margins of pharyngobranchial two has two cartilaginous heads: the anterolateral articulates with the uncinate process of epibrabranchial one and the posterolateral articulates with epibranchial two. Pharyngobranchial three is also trapezoidal, having a slightly lateral margin, broad posterior edge, and straight medial margin. The anteromedial edge of pharyngobranchial three has a cartilaginous cap that articulates with epibranchial three. The anterior margin projects anteromedially and bears a cartilaginous cap that articulates with pharyngobranchial two. From the articular cap, the anterior margin projects anterolaterally to form a broad anterolateral edge (Figure 10h).

Upper pharyngeal tooth plates

The upper pharyngeal toothplates first appear on the third pharyngobranchial at 11.4 mm SL (Figure 10f), although a pair of small pharyngeal teeth was associated with pharyngobranchial three at 8.2 mm SL. At 16.1 mm SL, the pharyngeal toothplate three already covers most of the ventral surface of pharyngobranchial three. The pharyngeal toothplate 2 is first observed at 13.9 mm SL and its occurrence is fixed in specimens larger than 16.1 mm SL. In its earliest stages, the pharyngeal toothplate two is restricted to the posterolateral edge of the second pharyngobranchial (Figure 10g). At 16.1 mm SL, the teeth

that will attach to the upper pharyngeal toothplates are already present, but they have not ankylosed to the toothplate yet (as observed in larger larvae and juveniles; Figure 10h). The earliest trace of the toothplate of epibranchial three is observed on the ventromedial region of epibranchial three at 18.6 mm SL, at which point there is only a single tooth present (Figure 10h). At 24.3 mm SL, the toothplate of epibranchial three still only has a single tooth, but the toothplate is already projecting laterally and has the initial stages of development of a second tooth. The sequence of development of gill arches is summarized in Figure 11.

3.7 | Vertebral column and intermuscular bones

The sequence of ossification of the vertebral column and intermuscular bones is: neural arches (first observed and fixed at 6.0 mm NL), haemal arches (fixed length at 6.4 mm NL; minimum length observed at 6.0 mm NL), epineural bone one (fixed, 8.2 mm SL, minimum, 7 mm SL), vertebral centra (fixed, 8.2 mm SL; minimum, 7.7 mm SL), haemal spines (fixed, 11.8 mm SL, minimum, 8.8 mm SL), neural spines (fixed, 13.1 mm SL, minimum, 8.8 mm SL), and remaining epineurals (minimum and fixed observed at 13.1 mm SL) (Figures 12–14).

In *Porichthys notatus* most neural and haemal arches and spines are membranous ossifications (as described for *Indostomus parodoxus* and some gobies; Britz & Johnson, 2002; Schultze & Arratia, 2013). Only the neural and haemal elements of the third and second preural centra and the basiventrals of vertebrae 2–5 are pre-formed in cartilage.

Neural arches and spines

Dorsal arcocentra of vertebrae 1–3 are present at 6.0 mm NL and are thin and elongate bones that surround the dorsolateral region of the spinal cord (Figure 12a). By 6.2 mm NL, dorsal arcocentra of vertebrae 1–14 are present (Figure 12b). At this size, dorsal arcocentra

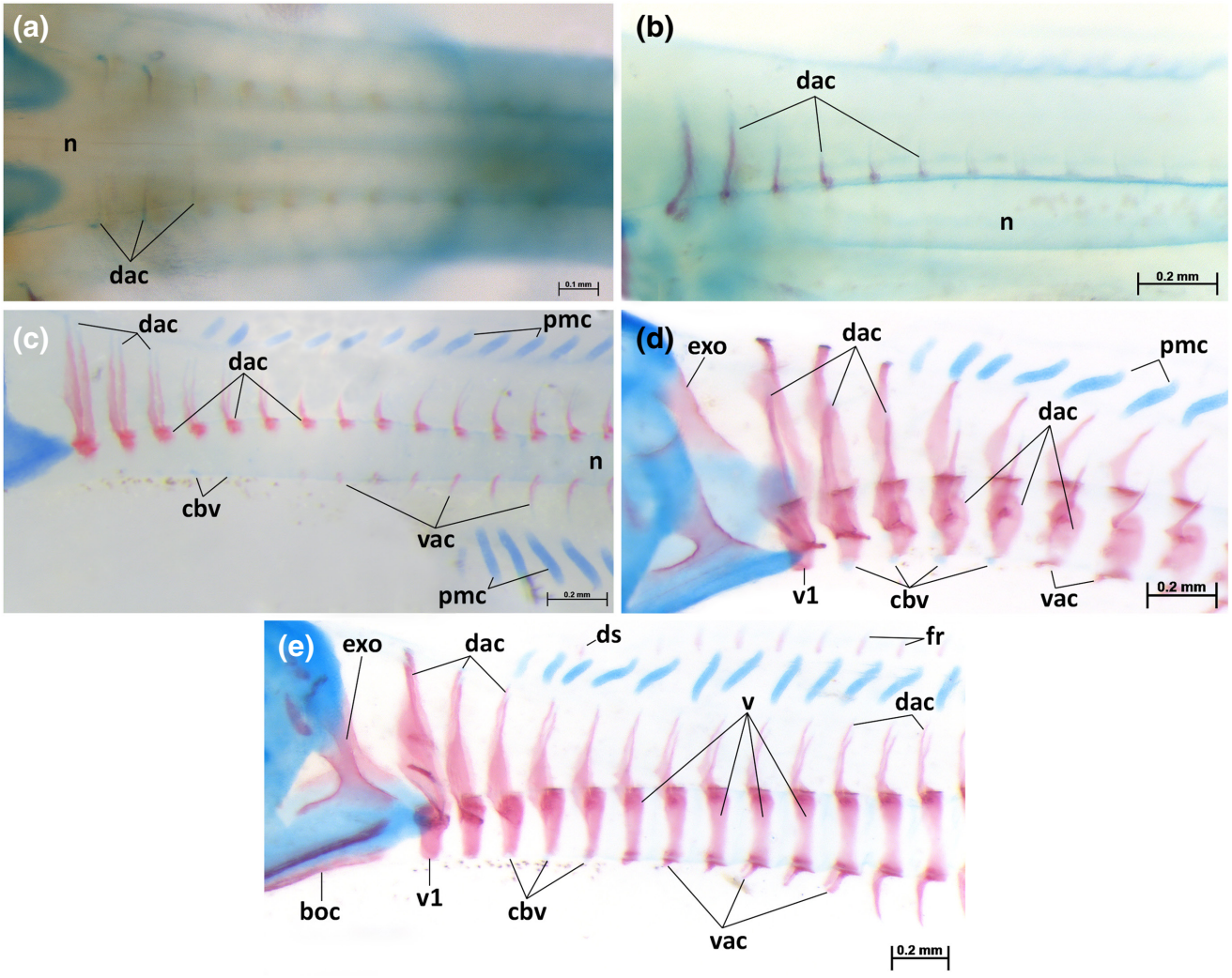

FIGURE 12 Ontogeny of the anterior region of the vertebral column of *Porichthys notatus* in dorsal (a) and lateral (b–d) views. (a) VIMS 40285, 6.0 mm NL. (b) VIMS 40282, 6.2 mm NL. (c) VIMS 40859, 7.4 mm SL. (d) VIMS 40278, 8.2 mm SL. (e) VIMS 40277, 9 mm SL. Abbreviations: boc, basioccipital; cbv, cartilaginous ventral arcocentrum; dac, dorsal arcocentrum; ds, dorsal spine; exo, exoccipital; fr, fin ray; n, notochord; pmc, proximal-middle cartilage; v, vertebral centrum; vac, ventral arcocentrum.

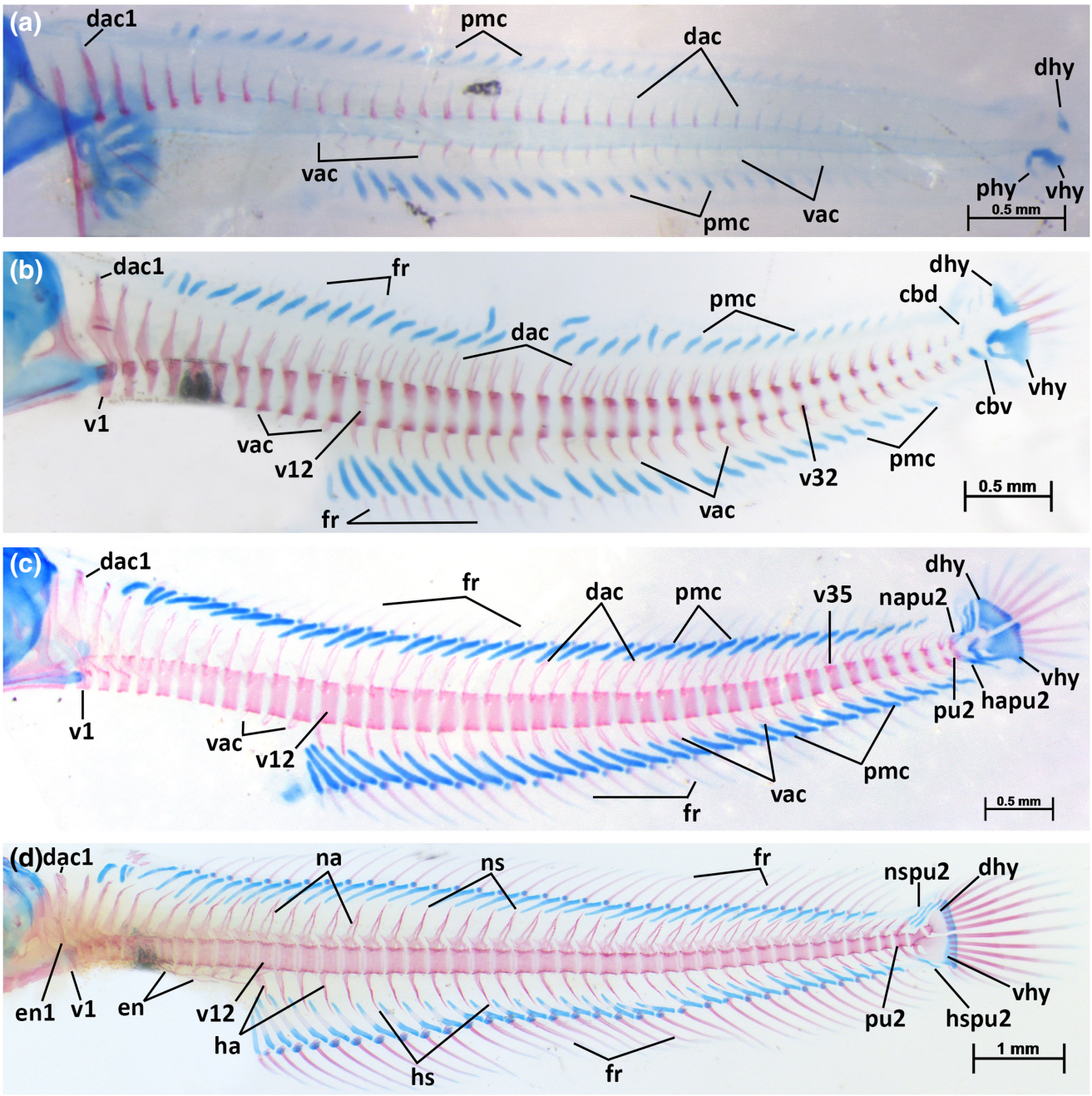

FIGURE 13 Ontogeny of the axial skeleton of *Porichtys notatus* in lateral view. (a) VIMS 40281, 7.8 mm NL. (b) VIMS 40275, 7.9 mm SL. (c) VIMS 40272, 10.9 mm SL. (d) VIMS 40258, 14.3 mm SL. Abbreviations: cbd, cartilaginous dorsal arcocentrum; cbv, cartilaginous ventral arcocentrum; dac, dorsal arcocentrum; dhy, dorsal hypural; en, epineural bone; fr, fin ray; ha, haemal arch; hapu2, haemal arch of pre-ural centrum two; hs, haemal spine; hspu2, haemal spine of pre-ural centrum two; na, neural arch; napu2, neural arch of pre-ural centrum two; ns, neural spine; nspu2, neural spine of pre-ural centrum two; pu2, pre-ural centrum two; phy, parhypural; pmc, proximal-middle cartilage; v, vertebral centrum; vac, ventral arcocentrum; vhy, ventral hypural.

1 and 2 extend to the level of the dorsal tip of the cleithrum. Dorsal arcocentral 3–6 are elongate but smaller than the more anterior dorsal arcocentra: about half (dorsal arcocentra 3, 4) to one-fourth (dorsal arcocentra 5, 6) the length of dorsal arcocentrum 1. The more posterior dorsal arcocentra are small and circular. At 6.4 mm NL, 28 dorsal arcocentra are present. By 7.5 mm SL, a total of 39 dorsal arcocentra are present. The dorsal arcocentra of vertebrae 1–11 of specimen VIMS 40275 (7.9 mm SL) are expanded and triangular but do not form a neural arch. At 9.7 mm SL, the tips of all dorsal arcocentra are expanded dorsal to the spinal cord but none have contacted their antimere to form neural arches. From vertebra 1 to 18, the early stages of dorsal pre-zygapophyses are evident. At 11.8 mm SL, dorsal arcocentra of vertebra 3–9 enclose into neural arches. All vertebrae except the first have complete neural arches and spines by 15.4 mm SL. At this size, antimeres of dorsal arcocentrum of vertebra 1 fuse to a neural arch. The neural arch of v1 is robust, triangular,

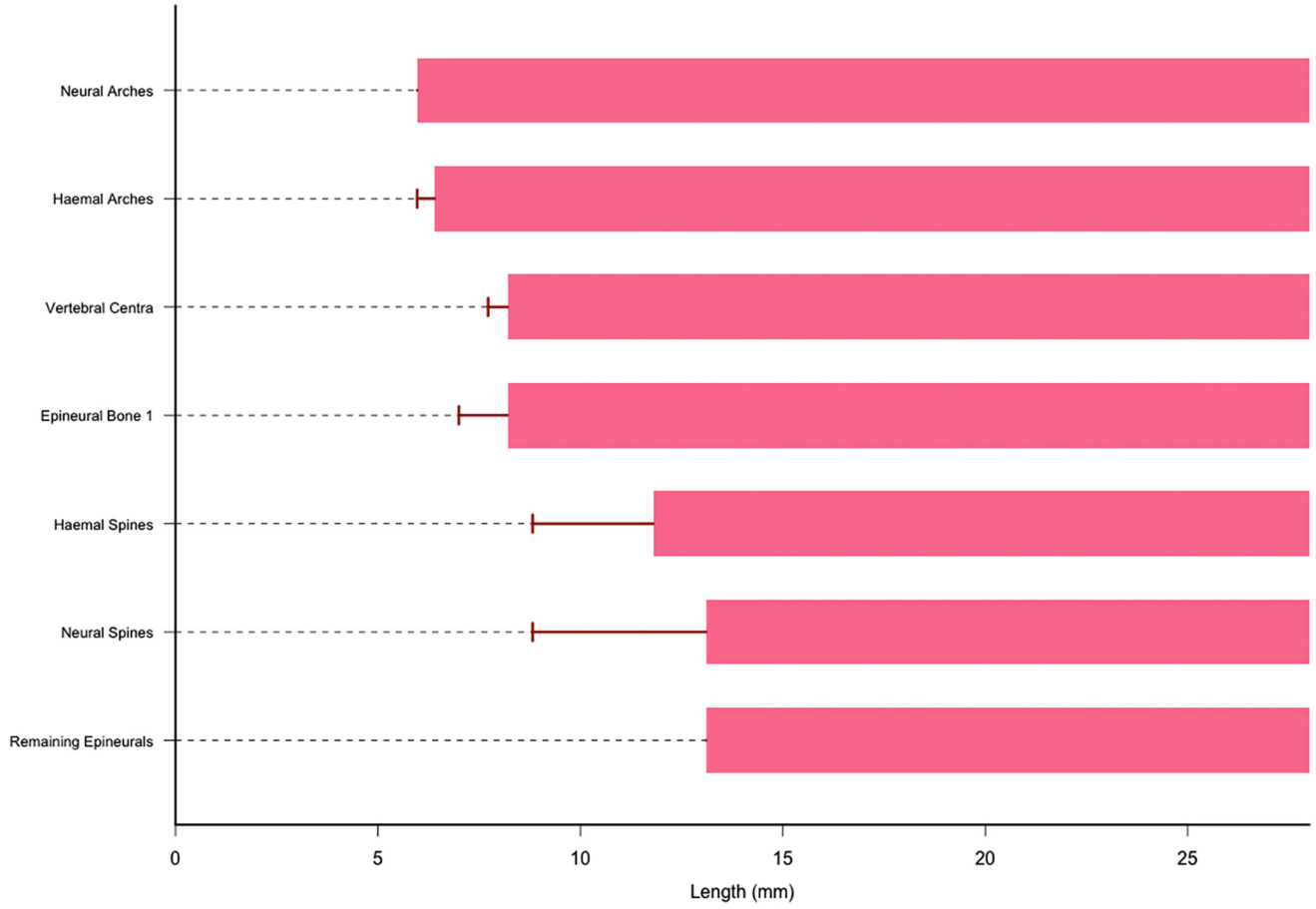

FIGURE 14 Diagram of sequence of development of the vertebral column and intermuscular bones of *Porichthys notatus*. Bars correspond to fixed length. Error bars correspond to the smallest size that a structure was found. Bars in red correspond to bone. Lengths presented in mm NL/SL.

and expanded dorsally, but the neural spine is not observed until 18.6 mm SL. The neural spine of the first vertebra is rectangular with an undulated dorsal margin. At this size, all other posterior vertebrae have neural arches and spines with the adult form: from vertebrae 2–7, the neural arches project anteriorly and bear acute dorsal pre-zygapophyses that extend close to the middle of the preceding vertebra. Posterior to vertebra 7, the neural arches are trapezoidal with short pre-zygapophyses and elongated neural spines.

Haemal arches, spines, and parapophyses

At 6.4 mm NL ventral arcocentra are rod-like bones associated with vertebra 12–23. By 7.5 mm SL, 34 ventral (v6-39) arcocentra are present. VIMS 40278 (8.2 mm SL) has the first ventral arcocentra fused with the dorsal arcocentra, forming a complete centrum. Vertebra 2–5 has cartilaginous basiventrals, contacting the dorsal arcentra (therefore, enclosing the notochord into centra 2–5). Ventral arcocentra from vertebra six to 42 are present.

At 9.7 mm SL, the tips of all 42 ventral arcocentra are extended ventral to the blood vessels, but none have contacted their antimere to form haemal arches. The haemal arches of vertebrae 12 and 13 (first two caudal vertebrae) are the first arches formed at 10.9 mm SL. At 11.8 mm SL, haemal arches with haemal spines are present from vertebrae 17–32. All caudal vertebrae have complete haemal arches and spines by 15.4 mm SL. At 18.6 mm SL, haemal arches are simple (i.e., without zygapophyses), and have simple elongate haemal spines, similar to the condition in larger larvae and juveniles.

Vertebral centra

The earliest traces of ossification surrounding the notochord (i.e., centra) 1–10 are observed at 7.1 mm NL as lateral expansions from the dorsal arcocentra. At this size dorsal arcocentra 1 and 2 start expanding ventrally. At 7.5 mm SL dorsal arcocentra of vertebrae 1–3 are expanded ventrally to almost completely encircle the notochord. The smallest specimen with fully formed centra is 7.7 mm SL, but centra are fixed only at 8.2 mm SL. VIMS 40278 (8.2 mm SL) has the centrum of the first vertebra entirely ossified perichordally. Vertebrae 2–5 of VIMS 40278 already encircle the notochord, although their dorsal arcocentra are expanded to the ventral surface of the notochord, and contact a still distinguishable cartilaginous basiventral (in contrast to the membranous ventral arcocentra observed in more posterior vertebrae; Figure 12d). Vertebrae six and seven have their centrum perichordally ossified, whereas vertebrae 8–10 have both expanded dorsal and ventral arcocentra, but these do not yet contact one another. All vertebrae posterior to v10 have dorsal and ventral

arconcentra in the early stages of formation. Specimen VIMS 40275 (7.9 mm SL) already has fully ossified centra from the vertebrae 1–31. The smallest specimen to have all 42 preural vertebrae with ossified centra is 10.9 mm SL (Figure 13c). From this and larger sizes (including juveniles), the vertebral column comprises 11 abdominal vertebrae, 31 caudal vertebrae, and two ural vertebrae.

Intermuscular bones

The first bone of the intermuscular series to appear is the anteriormost epineural bone, present in a 7 mm SL specimen but fixed only at 8.2 mm SL. Epineural 1 is slender, rod-like that projects posterolaterally from its origin at the level of the neural arch. The origin of epineural 1 first contacts neural arch 1 at 11.8 mm SL. At this size, epineural 1 has doubled its length and becomes thicker relative to the condition at 7.9 mm SL. By 13.1 mm SL, proximal tip of epineural 1 develops an articulatory head that contacts the first neural arch. In frontal view, epineural 1 is bent ventrally and its distal tip is dorsoventrally flattened where it contacts the cleithrum. This is the smallest specimen in which other abdominal epineural bones were also observed. The slender epineurals 4–9 are present in the horizontal septum of the abdominal region and are approximately half the length of epineural 1. At 16.1 mm SL, epineurals 10 and 11 develop. Between 18.6 mm SL and 24.3 mm SL, epineurals 12–15 appear, with more posterior caudal epineurals (16–24) developing at later juvenile sizes.

3.8 | Caudal fin and skeleton

Development of the skeleton of the caudal fin and skeleton of *Porichthys notatus* is described and discussed in Vaz and Hilton (2020); an overview is provided here but the reader is directed to Vaz and Hilton (2020) for details on the ontogeny of this complex. The sequence of ossification of the caudal-fin skeleton occurs in the following order: principal fin rays (fixed length at 7.9 mm SL; minimum observed length at 7 mm SL); compound ural centrum one, ural centrum two, and neural arch of second preural centrum (fixed, 9.7 mm SL; minimum, 8.7 mm SL); dorsal hypural, ventral hypural, procurrent fin rays, and haemal arch of second preural centrum (fixed, 10 mm SL; minimum, 8.7 mm SL); parhypural (fixed, 11.5 mm SL; minimum, 8.7 mm SL); haemal spine of second preural centrum (minimum and fixed at 13.1 mm SL); anterior and posterior epurals (fixed, 13.9 mm SL; minimum, 8.7 mm SL); and neural spine of second preural centrum (fixed, 16.1 mm SL; minimum, 13.9 mm SL) (Figures 15, 16).

The first element of the caudal skeleton to appear is the cartilage of the ventral hypural, fixed at 6.4 mm NL, followed by the dorsal hypural cartilage, fixed at 7.1 mm NL, and the parhypural cartilage, fixed at 7.5 mm SL (although the smallest occurrence of all these cartilages is 6.0 mm NL, VIMS 42847; Figures 15a–c). The parhypural and ventral hypural develop from a single group of cartilage cells. The arch of the parhypural first develops between 6.4–6.8 mm NL, but it is not until 7.3 mm NL-7.9 mm SL that the spine of the parhypural becomes distinct (Figures 15d–f). Two epurals are present in *Porichthys notatus*, with both cartilages first appearing at 7.9 mm SL; its occurrence is fixed by 8.7 mm SL (Figures 15g–i). The ventral arcocentrum of preural centrum two is present between 6.7 mm NL-7.8 mm SL (Figures 15e,f). A cartilaginous haemal spine of preural centrum two is first present at 7.5 mm SL but is fixed only after 8.7 mm SL (Figure 15g–i). The dorsal arcocentrum of preural centrum two is first observed at 7 mm SL, but its occurrence is fixed only at 9 mm SL (Figure 15h). The cartilage of neural spine of preural centrum two first occurs at 8.7 mm SL (Figures 15h,i).

Hypurals and Parhypural

Ossification of the dorsal and ventral hypural is fixed at 10 mm SL (Figures 15j,k), whereas for the parhypural it is fixed at 11.4 mm SL (Figures 15m,n). The smallest occurrence of ossification of these structures, however, all occur at 8.7 mm SL. At 18.6 mm SL, these elements are fully ossified (Figure 15r). Fusion of ventral and dorsal hypurals to their associated ural centra (first and second ural centra, respectively) is first observed by 14.3 mm SL (Figure 15o). The ossifications of the parhypural and ventral hypural fuse by 11.8 mm SL (Figure 15m).

Epurals

Ossification of epurals is first observed at 8.7 mm SL, but fixed only at 13.9 mm SL (Figures 15n–q). Complete ossification of epurals occur at 18.6 mm SL (Figure 15r).

Ural centra

The first and second ural autocentra ossify at 8.7 mm SL (fixed length at 9.7 mm SL; Figure 15i). Ossification of both ural central is complete at 11.9 mm SL (Figures 15m).

Preural centrum two

Ossification of the ventral arcocentrum of preural centrum two is first observed at 8.67 mm SL (and fixed at 10 mm SL; Figure 15i). Ossification of haemal spine of preural centrum two occurs at 13.1 mm SL. Ossification of neural arch of preural centrum two is first observed at 8.7 mm SL (fixed at 9.7 mm SL). Ossification of the cartilage of neural spine of preural centrum two first occurs at 13.9 mm SL, but is only fixed at 16.1 mm SL (Figure 15q).

Caudal-fin rays

The first fin rays to appear are the innermost pair of the principal series that delimit the diastema at 7 mm SL, but their occurrence are fixed at 7.9 mm SL (Figures 15d–f). Ossification of fin rays runs from the diastema to both dorsal and ventral margins. The principal series (I, 6, 6, I) are complete at 10.0 mm SL (Figure 15j–r). At this size, both ventral procurrent fin rays and the second dorsal procurrent ray are present (Figure 15j).

3.9 | Anal fin and support

The sequence of ossification of the anal fin is: anal-fin rays (fixed length at 7.9 mm SL; minimum length observed at 7 mm SL), anal-fin

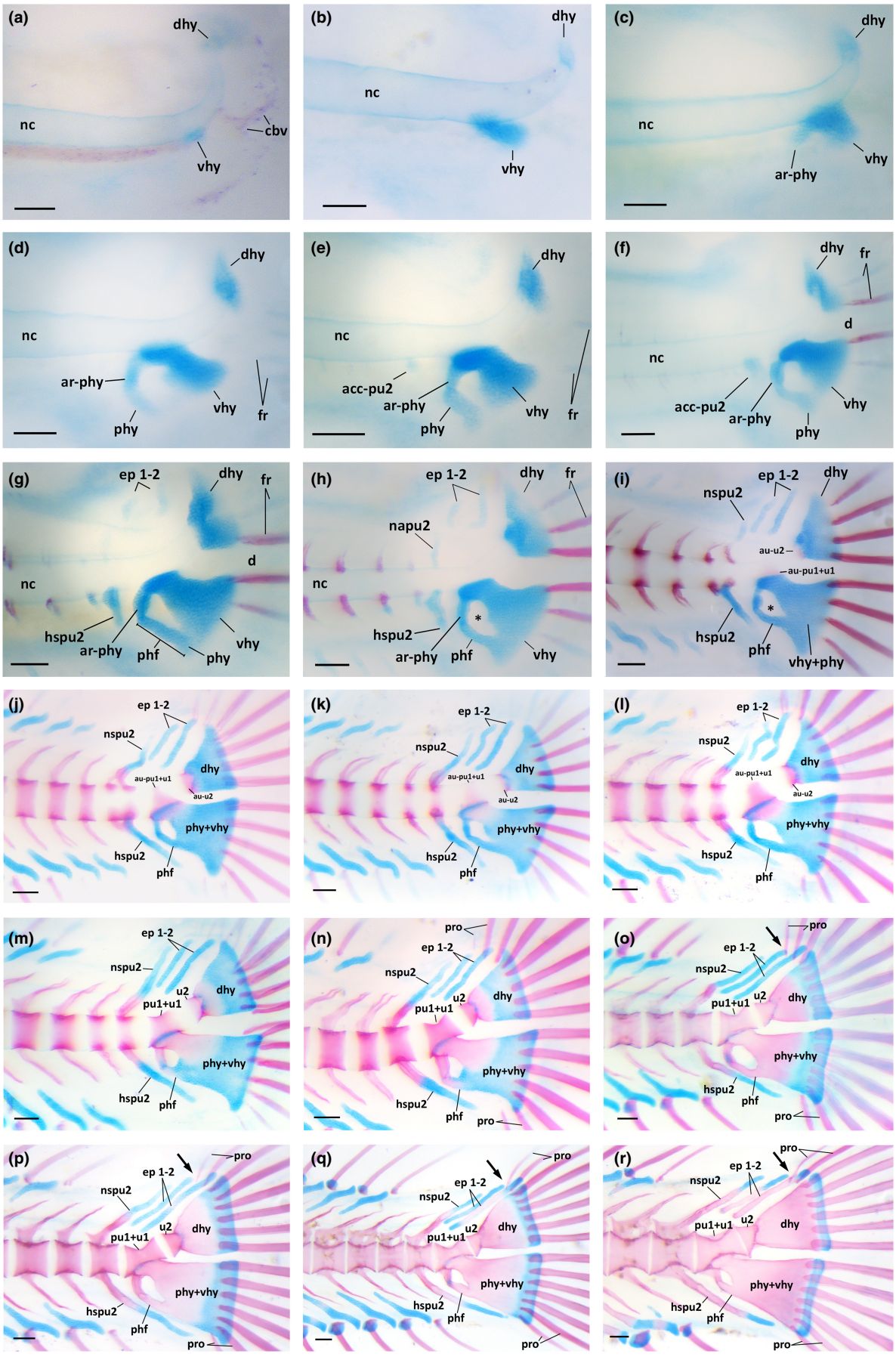

FIGURE 15 Early development of the caudal skeleton of *Porichthys notatus* (modified from Figures 3, 4 of Vaz & Hilton, 2020). (a) VIMS 40257, 6.5 mm NL. (b) VIMS 40274, 6.8 mm NL. (c) VIMS 40283, 7.3 mm NL. (d) VIMS 40281 7.8 mm NL. (e) VIMS 40859, 7.4 mm SL. (f) VIMS 40279, 7.9 mm SL. (g) VIMS 40278, 8.2 mm SL. (h) VIMS 40277, 9.0 mm SL. (i) VIMS 40273, 9.7 mm SL. (j) VIMS 40268, 10.0 mm SL. (k) VIMS 40272, 10.9 mm SL. (l) VIMS 40267, 10.6 mm SL. (m) VIMS 40266, 11.9 mm SL. (n) VIMS 40276, 11.5 mm SL. (o) VIMS 40270, 14.3 mm SL. (p) VIMS 40258, 14.3 mm SL. (q) VIMS 40260, 16.1 mm SL. (r) VIMS 40264, 18.6 mm SL. *foramen from which the caudal vessels exit. Black arrows indicate the support for the anteriormost dorsal procurrent fin ray. Abbreviations: acc, arcocentrum; ar-phy, arch of parhypural; au, autocentrum; cbv, caudal blood vessels; dhy, dorsal hypural; ep, epural; fr, fin rays; hspu, haemal spine of preural vertebra; mr, middle radial; nspu, neural spine of preural vertebra; phf, parhypural flange; phy, parhypural; pro, procurrent caudal-fin ray; pu, preural centrum; vhy, ventral hypural; u, ural centrum. Scale bars: 0.1 mm.

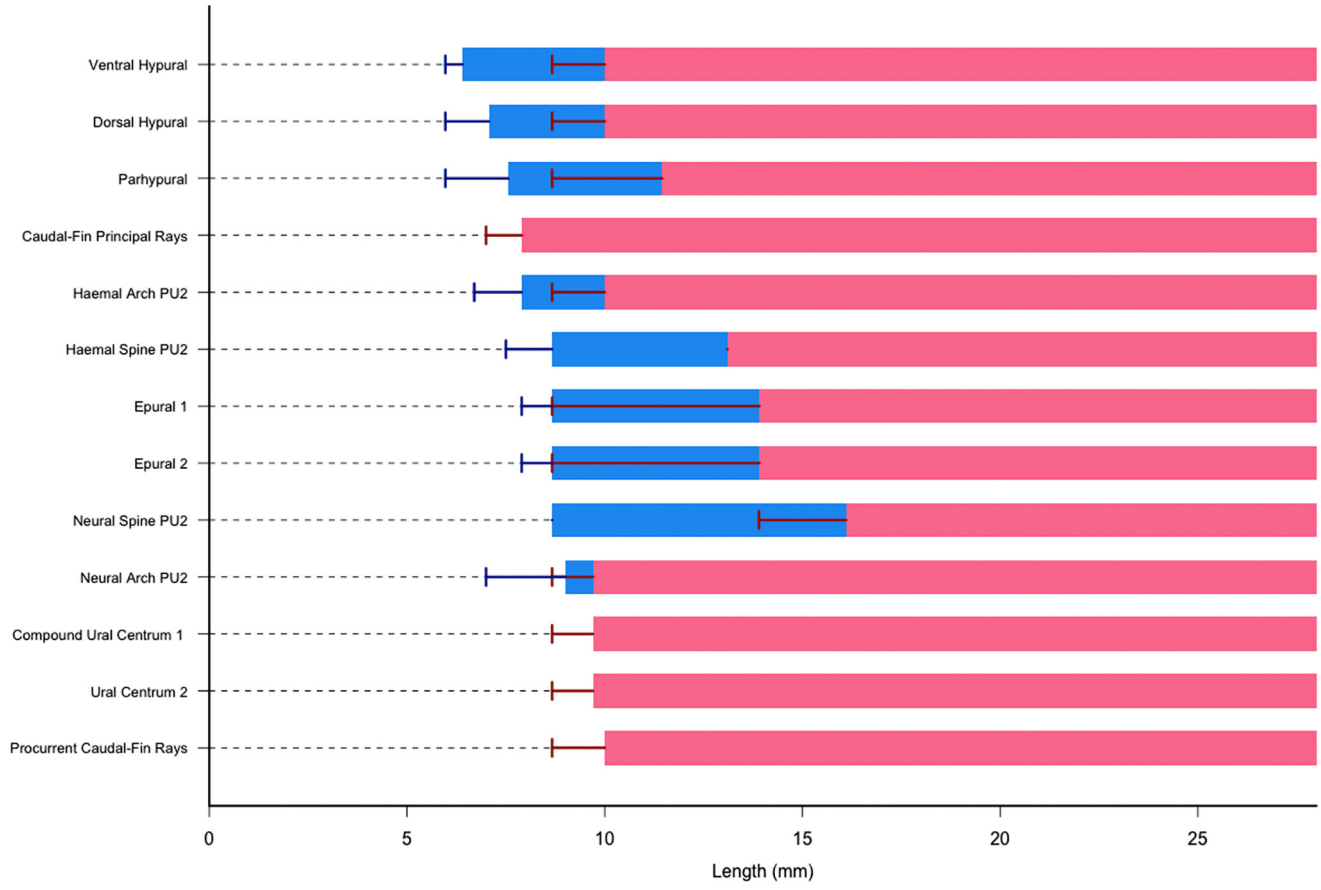

FIGURE 16 Diagram of sequence of development of the caudal skeleton of *Porichthys notatus*. Bars correspond to fixed length. Error bars correspond to the smallest size that a structure was found. Bars in blue correspond to cartilage, red to bone. Lengths presented in mm NL/SL.

proximal radials (minimum and fixed at 11.8 mm SL), and anal-fin middle radial (minimum and fixed at 13.9 mm SL) (Figures 17–19).

Proximal-middle radial cartilages of the anal fin are first seen at 6.0 mm NL and have their occurrence fixed at 6.9 mm NL. A 6.2 mm NL specimen (VIMS 40282) has nine distinct proximal-middle cartilages in the anal fin. At 6.4 mm NL there are 16 anal proximal-middle radial cartilages present. The posteriormost proximal-middle radial cartilages develop by 11.8 mm SL, totaling 32 radials in the anal fin supporting soft fin rays. Distal radial cartilages of the anal fin are first observed in the anterior portion of the caudal regions at 8.7 mm SL but fixed only at 9.7 mm SL. At 11.8 mm SL, the distal radial cartilages are present at the base of all soft fin rays (Figure 17).

Proximal radial

Ossification of the proximal radials occurs at 11.8 mm SL in the first seven anterior pterygiophores of the anal fin (Figure 17a). Ossification of the proximal radials follows a proximal-to-distal direction. By 14.3 mm SL (Figure 17b), ossification is observed in the 24 anterior proximal-middle radial cartilages (with exception of the anteriormost, which remains cartilaginous). By 16.1 mm SL (Figure 17c), all but the two most posterior proximal radials of the anal fin are ossified; all proximal radials of the anal fin are ossified by 18.6 mm SL (Figure 17d). In larger larval specimens and juveniles, the proximal radials of the anal fin are elongated, rectangular, laterally compressed, and slightly wider on the ventral edge.

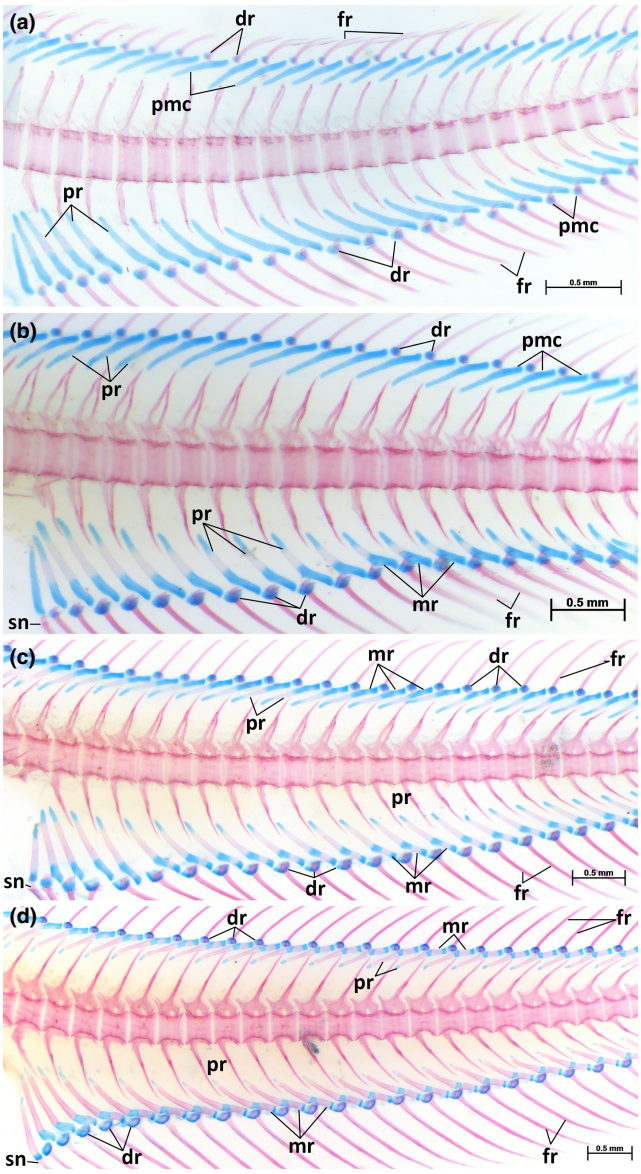

FIGURE 17 Ossification of dorsal and anal fins of *Porichthys notatus* in lateral view. (a) VIMS 40269, 11.8 mm SL. (b) VIMS 40258, 14.3 mm SL. (c) VIMS 40260, 16.1 mm SL. (d) VIMS 40264, 18.6 mm SL. Abbreviations: dr, distal radial cartilage; fr, fin rays; mr, middle radial; pmc, proximal-middle cartilage; pr, proximal radial; sn, supernumerary ray.

Middle radial

First ossification of the middle radial of anal fin occurs at 13.1 mm SL. At 14.3 mm SL, ossification of the middle radial is observed on pterygiophores 11 to 17 (Figure 17b). All but the four most anterior and two most posterior middle anal-fin radials are ossified at 16.1 mm SL. At 18.6 mm SL, the four anterior middle radials remain cartilaginous (Figure 17d). At this size, the middle radials of the anal fin are rectangular and laterally compressed. In juveniles, the middle radial become spool-shaped.

Distal radial

In all larval specimens, distal radials remain rounded and cartilaginous. In juveniles, the center of the anal-fin radials ossify, although their external surfaces are cartilaginous where they contact the bases of the anal-fin rays (Figure 18a).

Anal-fin rays

The first soft fin rays of the anal fin to develop are the five anterior rays (smallest size observed at 7 mm SL; fixed at 7.9 mm SL). In the earliest stages, the hemitrichia are small (less than a third of the length of the associated proximal-middle radial cartilages). All more posterior anal-fin rays are present by 11.8 mm SL (Figure 17a), although the hemitrichia are unsegmented and unbranched and still have actinotrichia exposed at the tip of the most posterior fin rays; the length of these fin rays is similar to that of the proximal-middle radial cartilages. Segmentation and branching of anal-fin rays are first observed at 14.3 mm SL (Figure 17b). At 18.6 mm SL (Figure 17d), all anal-fin rays are segmented and branched, their length are approximately two to three times longer than the length of their supporting pterygiophore.

3.10 | Dorsal fins and supports

The sequence of ossification of the dorsal fin is: dorsal-fin rays (fixed, 8.2 mm SL; minimum, 7.7 mm SL), dorsal-fin spine (minimum and fixed at 8.7 mm SL), dorsal-fin proximal radial (minimum and fixed at 13.1 mm SL), dorsal-fin middle radial (minimum and fixed at 16.1 mm SL) (Figures 17–19).

Proximal-middle radial cartilages of the dorsal fin are first observed at 6.4 mm NL; there are15 cartilages present. The posteriormost proximal-middle radial cartilages develop by 11.8 mm SL, at which size 39 proximal-middle cartilages are present in the dorsal fin (with the three anterior proximal-middle radials supporting spines). Dorsal-fin distal radial cartilages are first observed at 8.7 mm SL and their occurrence is fixed by 9.7 mm SL. In the earliest stages, the distal radial cartilages are present only in the abdominal and anterior portion of the caudal regions. At 11.8 mm SL, the distal radial cartilages are present at the base of all soft fin spines. Distal radials of the dorsal fins remain cartilaginous in larger juveniles.

Proximal radial

Ossification of the proximal part of the dorsal proximal-middle cartilages of both the spinous and soft rays is first seen at 13.1 mm SL in the proximal-middle cartilages of the third dorsal spine to the tenth soft fin ray pterygiophores. At 16.1 mm SL (Figure 17c), all proximal radials start ossifying with the exception of the two most anterior (supporting the first and second dorsal spines) and the four most posterior proximal-middle cartilages. At 18.6 mm SL (Figure 17d), all proximal radials of the second dorsal fin are ossified. The proximal radials are elongated, rectangular, laterally compressed, and slightly wider dorsally, acquiring the conformation observed in juveniles. The proximal-middle radial cartilages that support spines are also all ossified at 18.6 mm SL. The first and second proximal-middle radials that support the spinous fin rays are robust elements and the proximal

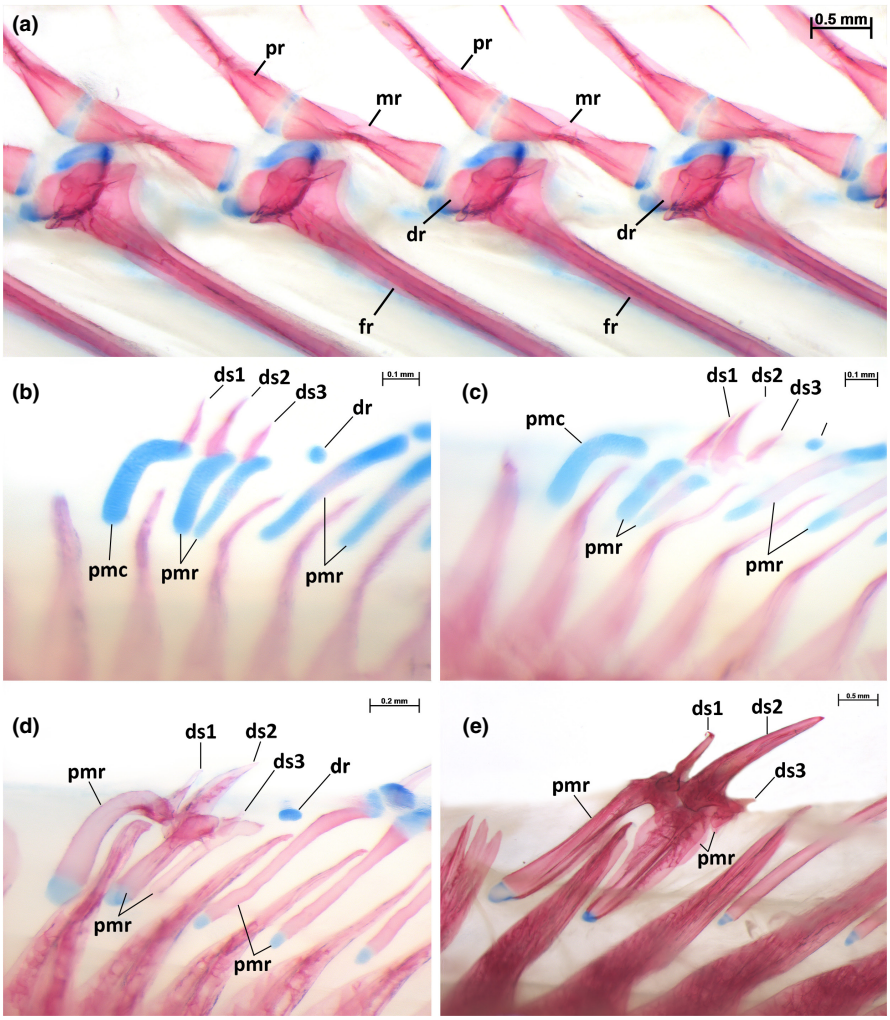

FIGURE 18 Morphology of juvenile anal-fin rays (a) and ontogeny of dorsal-fin spines of *Porichthys notatus* in lateral view (b–e). (a) Anal fin of VIMS 38018 (84.5 mm SL). Note the ossified core in the middle of distal radials. (b) Dorsal pterygiophores and spines of VIMS 40259, 13.1 mm SL. (c) Dorsal pterygiophores and spines of VIMS 40260, 16.1 mm SL. (d) Dorsal pterygiophores and spines of VIMS 42863, 24.5 mm SL. (e) Dorsal pterygiophores and spines of VIMS 38018, 84.5 mm SL. Abbreviations: dr, distal radial; ds, dorsal spine; fr, fin ray; mr, middle radial; pmc, proximal-middle cartilage; pmr, proximal-middle radial; pr, proximal radial.

and middle radials are fully fused (i.e., they are proximal-middle radials). The third proximal-middle radial is also a single elongate bone, although it lacks the cartilaginous tips found in the more anterior proximal-middle radials. At 24.5 mm SL, this proximal-middle radial is still distinct but the third dorsal-fin spine is smaller than a distal radial cartilage. In large juveniles (84.8 mm SL; Figure 18d), the third proximal-middle radial is no longer than the base of the second dorsal-fin spine.

Middle radial

Ossification of middle radials of the second dorsal fin 11–28 is observed at 16.1 mm SL (Figure 17c). By 18.6 mm SL, ossification of the middle radials are observed in all but the four most anterior soft-fin ray pterygiophores and in the two most posterior radials (Figure 17d). At this size, the middle radials are rectangular and laterally compressed. In juveniles, the middle radials acquire a spool shape.

Dorsal-fin rays

The smallest specimen with soft dorsal-fin rays is 7.7 mm SL, but their occurrence is fixed only at 8.7 mm SL. In the earliest stages, hemitrichia are small (length less than one-third that of proximal-middle cartilages) and are associated with proximal-middle cartilages 5–14 (Figure 17A). Soft rays and spines of the dorsal fin develop in both anterior and posterior directions. The posteriormost soft dorsal-fin ray develops at 13.7 mm SL. At this size, most dorsal hemitrichia are still unsegmented and unbranched but are as long or longer than the proximal-middle radial cartilages. At 18.6 mm SL (Figure 17d), all dorsal-fin rays are segmented and branched, their length are approximately two to three times longer than the length of their supporting pterygiophore.

Dorsal-fin spines

Three dorsal-fin spines are present in the earliest sizes of development of *Porichthys notatus* studied (Figure 18b). The third dorsal-fin

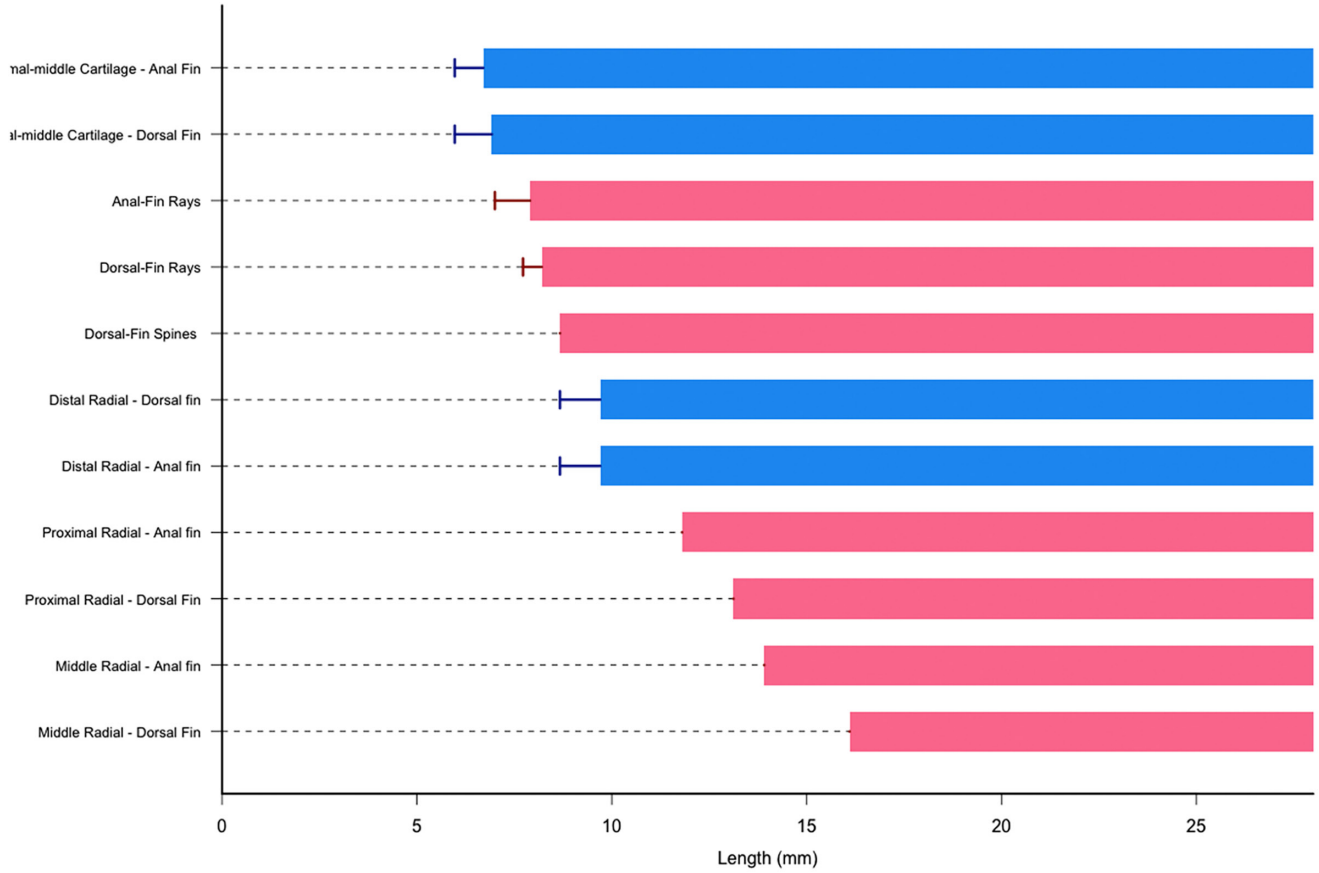

FIGURE 19 Diagram of sequence of development of dorsal and anal fins of *Porichthys notatus*. Bars correspond to fixed length. Error bars correspond to the smallest size that a structure was found. Bars in blue correspond to cartilage, red to bone. Lengths presented in mm NL/SL.

spine to is the first to develop (at 8.7 mm SL), with the second appearing at 9.7 mm SL and the first at 10.9 mm SL. At 11.8 mm SL, the left and right halves of the first and second dorsal spines are not yet fused; all spines are fully fused at 13.1 mm SL. By 16.1 mm SL, it is apparent that the growth of the third dorsal-fin spine is interrupted, in that it is only about half of the size of dorsal spines one and two and is not protruding externally; the more anterior spines are visible externally (Figure 18c–e).

3.11 | Pectoral girdle

The sequence of ossification of the pectoral girdle is as follows: cleithrum (minimum and fixed length at 5.4 mm SL), supracleithrum, and postcleithrum (fixed length at 6.2 mm SL; minimum length observed at 6.0 mm NL), posttemporal (fixed, 7.4 mm SL, minimum, 6.0 mm NL), pectoral-fin rays (fixed, 7.9 mm SL; minimum 6.0 mm NL), pectoral-fin spine (fixed, 7.9 mm SL; minimum, 7 mm SL), pectoral-fin radials (minimum and fixed at 10.9 mm SL), propterygium (minimum and fixed at 11.8 mm SL), coracoid (minimum and fixed at 13.1 mm SL), and scapula (fixed, 18.6 mm SL; minimum, 13.9 mm SL) (Figures 20, 21).

The scapulocoracoid cartilage is rectangular and the scapular fenestra is present at its first appearance (6.0 mm NL). At 6.2 mm NL (Figure 20a), the coracoid process is distinct and projects anteroventrally from the main body of the scapulocoracoid cartilage. The anteroventral portion of the scapulocoracoid cartilage attaches to the cleithrum at 7.1 mm NL (Figure 20b).

At 6.0 mm NL, two cartilaginous elements inside the pectoral-fin bud articulate with the scapulocoracoid cartilage: a large pectoral radial plate, which is as long as the scapulocoracoid cartilage, and a smaller cartilaginous propterygium (Figure 20a). The pectoral radial plate is partially divided into four elements (i.e., the four ventral pectoral radials). Between 6.4 and 7.3 mm NL, a group of chondrocytes is observed posterior to the propterygium (Figure 20b). In specimens larger than 7.4 mm SL they are found consistently fused to the propterygium (e.g., VIMS 40858, 6.7 mm NL these chondrocytes are fused to the propterygium, while others of similar sizes do not). The resulting large pad-like propterygium is of similar shape to the ventralmost pectoral radial (Figure 20c). The other pectoral radials are simple bars of cartilage and the shapes of these elements (propterygium and radials) reflect those of adults. VIMS 40262 (7.1 mm NL) and VIMS 40283 (7.3 mm NL) have the propterygium not contacting the pectoral radial plate, although in larger specimens (e.g., VIMS 40859, 7.4 mm SL; VIMS 40284, 7.5 mm SL) the dorsalmost pectoral radial contacts the propterygium. From 7.4 to 11.5 mm SL, the propterygium and pectoral radials are all connected distally.

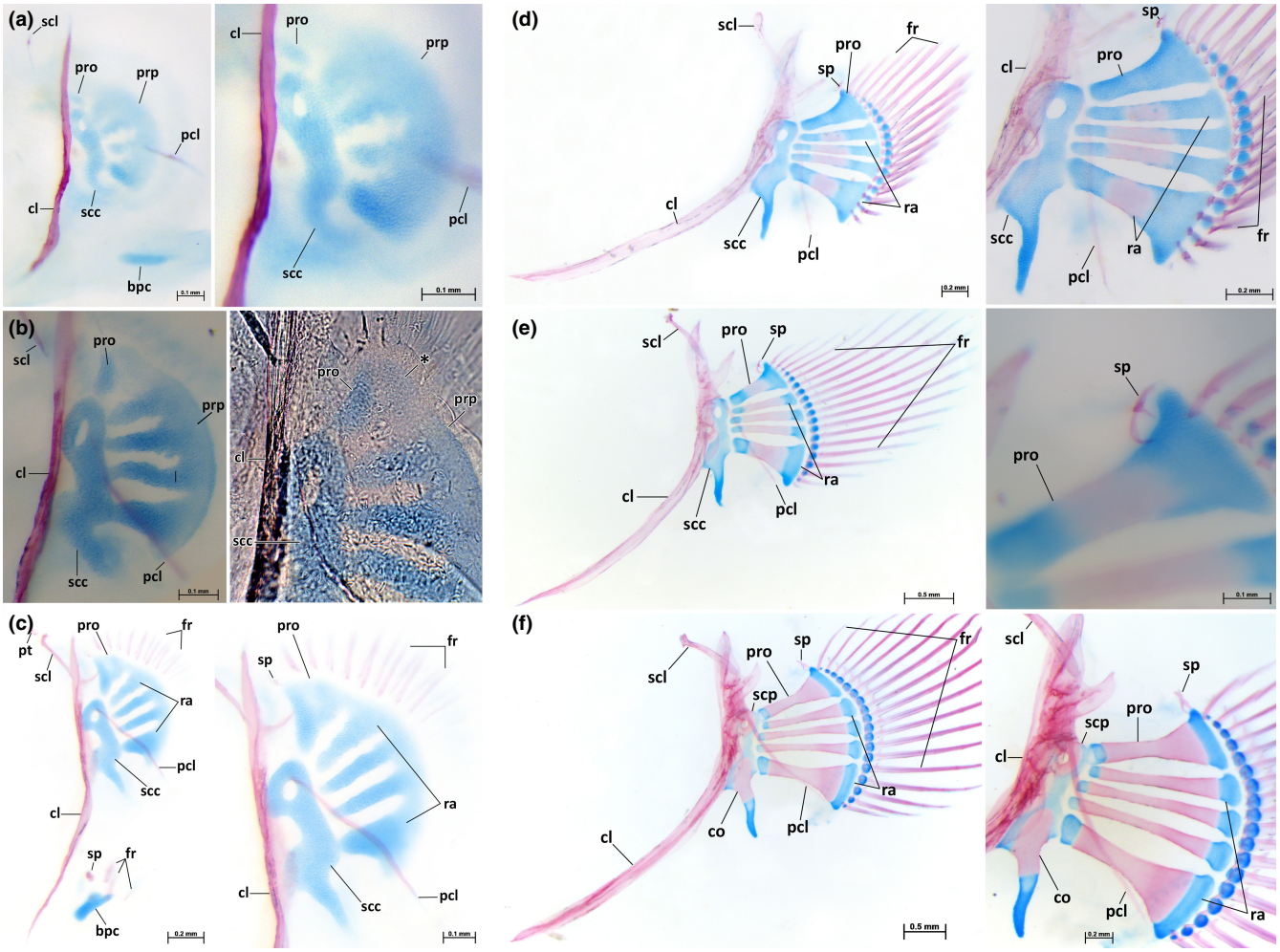

FIGURE 20 Ontogeny of the pectoral fin of *Porichthys notatus* in lateral view and higher magnification of the pectoral radials (a, c, d, f). In (b), close-up image from a stereomicroscope (left) and higher magnification (100×) in a compound microscope (right) highlighting the margins of the propterygium and the pectoral radial plate. Note the absence of cells between the pectoral radial plate and the propterygium. Asterisk indicates the group of cells that later fuse to the propterygium. In (e), the high-magnified picture shows details of the pectoral fin spine showing complete fusion and lack of segmentation. (a) VIMS 40282, 6.2 mm NL. (b) VIMS 40262, 7.1 mm NL. (c) VIMS 40284, 7.5 mm SL. (d) VIMS 40269, 11.8 mm SL. (e) VIMS 40258, 14.3 mm SL. (f) VIMS 40264, 18.6 mm SL. Abbreviations: bpc, basipterygial cartilage; cl, cleithrum; co, coracoid; fr, fin ray; pcl, postcleithrum; pro, propterygium; prp, pectoral radial plate; ra, pectoral radial; scc, scapulocoracoid cartilage; scl, supracleithrum; scp, scapula; sp, spine.

Cleithrum

At the smallest size examined (5.4 mm NL) the cleithrum is present as a slender rod of bone, extending from the base of the occipital region of the neurocranium to the ventral margin of the abdominal cavity (Figure 20a). At 7.1 mm NL, the cleithrum is slightly expanded laterally (Figure 20b), and by 7.9 mm SL its ventral tip is projected anteriorly (Figures 20d,e). By 16.1 mm SL, the cleithrum attains its adult form (Figure 20f). The posterodorsal process of the cleithrum first appears at 7.5 mm SL (Figure 20c) as a slender process. It gradually widens until achieving a trapezoidal shape at 16.1 mm SL, which is similar to its form in adults (Figure 20f).

Supracleithrum

The smallest specimen with a supracleithrum is 6.0 mm NL and it is fixed at 6.2 mm NL. In its earliest stages, the supracleithrum is a slender bone that is less than 25% the width of the cleithrum (Figure 20a). It projects dorsally at 7.1 mm NL (Figure 20b), forming a rounded process that articulates with the posttemporal by 8.2 mm SL (Figure 20c). Between 11.8 mm SL and 16.1 mm SL, the posterior region of the supracleithrum becomes thicker and assumes its adult shape (Figures 20d–f).

Postcleithrum

The postcleithrum is a slender rod-like bone, first appearing at 6.0 mm NL; its occurrence is fixed at 6.2 mm NL (Figure 20). The postcleithrum does not reach juvenile proportions until 24.3 mm SL.

Posttemporal

The fixed occurrence of the posttemporal bone is at 7.5 mm SL (Figure 20c), although specimen VIMS 42847 (6.0 mm NL) has a

distinct posttemporal in its earliest stages. The posttemporal first appears as a small, slender bone positioned close to (but not in contact with) the posterodorsal region of the auditory capsule of the neurocranium. By 9 mm SL, the posterior portion of the posttemporal is thick and cylindrical in shape, foreshadowing the articulatory condyle for its contact with the supracleithum. The posterior process of the posttemporal is first observed at 13.1 mm SL. Despite its close association with the otic region, the dorsal limb of the posttemporal becomes ankylosed with the epioccipital only in larger sizes, this fusion being first observed in this series at 24.3 mm SL. At this size, the posterior process of the posttemporal projects anterolaterally and is in loose contact with the pterotic, as seen in juveniles and adults. The ventral limb of the posttemporal is reduced to a small knob in large juveniles and adults.

Scapula

The scapula is first observed at 13.9 mm SL but its occurrence is fixed only at 18.6 mm SL (Figure 20f). The scapula is mostly rectangular with a convex posterior margin in all larvae, similar to the shape the observed in juveniles. The scapula is pierced by the scapular fenestra (Figure 20f).

Coracoid

The first indication of ossification of the coracoid is at 13.1 mm SL. The coracoid has a trapezoidal outline and its ventral margin bears an anteroventrally directed process. Ossification of this process is incomplete even in adults; the tip of the coracoid process remains cartilaginous (Figure 20f).

Propterygium and pectoral radials

Complete separation among all pectoral radials and the propterygium first occurs at 11.8 mm SL (Figure 20d). Ossification of pectoral radials starts in the middle of the cartilage at 10.9 mm SL and progresses both anteriorly and posteriorly. The propterygium ossifies in a similar manner, but ossification is first observed at 11.8 mm SL. In larger larvae and juveniles, the propterygium is a large pad-shaped bone, having its base articulating with the posterodorsal edge of the scapula. The posterior margin of the propterygium supports five pectoral-fin rays and its posterodorsal edge articulates with the pectoral-fin spine (Figure 20f). In larger larvae and juveniles, the three dorsal pectoral radials are rod-shaped bones with their bases positioned between the ventral edge of the scapula and dorsal edge of the coracoid. Each pectoral radial supports two pectoral fin rays. The ventralmost pectoral radial is pad-shaped, similar to the propterygium, and has its base articulating with the posterior edge of the coracoid. The posterior margin of the ventralmost pectoral radial supports five fin rays (Figure 20f).

Pectoral-fin rays

The pectoral-fin rays are first found in a 6.0 mm NL specimen, but the ossification of the rays is not fixed until 7.4 mm SL. The first rays to appear are located at the dorsal margin of the propterygium (Figure 20c). The other fin rays develop in a ventral direction gradually at later sizes. By 18.6 mm SL, there are 18 pectoral-fin rays present; 21 fin rays are present in juveniles. Segmentation of the fin rays is first observed at 11.8 mm SL. Between 11.8 and 16.1 mm SL, the pectoral-fin rays develop a triangular dorsal projection on the base of the medial hemitrichium; this projection contacts the adjacent hemitrichium. Distal radial cartilages are first observed at 7.9 mm SL at the tips of the two dorsal pectoral radials. The series of distal radials gradually develops both dorsally and ventrally. A small, unsegmented pectoral-fin ray element that we interpret as a pectoral-fin spine articulates with the posterodorsal edge of the propterygium and projects dorsally (Figure 20d–f). Fusion of the halves of the pectoral-fin spine occurs after 10.9 mm SL.

3.12 | Pelvic girdle and fin

The sequence of ossification of the pelvic fin is: pelvic-fin rays (fixed length at 7.1 mm NL; minimum length observed at 6.0 mm NL), pelvic-fin spine (fixed, 7.9 mm SL; minimum 6.0 mm NL), and basipterygium (fixed, 11.4 mm SL; minimum, 8.7 mm SL) (Figures 21, 22).

Pelvic buds are present in the smallest sizes after hatching (>5.4 mm NL), and are positioned in the posterior end of the abdominal cavity. The cartilaginous basipterygium is first observed at 6.0 mm NL as an elongated element in the ventral region of the body cavity at the level of the distal tips of the pectoral-fin radials. By 6.8 mm NL, the basipterygium cartilage is more anteriorly positioned at the level of the scapulocoracoid cartilage. The basipterygium cartilage is ventral to the cleithrum by 7.4 mm SL, at which size its posterior region is wide and bears a deep indentation in its posterior margin. By 10.9 mm SL (Figure 22a), the anterior margin of the basipterygium cartilage contacts the medial surface of the anteroventral region of the cleithrum. The anterior portion of the basipterygium cartilage is elongate and rectangular; the posterior region is about twice as wide as the anterior portion.

Basipterygium

Endochondral ossification of the basipterygium cartilage is first observed at 8.7 mm SL, but it is fixed only at 11.4 mm SL and is mostly restricted to its posterior region (Figure 22b). At this size, the posterior region of the lateral margin of the basipterygium is projected anterolaterally. A flange formed by membrane bone is developed posteriorly along the medial margin. By 14.3 mm SL (Figure 22c) ossification of the basipterygium reaches its anterior region as well as the lateral process, which becomes angular and completely ossified by 16.1 mm SL. The membranous medial flange extends to the middle of the basipterygium in a semi-elliptical shape by 14.3 mm SL; it acquires a trapezoidal shape by 18.6 mm SL (Figure 22d).

Pelvic-fin rays and spine

The pelvic fin comprises one spine and two fin rays. Fin rays and the pelvic-fin spine are first seen at 6.0 mm NL, but their

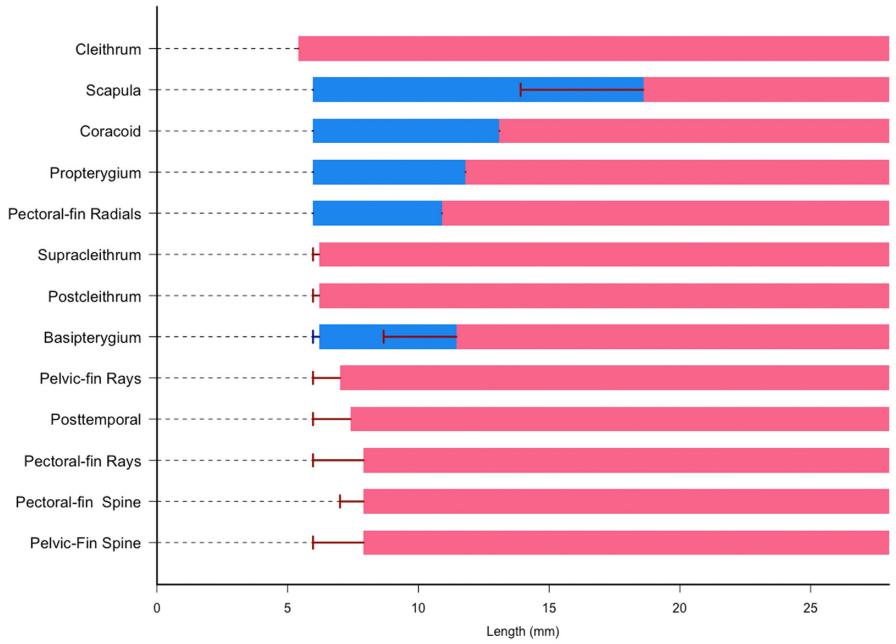

FIGURE 21 Diagram of sequence of development of pectoral and pelvic fins of *Porichthys notatus*. Bars correspond to fixed length. Error bars correspond to the smallest size that a structure was found. Bars in blue correspond to cartilage, red to bone. Lengths presented in mm NL/SL.

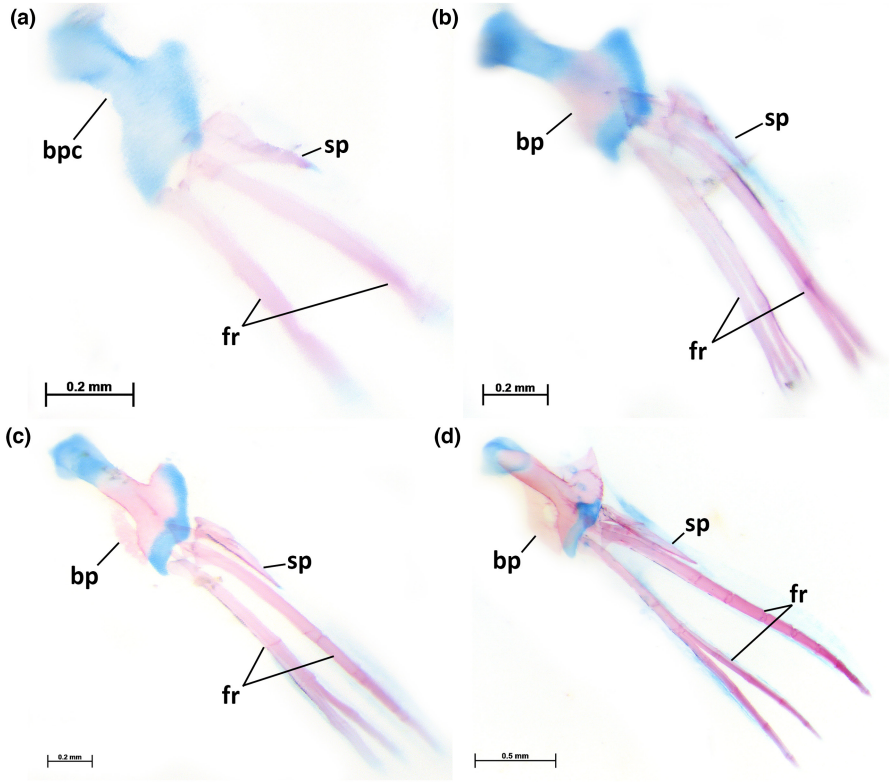

FIGURE 22 Ontogeny of the pelvic fin of *Porichthys notatus* in ventral view. (a) VIMS 40272, 10.9 mm SL. (b) VIMS 40269, 11.8 mm SL. (c) VIMS 40258, 14.3 mm SL. (d) VIMS 40264, 18.6 mm SL. Abbreviations: bp, basipterygium; bpc, basipterygial cartilage; fr, fin ray; sp, spine.

occurrences are fixed at 7 mm SL (rays) and 7.9 mm SL (spine). By 10.9 mm SL, the length of the pelvic-fin rays is twice that of the spine (Figure 22a). By 11.8 mm SL, the pelvic-fin rays become segmented (Figure 22b). From this size through the juvenile stages, the pelvic-fin rays are three to four times longer than the pelvic-fin spine (Figure 22c,d).

4 | DISCUSSION

The description of the early skeletal development confirms that *Porichthys notatus* lacks the mesethmoid and parietal bones in all stages of ontogeny. The mesethmoid and parietal are not found in any other species of Batrachoidiformes examined to date. Assuming *Porichthys notatus* as an exemplar of the order, this study offers additional support for the absence of these bones as synapomorphies of Batrachoidiformes (Wiley & Johnson, 2010).

This dataset demonstrated that *Porichthys notatus* lacks the intercalar throughout its ontogeny. The intercalar is present in most species of Halophryninae (except *Halobatrachus and Colletteichthys*). All representatives of Batrachoidinae, Porichthyinae, and Thalassophryninae observed to date lack an intercalar. Preliminary analysis suggests that the absence of the intercalar is a potential synapomorphy grouping these three subfamilies, being lost homoplastically in *Halobatrachus* and *Colletteichthys* (Vaz, 2020).

The coronomeckelian is not present in any larval, juvenile, or adult specimen of *Porichthys notatus*. This bone is also absent in all other species of Porichthyinae, Batrachoidinae, Thalassophryninae, and the halophryine genera *Allenbatrachus*, *Batrachomeus*, *Halophryne*, and *Bifax*. The coronomeckelian, however, is present in the halophrynine genera *Triathalassothia*, *Riekertia*, *Perulibatrachus*, *Chatrabus*, *Barchatus*, *Halobatrachus*, *Colletteichthys*, and *Batrichthys*. A preliminary phylogenetic analysis suggests that the absence of this bone is a synapomorphy grouping Batrachoidinae, Thalassophryninae, Porichthyinae, *Allenbatrachus*, *Batrachomoeus*, and *Halophryne*, with a homoplastic loss in *Bifax* (Vaz, 2020).

The description of the early skeletal development of *Porichthys notatus* presented herein confirms that basibranchial two is absent through ontogeny. This bone was also not found in any of the other species of Porichthyinae. The occurrence of basibranchial two is highly variable across Batrachoidiformes. The second basibranchial is completely absent in the genera *Potamobatrachus* (Batrachoidinae), *Daector* (Thalassophryninae), *Batrichthys*, *Chatrabus*, *Colletteichthys*, *Halophryne*, and *Perulibatrachus* (Halophryninae) (Figure 23). In the genus *Batrachoides* (Batrachoidinae), the presence of basibranchial two varies intrageneric ally, being present in *Batrachoides liberiensis* and *B. goldmani*, but completely absent in *B. pacifici*, *B. gilberti*, *B. waltersi*, *B. surinamensis*, *B. manglae*, and *B. boulengeri*. Most species that lack the second basibranchial bone still have the *copula communis* cartilage present. In species of *Halophryne*, the *copula communis* is reduced to two small cartilaginous elements: an elongated cartilage ventral to basibranchial one and a small circular element that is ventral to the posterior copula cartilage (Figure 23d).

4.1 | Developmental comparisons to other percomorphs and teleostean fishes

There is a broad range of data available related to the early development of the skeleton of fishes, many of which have been fundamental to hypotheses of homology for various structures within Actinopterygii (e.g., Arratia & Schultze, 1990, 1991, 1992; Johnson & Britz, 2005). Several of these studies are focused on particular anatomical regions, such as skull (de Beer, 1937), jaws, and hyopalatine arch (e.g., Arratia, 1990, Siluriformes; Arratia & Schultze, 1991, basal Actinopterygii; Konstantinidis & Johnson, 2012b, Tetraodontiformes), caudal skeleton (Britz & Johnson, 2005; Johnson & Britz, 2005; Konstantinidis & Johnson, 2012a). The series of papers by Potthoff (1974, 1975, 1980; Potthoff and Kelly, 1982; Potthoff & Tellock, 1993; Potthoff et al., 1980, 1984, 1988) is a rich source of information for development of the axial skeleton, appendicular, and gill arches for several scombrids and some other acanthomorphs (e.g., Centropomidae, Haemulidae). Detailed descriptions of sequences of ossification of the entire skeleton, however, are available for very few species of Teleostei; including five ostariophysians (*Danio rerio*: Cubbage and Mabee, 2003; Bird & Mabee, 2003; *Salminus brasiliensis*: Mattox et al., 2014; *Moenkhausia pittieri*: Marinho, 2022; *Ictalurus punctatus* and *Notorus gyrinus*: Kubicek, 2022), and two acanthomorphs: *Sciaenops ocellatus* and *Cynoscion nebulosus* (Sciaenidae; Kubicek & Conway, 2016). The complete sequence of ossification of *Porichthys notatus* is summarized in Figure 24. The following comparisons were made based on available ontogenetic data from fishes that are not necessarily closely related to Batrachoidiformes. More detailed comparisons on the sequence of ossification are made with representatives of Sciaenidae (from Kubicek & Conway, 2016) because this family is within Percomorphacea, as is Batrachoidiformes (sensu Betancur-R et al., 2017).

The embryonic cartilaginous neurocranium of *Porichthys notatus* has only the posterior portion of the cartilage *taenia marginalis*, which is a triangular element at the posterodorsal edge of the orbital region, and lacks entirely the epiphyseal bar (Figures 3c–e). Conversely, *Sciaenops ocellatus* has the *taenia marginalis* extending throughout the dorsal margin of the optic region (i.e., both the anterior and posterior *taenia marginalis* are present) and the epiphyseal bar extends transversely over the anterodorsal region of the head. The condition observed in *Sciaenops* is similar to that in other percomorphs, such as *Dentex* (Scaridae; Koumondorous et al., 2000) and *Morone* (Moronidae; Fritzsche & Johnson, 1980), as well in other more basal teleosts, such as *Salminus brasiliensis* (Characiformes; Mattox et al., 2014), *Danio rerio* (Cypriniformes; Cubbage & Mabee, 1996), *Puntius semifasciatus* (Cypriniformes; Block & Mabee, 2012), *Paedocypris* (Cypriniformes; Britz & Conway, 2009), and *Danionella* (Cypriniformes; Britz & Conway, 2016).

The sequence of ossification of the neurocranium of *Porichthys notatus* and *Sciaenops ocellatus* is different in several ways. In *P. notatus*, the basioccipital develops after the exoccipital, with the frontal developing after both of these bones. In *S. ocellatus*, these three bones appear at the same time. In *P. notatus*, the autosphenotic and the epioccipital develop before the pterotic. The vomer is the first bone of the neurocranium to ossify after the pterotic and is followed by the basisphenoid, prootic, and supraoccipital. In *Sciaenops ocellatus*, the prootic develops after the frontal, followed by supraoccipital,

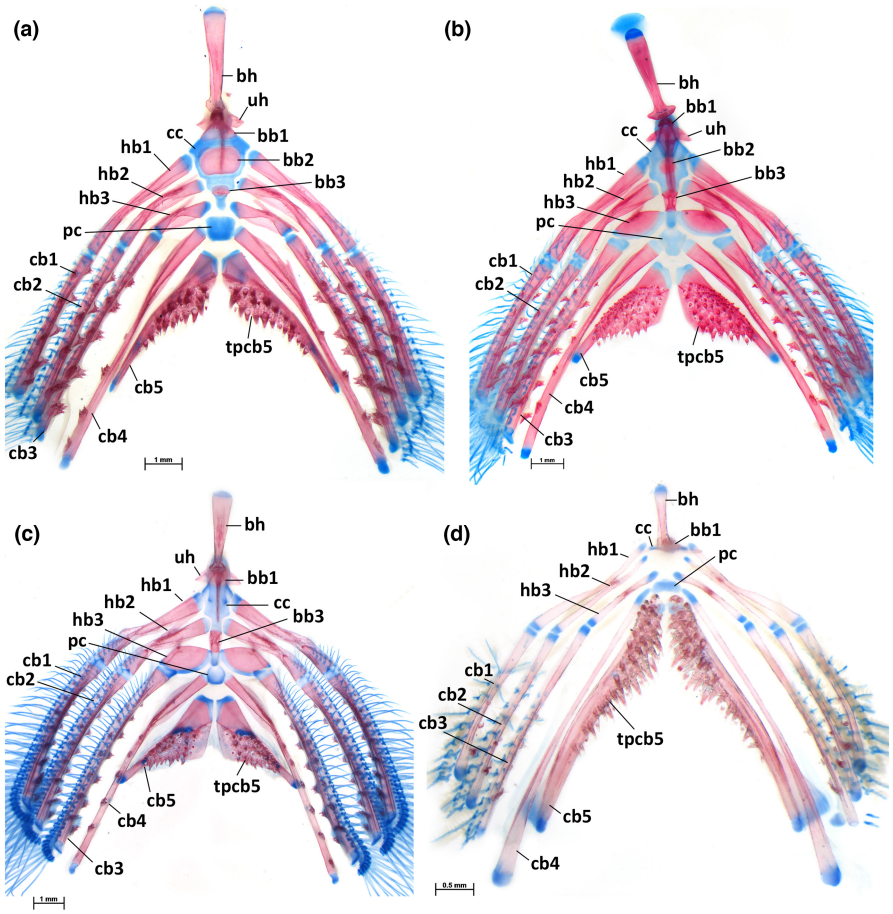

FIGURE 23 Comparative morphology of ventral gill arches in Batrachoidiformes. (a) *Allenbatrachus reticulatus*, USNM 333283 (45.8 mm SL). (b) *Opsanus tau*, VIMS 34472 (52.1 mm SL). (c) *Batrachoides waltersi*, USNM 367548 (60.2 mm SL). (d) *Halophryne diemensis*, AMI 23930–1 (24 mm SL). Abbreviations: bb, basibranchial; bh, basihyal; cb, ceratobranchial bone; cc, copula communis; hb, hypobranchial bone; hbc, hypobranchial cartilage; pc, posterior copula; tp, tooth plate; uh, urohyal.

vomer, pterotic (these three at same size), followed by the epioccipital, then later the autosphenotic. The pterosphenoid is the last bone of the neurocranium to ossify in *P. notatus*, whereas in *S. ocellatus* the last bone to appear is the basisphenoid.

Within the suspensorium, jaws, and opercular series, the opercle is the first bone to form in *Porichthys notatus*, followed by the subopercle, and then the interopercle, which appears at the same time of the dentary. After these elements, the angular, maxilla, and the preopercle appear. In *Sciaenops*, the maxilla is the first bone to develop, followed by the dentary, opercle, and premaxilla. Following the ossification of the preopercle, the sequence of ossification in *P. notatus* is premaxilla, articular, retroarticular, hyomandibular, symplectic, and the quadrate. In contrast, in *S. ocellatus* the bones that ossify before the preopercle are the anguloarticular, symplectic, endopterygoid, quadrate, and subopercle; after the preopercle is present, the subopercle, hyomandibula, retroarticular, and ectopterygoid appear. It is notable that in *P. notatus* the endopterygoid is one of the last bones to ossify in the entire skeleton, while in *S. ocellatus* it develops relatively early.

Because of the phylogenetic distance between *Porichthys* and *Sciaenops*, as well as the complexity of the variation involved in the sequence of ossification, these differences are difficult to interpret, particularly having multiple bones of the skull being coopted to multiple functions (e.g., oral jaws acting in both breathing and feeding). However, it is possible to make a few generalizations from the developmental data for *P. notatus* presented above compared to that of *S. ocellatus* and other teleosts.

In *Porichthys notatus* bones that are closely associated with breathing (e.g., opercular series and branchiostegals) ossify at smaller sizes (i.e., earlier stages) than those that are exclusively associated with feeding (e.g., tooth plates and tooth patches of the pharyngeal jaws; Figure 24); the pharyngeal tooth plates are the last elements to develop among elements of the visceral arches in *P. notatus*. This is possibly related to endogenous feeding through absorption of the yolk during the larval development of *P. notatus* (Arora, 1948; this study). This is in contrast to *S. ocellatus*, a species that begins exogenous feeding in their earliest stages (FAO, 2022); in *S. ocellatus* tooth plates and ceratobranchials among the earliest elements to ossify (Kubicek & Conway, 2016). A similar overall sequence pattern is observed in other Teleostei, such as *Danio rerio* and *Salminus brasiliensis*, especially in the latter in which the tooth plates of pharyngobranchial 4 and ceratobranchial 5 are the first elements to ossify (Cubbage & Mabee, 1996; Mattox et al., 2014).

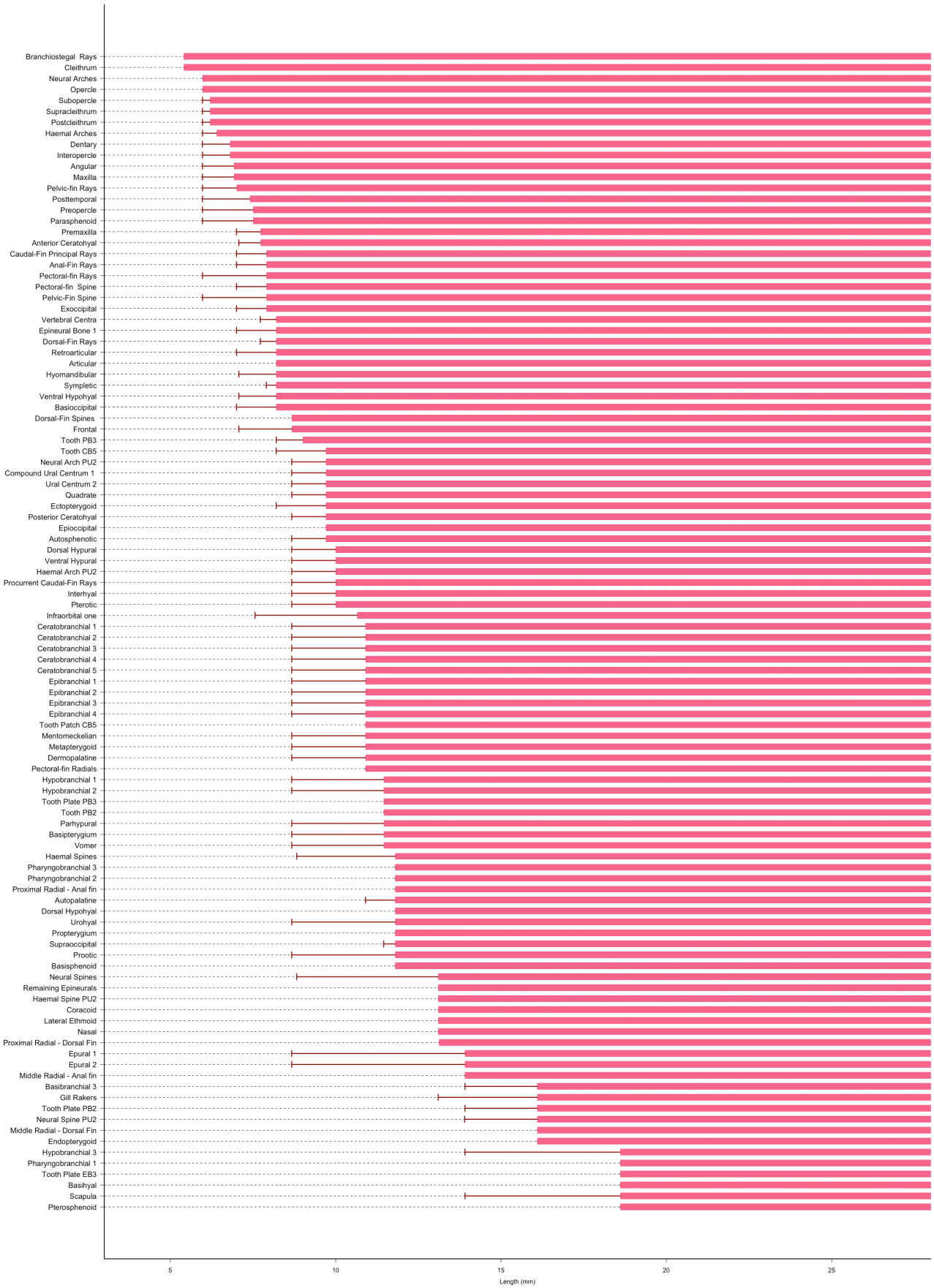

FIGURE 24 Sequence of ossification of the entire skeleton of *Porichthys notatus*. Bars correspond to fixed length. Error bars correspond to the smallest size that a structure was found. Lengths are described in mm NL/SL.

A remarkable difference between the sequence of ossification of *Porichthys notatus* and that of other fishes is the early development of dermal bones of the pectoral girdle. In all groups surveyed in this study, the cleithrum is among the first bones of the skeleton to develop (Kubicek, 2022; Kubicek & Conway, 2016; Marinho, 2022; Mattox et al., 2014). In *P. notatus* the supracleithrum and postcleithrum also develop early (at 6.2 mm NL), before the interopercle and the dentary. In *Sciaenops*, *Salminus*, *Ictalurus*, *Noturus*, and *Moenkhausia* the supracleithrum develops after the jaw bones. In *Sciaenops* and *Salminus*, the postcleithrum (or series of postcleithra) usually develops late in ontogeny (near the end of the ossification sequence; Kubicek & Conway, 2016; Mattox et al., 2014). The pectoral-fin rays of *P. notatus* develop at smaller sizes than the dorsal, anal, and caudal-fin rays. In *Sciaenops* and *Salminus*, however, the pectoral-fin rays develop after the fin rays of the unpaired fins. It is unclear if the relative early ossification of the supracleithrum, postcleithrum, and pectoral-fin rays in *P. notatus* is related to a particular function during larval stages.

4.2 | Posterior copula cartilage

In other Teleostei, the posterior copula, a diamond-shaped cartilage posterior to basibranchial 3, is commonly identified as a cartilaginous basibranchial 4 (Hilton et al., 2010; Hilton et al., 2019; Schnell & Hilton, 2015). The ontogenetic descriptions of Potthoff and Tellock (1993), Potthoff et al. (1984, 1988), Engeman et al. (2009), Engeman & Mabee (2012), Kubicek and Conway (2016) describe a single embryonic cartilage continuous with the *copula communis* that remains cartilaginous in adults, supporting the hypothesis of a cartilaginous basibranchial 4.

The gill arches of specimens at the earliest ontogenetic stages of *Porichthys notatus* examined in this study, conversely, have a pair of cartilages positioned posterior to the *copula communis*. Between sizes of 6.8 and 7.3 mm NL, the left and right elements appear as distinct circular cartilages that remain separate from one another until 7.4 mm SL, at which point they fuse in the midline (Figure 10). This results in a single posterior copula (= basibranchial 4) that remains cartilaginous in adults. The shape of the posterior copula is similar across diversity of Batrachoidiformes (Figure 23). The ontogeny of the posterior copula is unknown for most species, especially within Batrachoidiformes and their closest related groups (sensu Betancur-R et al., 2017). Assessing the distribution of the distinct ontogenetic pathway described for *P. notatus* is crucial as this unique trajectory could be used as a character for phylogenetic analyses.

4.3 | Homology of pectoral-fin radials and phylogenetic implications

Batrachoidiformes are historically described as having five pectoral fin radials (Günther, 1861; p. 168, "five carpal bones distinctly developed"), in contrast to the condition observed in most Teleostei, which typically have four pectoral radials. Monod (1960) described the dorsalmost pectoral radial of *Halobatrachus didactylus* (named as "R1") being as long as the other radials, but remaining cartilaginous; Gunther (1861) described it as rudimentary. Greenfield et al. (2008) confirmed the presence of five pectoral radials across the generic diversity of Batrachoidiformes. These authors also found that in addition to *Halobatrachus* a cartilaginous dorsalmost pectoral radial (their "upper accessory radial") is present also in *Triathalassothia*, *Austrobatrachus*, *Riekertia*, *Batrichthys*, and *Perulibatrachus*. Greenfield et al. (2008) did not discuss their hypothesis of homology for the dorsalmost pectoral radial and Wiley and Johnson (2010) proposed five pectoral fin radials as a synapomorphy for Batrachoidiformes, again with no discussion of the homology of each of these elements.

This study of *Porichthys notatus* offers the first robust hypothesis for the homology of each individual radial supporting the pectoral fin of Batrachoidiformes. Data from the early ontogeny demonstrates that the embryonic pectoral radial plate forms the four ventral radial elements of the pectoral fin. Therefore, the four ventral radial elements of Batrachoidiformes are homologous to the pectoral radials of other teleostean fishes. The dorsalmost pectoral "radial," however, is actually formed by the propterygium that elongates during its early development (Figure 20). The occurrence of this uniquely hypertrophied propterygium in *P. notatus* is evidence that previous interpretations suggesting that Batrachoidiformes have five pectoral radials is incorrect. The pectoral fin supports of Batrachoidiformes have four radials (the four ventral bones) and one hypertrophied propterygium. Therefore, the synapomorphy of Batrachoidiformes is the hypertrophied propterygium and not the presence of five pectoral radials.

Among Batrachoidiformes, the propterygium remains cartilaginous in adults of the halophrynine genera *Triathalassothia*, *Halobatrachus*, *Perulibatrachus*, and *Austrobatrachus* (Greenfield et al., 2008; this study, Figure 25). Batrachoidinae, Thalassophryninae, Porichthyinae, and the remaining Halophryninae all have a hypertrophied propterygium that is completely or partially ossified (the latter condition observed only in *Batrichthys apiatus* and *Riekertia ellisi*). The phylogenetic analysis of Greenfield et al. (2008) resulted in optimizing the cartilaginous state as apomorphic (character [5]: Upper accessory pectoral-fin cartilage: 0 = ossified; 1 = not ossified). Greenfield et al. (2008) coded this character in outgroups with a question mark because their study did not have ontogenetic data to establish the homology of the propterygium. The propterygium of other fishes ossifies during early ontogeny ossifies and fuses with the upper hemitrichium (Kubicek, 2022; Kubicek & Conway, 2016; Marinho, 2022; Mattox et al., 2014), including Sciaenidae, the family of fishes phylogenetic closer to Batrachoidiformes with ontogenetic information on the ossification of the propterygium (sensu Betancur-R et al., 2017). Based on our ontogenetic data, we infer that an ossified propterygium is the plesiomorphic state and a cartilaginous propterygium would be considered apomorphic. The distribution of this apomorphic state of character could support the hypothesis that *Triathalassothia*, *Halobatrachus*, *Perulibatrachus*, and

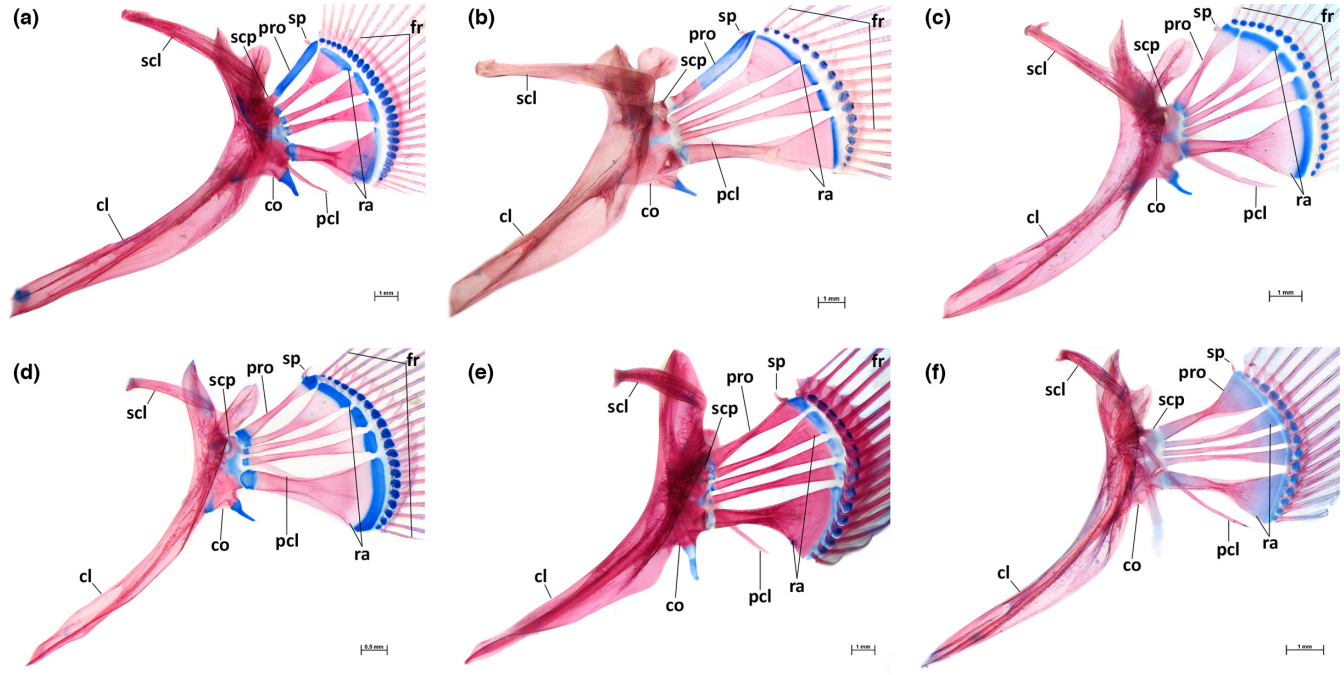

FIGURE 25 Comparative morphology of pectoral fins in Batrachoidiformes. (a) *Halobatrachus didactylus* (Halophryninae), USNM 205066 (59.16 mm SL). (b) *Batrichthys apiatus* (Halophryninae), SAIAB 70353 (72 mm SL). (c) *Allenbatrachus reticulatus* (Halophryninae), USNM 333283 (45.8 mm SL). (d) *Opsanus tau* (Batrachoidinae), VIMS 34756 (29.9 mm SL). (e) *Daector dowi* (Thalassophryninae), USNM 206532 (79.1 mm SL). *Porichthys greenei* (Porichthyinae), UF 226105 (56.7 mm SL). Abbreviations: cl, cleithrum; co, coracoid; fr, fin ray; pcl, postcleithrum; pro, propterygium; ra, pectoral radial; scl, supracleithrum; scp, scapula; sp, spine.

Austrobatrachus form a monophyletic group. The preliminary phylogenetic analysis from Vaz (2020) did not recover these four species forming a monophyletic group. The phylogenetic implications of this character, however, are still under investigation.

Outside of Batrachoidiformes, the only other teleostean fish reported to have five elongate radial or radial-like elements supporting the pectoral fin is *Gigantactis longicirra* (Lophiiformes; Waterman, 1948; Rosen and Patterson, 1969). There is no developmental evidence to determine whether the cartilaginous radial-like element of *Gigantactis* is homologous to the propterygium or if it is an additional pectoral radial. Even if the elongated cartilage of *Gigantactis* is homologous to the propterygium as in Batrachoidiformes, the currently accepted phylogenetic relationships of toadfishes and anglerfishes within Percomorphacea (Betancur-R et al., 2013; Betancur-R et al., 2017) suggest that these are independent (i.e., homoplastic) occurrences.

4.4 | Reabsorption of the third dorsal-fin spine during development

Representatives of Porichthyinae and Thalassophryninae have been historically described having two dorsal-fin spines, in contrast to the three observed in Batrachoidinae and Halophryninae (Collette, 1966, 1973; Gilbert, 1968; Greenfield et al., 2008; Günther, 1861; Walker & Rosenblatt, 1988). The number of dorsal-fin spines has been used for identification purposes and proposing phylogenetic relationships. Our study clearly shows that there are three distinct dorsal-fin spines in the early development of *Porichthys notatus* (Figure 18). The third dorsal-fin spine develops similarly to other spines until approximately 13 mm SL (Figure 18b). Its development is then interrupted (first observed at 16.1 mm SL; Figure 18c), resulting in a rod-like pterygiophore with a diminutive spine at 24.5 mm SL (Figure 18d). In juveniles, the pterygiophore is further reduced to a small, comma-shaped structure that is closely associated with the pterygiophore of the second dorsal-fin spine (Figure 18e).

A reduced third dorsal-fin spine in *Porichthys notatus* is clearly seen in ontogeny and suggests the need for reevaluation of the condition in other Batrachoidiformes. A similar structure was found in other species of Porichthyinae, as well as in Thalassophryninae; both subfamilies have been described as having only two dorsal-fin spines (Collette, 1966, 1973; Gilbert, 1968; Greenfield et al., 2008; Walker & Rosenblatt, 1988). In Thalassophryninae, however, the only structure left is a small ossified spine (a reduced pterygiophore is not present). In *Daector dowi*, *Thalassophryne amazonica*, and *T. nattereri* this spine is circular and small, but in *T. maculosa* this element is elongate, similar to other pterygiophores supporting soft fin rays (Figure 26). The presence of a reduced third dorsal-fin spine in these taxa necessitates reconsidering the homology of fin-support structures within Batrachoidiformes. These data suggest that the two complete dorsal-fin spines and pterygiophores of Porichthyinae and Thalassophryninae are homologous to the first and second dorsal-fin spines of Batrachoidinae and Halophryninae. The presence of

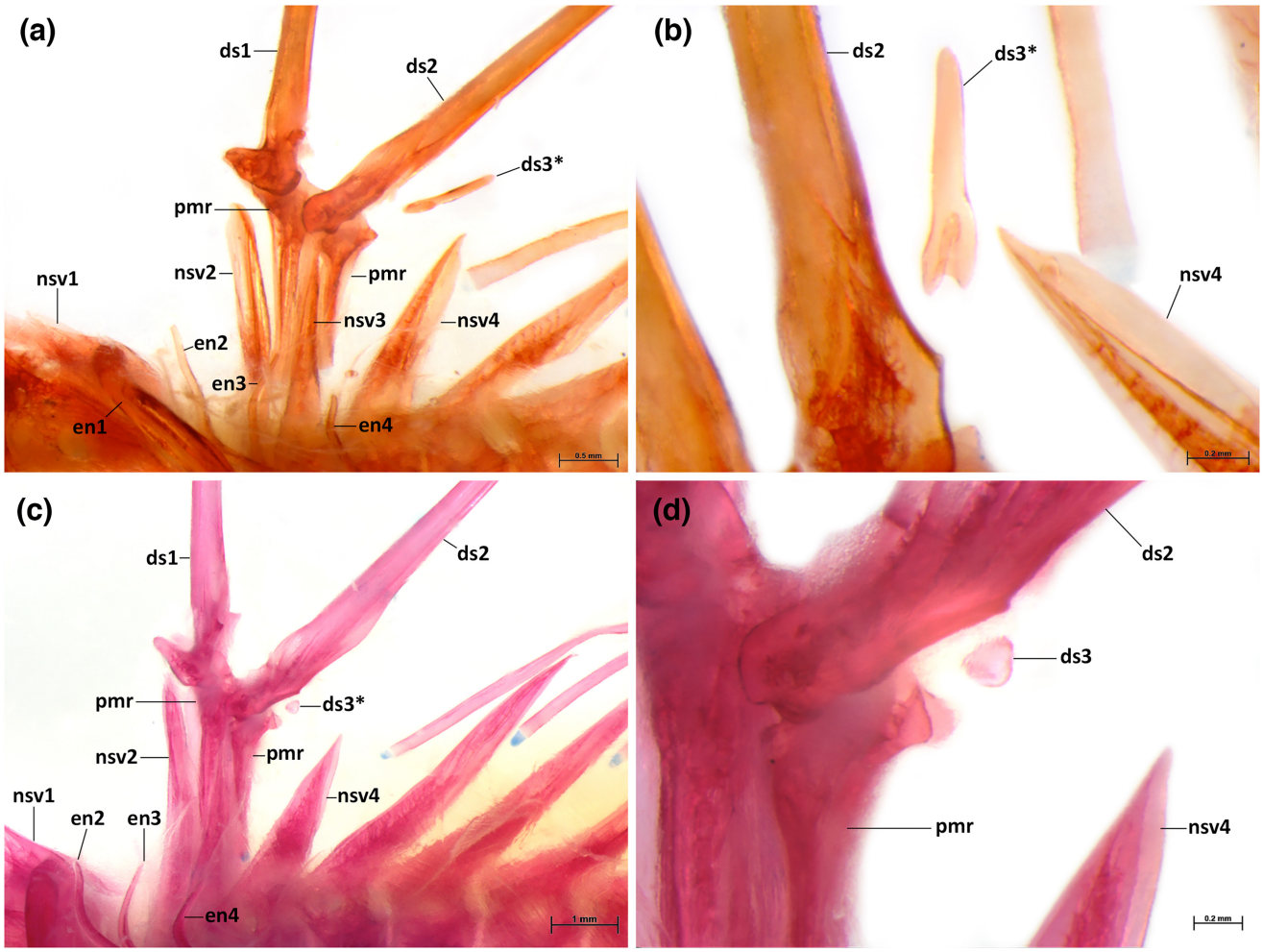

FIGURE 26 Fin spines and pterygiophores in Thalassophryninae. (a, b) *Thalassophryne maculosa*, USNM 200558 (36.1 mm SL), in lateral (a) and dorsal (b) views. (c, d) *Daector dowi*, USNM 206532 (79.1 mm SL) in lateral view. Figures (b) and (d) show the third dorsal spine in high magnification. Abbreviations: ds, dorsal spine; en, epineural bone; pmr, proximal-middle radial; nsv, neural spine of vertebra.

three dorsal-fin spines in all Batrachoidiformes (complete or reduced) suggests that the common ancestor of this order had three dorsal-fin spines.

Greenfield et al. (2008) used the number of dorsal-fin spines in their identification key, and considered Porichthyinae and Thalassophryninae as having only two dorsal-fin spines. The presence of a reduced third dorsal-fin spine and pterygiophore in *Porichthys notatus* (and the recognition of their homologues in other representatives of Porichthyinae and Thalassophryninae) implies that the correct character for using in a key would be two or three complete dorsal spines in juveniles and adults. Further, Greenfield et al. (2008) used in their phylogenetic analyses the character "two dorsal-fin spines: 0=no; 1=yes". By examination of their character matrix, the states "no" and "yes" meant the total number of complete dorsal-fin spines in juveniles and adults, as all taxa coded with "yes" are those from Porichthyinae and Thalassophryninae (taxa with two complete dorsal spines) and those coded with "no" have three dorsal-fin spines (Batrachoidinae and Halophryninae). In addition to the evidence of all Batrachoidiformes having three dorsal-fin spines at some stage of their life, the codification of that character itself has problems. Following Sereno's (2007) terminology and methodology for character construction, the character statement proposed by Greenfield et al. (2008) is not an independent variable. All Batrachoidiformes have at least two fully developed dorsal-fin spines and pterygiophores. The variation relates to the presence of a third dorsal-fin spine. Therefore, incorporating the ontogenetic data from this study, the correct character statement is the development of the third dorsal-fin spine in juveniles and adults. The exclusive conditions (i.e., states of character) would be "complete with fully developed spine" versus "reduced with spine restricted to a circular or elongate bone"

4.5 | Development of the vertebral column

In *Porichthys notatus* the dorsal arcocentra develop in an anteroposterior direction, whereas the ventral arcocentra first appear in the midpoint of the body (between vertebrae 12 to 23) and develop in both anterior and posterior directions. In most percomorph fishes for which developmental information is available, the

direction of development of dorsal and ventral arcocentra typically are similar (e.g., in Sciaenidae, Kubicek & Conway, 2016; most Zoarcoidei, Hilton et al., 2019; and *Lutjanus*, Potthoff et al., 1988), regardless whether the dorsal arcocentra and ventral arcocentra develop anterior to posterior or from the midpoint to the extremities. Potthoff (1975) describes *Thunnus atlanticus* having a completely inverse direction of development between dorsal arcocentra (which develop anterior to posterior) and ventral arcocentra (which develop posterior to anterior). The ossification of other vertebral elements of *Thunnus atlanticus*, however, develops anterior to posterior. Few fishes display a pattern of development similar to that seen in *P. notatus*; we are only aware of species of *Morone* (Moronidae; Fritzsche & Johnson, 1980) having this pattern. However, given the relative paucity of ontogenetic data across the diversity of Acanthomorphacea, the phylogenetic significance of such vertebral developmental pathways remains unclear. Additional ontogenetic studies across closely related taxa are necessary to have a better assessment of its phylogenetic potential.

5 | CONCLUSIONS

The propterygium of *Porichthys notatus* is hypertrophied and ossified, elongating during development to become as long as the pectoral radials. Considering the similarities observed in the pectoral fin across Batrachoidiformes, we infer that a similar developmental pathway occurs in other species of toadfishes. Therefore, we propose that the dorsal most element of the pectoral fin, previously thought to be a pectoral radial, is a hypertrophied propterygium.

Porichthys notatus has three complete dorsal-fin spines in its early life history, and the development of the third dorsal-fin spine interrupted, resulting in a spine that is reduced to a small bone in juveniles. The recognition of this reduced third spine allowed the identification of this reduced spine in other species of subfamilies Porichthyinae and Thalassophryninae, both of which were previously thought to have only two dorsal-fin spines. Beyond the implications of homology, the discovery of a reduced third dorsal spine in these subfamilies leads to changes in their diagnoses. Instead of describing these subfamilies as having only two dorsal-fin spines, the correct characteristic is having a reduced third dorsal-fin spine.

A pair of posterior copula cartilages (=basibranchial 4) is present in the earliest stages of development of *Porichthys notatus*. These elements fuse during ontogeny, forming the single cartilaginous element positioned posterior to basibranchial 3. This ontogenetic pathway is not described for any other teleost fishes.

Most neural and haemal arches and spines develop as membrane bone in *Porichthys notatus*. The only elements of the vertebral column that have a cartilaginous precursor are both neural and haemal arches and spines of the second and third pre-ural centra, as well the ventral arcocentra of vertebra 2–5. Similar occurrences are reported only in *Indostomus* and a few gobies (Britz & Johnson, 2002; Schultze & Arratia, 2013). The biological and phylogenetic significances of this unique developmental pathway are unknown.

Bones related to breathing, such as those of the opercular series and the cleithrum, develop before the pharyngeal tooth plates, in contrast to other Teleostei, in which the pharyngeal tooth plates are usually the first bones to develop.

AUTHOR CONTRIBUTIONS

D. F. B. V and E. J. H conceived, outlined the study, and wrote the manuscript. D. F. B. V collected specimens in the field, prepared and examined the material, and collected and analyzed the data.

ACKNOWLEDGMENTS

J. Sisneros, R. Mohr, J. Perelmuter, and B. Vetter are sincerely thanked for helping and supporting the first author to reach the field site and obtain the series of development used in this study. A. Summers is thanked for allowing access to Friday Harbor Laboratories facilities during the field season and for putting the authors in contact with J. Sisneros. C. White (MCZ) is thanked for helping to analyze the data and construct the development tables in RStudio. G. Lauder (MCZ) is thanked for allowing the use of the compound microscope available in his lab and for his constant support and contagious enthusiasm when talking anything fish related, absolutely needed during these pandemic times. B. Collette (USNM), J. McDowell (VIMS), W. Vogelbein (VIMS), and K. Weng (VIMS) reviewed this manuscript. We are grateful to S. Huber (VIMS), B. Collette, D. Johnson, L. Parenti, J. Williams, J. Clayton, S. Raredon, K. Murphy, D. Pitassy (USNM), K. Hartel, A. Williston, and M. Sorce (MCZ), L. Page and R. Robins (UF), M. McGrouther and A. Hay (AMI), A. Graham and W. White (CSIRO), R. Bills and M. Dwani (SAIAB), A. Datovo and M. Gianeti (MZUSP), C. McMahan (FMNH) and B. Frable (SIO) for providing access to specimens that were crucial to the development of this study. P. Konstantinidis (OSU) is thanked for his friendship over the years and mentoring on imaging on the microscope. J. Silva is thanked for his decade-long friendship and for offering his insights on the homology of the pectoral-fin elements. Lastly, the first author is immensely thankful to the Polynesian civilizations who invented surfing hundreds of years ago – this is the only thing that keeps him sane. This study was funded by the Graduate Support Package of the Virginia Institute of Marine Science, College of William and Mary, VIMS Research Grant, VIMS GSA Research Grant, Stephen & Ruth Wainwright Endowed Fellowship at FHL, Friday Harbor Laboratories Graduate Research Fellowship, and Enrst Mayr Travel Grant in Animal Systematics to D.F.B.V., and National Science Foundation (DBI-1349327) to E.J.H., S. K. Huber & D. K. Steinberg. D.F.B.V. was funded by the E. O. Wilson Postdoctoral Fellowship, Museum of Comparative Zoology, Harvard University and is currently funded by NSF Guam EPSCoR (OIA-1946352).

CONFLICT OF INTEREST

Authors have no conflicts of interest to declare.

DATA AVAILABILITY STATEMENT

The data supporting the results of this manuscript are available through direct (and reasonable) request to the corresponding author.

ORCID

Diego F. B. Vaz https://orcid.org/0000-0001-8161-2620
Eric J. Hilton https://orcid.org/0000-0003-1742-3467

REFERENCES

Arora, H.L. (1948) Observations on the habits and early life history of the batrachoid fish, *Porichthys notatus* Girard. *Copeia*, 2, 89–93.

Arratia, G. (1990) Development and diversity of the suspensorium of trichomycterids and comparison with loricarioids (Teleostei: Siluriformes). *Journal of Morphology*, 205, 193–218.

Arratia, G. & Schultze, H.-P. (1990) The urohyal: development and homology within osteichthyans. *Journal of Morphology*, 203, 247–282.

Arratia, G. & Schultze, H.-P. (1991) Palatoquadrate and its ossifications: development and homology within osteichthyans. *Journal of Morphology*, 208, 1–81.

Arratia, G. & Schultze, H.-P. (1992) Reevaluation of the caudal skeleton of certain actinopterygian fishes: III. Salmonidae. Homologization of caudal skeletal structures. *Journal of Morphology*, 214, 187–249.

Balbontín, F., Bustos, C.A. & Landaeta, M.F. (2018) Comportamiento reproductivo y desarrollo de los estadios tempranos del bagre marino *Aphos porosus*, de la bahía de Valparaíso, Chile. *Revista de Biología Marina y Oceanografía*, 53(S1), 77–87.

Betancur-R, R., Broughton, R.E., Wiley, E.O., Carpenter, K., López, J.A., Li, C., et al. (2013) The tree of life and a new classification of bony fishes. *PLoS Currents*, 5. https://doi.org/10.1371/currents.tol.53ba26640df0ccaee75bb165c8c26288

Betancur-R, R., Wiley, E.O., Arratia, G., Acero, A., Bailly, N., Miya, M. et al. (2017) Phylogenetic classification of bony fishes. *BMC Evolutionary Biology*, 17, 162.

Bird, N.C. & Mabee, P.M. (2003) Developmental morphology of the axial skeleton of the zebrafish, *Danio rerio* (Ostariophysi: Cyprinidae). *Developmental Dynamics*, 228, 337–357.

Block, A.J. & Mabee, P.M. (2012) Development of the mandibular, hyoid arch and gill arch skeleton in the Chinese barb *Puntius semifasciolatus*: comparisons of ossification sequences among Cypriniformes. *Journal of Fish Biology*, 81, 54–80.

Britz, R. & Conway, K.W. (2009) Osteology of *Paedocypris*, a miniature and highly developmentally truncated fish (Teleostei: Ostariophysi: Cyprinidae). *Journal of Morphology*, 270, 389–412.

Britz, R. & Conway, K.W. (2016) *Danionella dracula*, an escape from the cypriniform Bauplan via developmental truncation? *Journal of Morphology*, 277, 147–166.

Britz, R. & Johnson, G.D. (2002) "Paradox lost": skeletal ontogeny of *Indostomus paradoxus* and its significance for the phylogenetic relationships of Indostomidae (Teleostei, Gasterosteiformes). *American Museum Novitates*, 3383, 1–43.

Britz, R. & Johnson, G.D. (2005) Leis' conundrum: homology of the clavus of the ocean sunfishes. 1. Ontogeny of the median fins and axial skeleton of *Monotrete leiurus* (Teleostei, Tetraodontiformes, Tetraodontidae). *Journal of Morphology*, 266, 1–10.

Britz, R. & Toledo-Piza, M. (2012) Egg surface structure of the freshwater toadfish *Thalassophryne amazonica* (Teleostei: Batrachoididae) with information on its distribution and natural habitat. *Neotropical Ichthyology*, 10(3), 593–599.

Collette, B.B. (1966) A review of the venomous toadfishes, subfamily Thalassophryninae. *Copeia*, 4, 846–864.

Collette, B.B. (1973) *Daector quadrizonatus*, a valid species of freshwater venomous toadfish from the Río Truandó, Colombia with notes on additional material of other species of *Daector*. *Copeia*, 2, 355–357.

Collette, B.B. (2005) Batrachoidiformes, Batrachoidide, toadfishes. Chapter 51. In: Richards, W.J. (Ed.) *Early stages of Atlantic fishes: an identification guide for the western Central North Atlantic*. Boca Raton: CRC Press, pp. 759–767.

Cubbage, C.C. & Mabee, P.M. (1996) Development of the cranium and paired fins in the zebrafish *Danio rerio* (Ostariophysi, Cyprinidae). *Journal of Morphology*, 229, 121–160.

de Beer, G.R. (1937) *The development of the vertebrate skull*. Oxford: Oxford University Press, p. 554.

Dingerkus, G. & Uhler, L.D. (1977) Enzyme clearing of alcian blue stained whole small vertebrates for demonstration of cartilage. *Journal of Stain Technology*, 52, 229–232.

Dovel, W.L. (1960) Larval development of the oyster toadfish. *Opsanus tau Chesapeake Science*, 1(3–4), 187–195.

Engeman, J.M. & Mabee, P.M. (2012) Segmentation and fusion on the midline: Basibranchial homologies in cypriniform fishes. *Journal of Morphology*, 273, 725–736.

Engeman, J.M., Aspinwall, N. & Mabee, P.M. (2009) Development of the pharyngeal arch skeleton in *Catostomus commersonii* (Teleostei: Cypriniformes). *Journal of Morphology*, 270, 291–305.

FAO. (2022) Sciaenops ocellatus. Cultured Aquatic Species Information Programme. Text by Cynthia K. Faulk, A. Fisheries and Aquaculture Division [online]. Rome. Updated 2006-11-06 [Cited Tuesday, May 24th 2022]. https://www.fao.org/fishery/en/culturedspecies/sciaenops_ocellatus/en

Felix, P.M., Gonçalves, A., Vicente, J.R., Fonseca, P.J., Amorim, M.C.P., Costa, J.L. et al. (2016) Optical micro-tomography "OPenT" allows the study of large toadfish *Halobatrachus didactylus* embryos and larvae. *Mechanisms of Development*, 140, 19–24.

Fritzsche, R.A. & Johnson, G.D. (1980) Early osteological development of white perch and striped bass with emphasis on identification of their larvae. *Transactions of the American Fisheries Society*, 109, 387–406.

Gilbert, C.R. (1968) Western Atlantic batrachoid fishes of the genus *Porichthys*, including three new species. *Bulletin of Marine Science*, 18, 671–730.

Grande, L. (2004) Categorizing types of morphological variation in comparative morphology, and the importance of this to vertebrate paleontology. In: Arratia, G. & Tintori, A. (Eds.) *Mesozoic fishes 3—systematics, paleoenvironments and biodiversity*. Munich: Dr. Friedrich Pfeil, pp. 123–136.

Greenfield, D.W. (2014) A new toadfish species from Somalia (Teleostei: Batrachoididade). *Copeia*, 2014, 668–672.

Greenfield, D.W., Winterbottom, R. & Collette, B.B. (2008) Review of the toadfish genera (Teleostei: Batrachoididae). *Proceedings of the California Academy of Sciences*, 59, 665–710.

Günther, A. (1861) *Catalogue of the fishes in the British museum*. 3rd Volume. London: Taylor and Francis, p. 586.

Hilton, E.J. (2011) Bony fish skeleton. In: Farrel, A.P., Cech, J.J., Jr., Richards, J.G. & Stevens, E.D. (Eds.) *Encyclopedia of fish physiology: from genome to environment* Volume 1. London: Academic Press, pp. 434–448.

Hilton, E.J. & Bemis, W.E. (2012) External morphology of shortnose sturgeon, *Acipenser brevirostrum* (Acipenseriformes: Acipenseridae), from the Connecticut River, with notes on variation as a natural phenomenon. In: Kynard, B., Bronzi, P. & Rosenthal, H. (Eds.) *Life history and behaviour of Connecticut River Shortnose and other sturgeons*, pp. 243–265. Special Publication 4. Norderstedt: World Society of Sturgeon Conservation.

Hilton, E.J., Johnson, G.D. & Smith-Vaniz, W.F. (2010) Osteology and systematics of *Parastromateus Niger* (Perciformes: Carangidae), with comments on the carangid dorsal gill-arch skeleton. *Copeia*, 2, 312–333.

Hilton, E.J., Stevenson, D.E. & Matarese, A.C. (2019) Osteology of *Ronquilus jordani* (Zoarcoidei: Bathymasteridae), with a discussion of the developmental osteology and systematics of bathymasterid fishes. *Acta Zoologica*, 100, 389–407.

Johnson, G.D. & Britz, R. (2005) Leis' conundrum: homology of the clavus of the ocean sunfishes. 2. Ontogeny of the median fins and axial skeleton of *Ranzania laevis* (Teleostei, Tetraodontiformes, Molidae). *Journal of Morphology*, 266, 11–21.

Konstantinidis, P. & Johnson, G.D. (2012a) A comparative ontogenetic study of the tetraodontiform caudal complex. *Acta Zoologica (Stockholm)*, 93, 98–114.

Konstantinidis, P. & Johnson, G.D. (2012b) Ontogeny of the jaw apparatus and suspensorium of the Tetraodontiformes. *Acta Zoologica (Stockholm)*, 93, 351–366.

Kubicek, K.M. (2022) Developmental osteology of *Ictalurus punctatus* and *Noturus gyrinus* (Siluriformes: Ictaluridae) with a discussion of siluriform bone homologies. *Vertebrate Zoology*, 72, 661–727.

Kubicek, K.M. & Conway, K.W. (2016) Developmental osteology of *Sciaenops ocellatus* and *Cynoscion nebulosus* (Teleostei: Sciaenidae), economically important sciaenids from the Western Atlantic. *Acta Zoologica (Stockholm)*, 97, 267–301.

Marinho, M.M. (2022) Ontogeny of the skeleton of *Moenkhausia pittieri* (Ostariophysi: Characiformes) with discussion on functional demands and ossification patterns in the Characidae. *Zoological Journal of the Linnean Society*, 2022, 1–40.

Mattox, G.M.T., Britz, R. & Toledo-Piza, M. (2014) Skeletal development and ossification sequence of the characiform *Salminus brasiliensis* (Ostariophysi: Characidae). *Ichthyological Exploration of Freshwaters*, 25(2), 103–158.

Monod, T. (1960) A propos du pseudobrachium des *Antennarius* (Pisces, Lophiiformes). *Bulletin d'Institut Français d'Afrique Noire*, 22a, 620–698.

Potthoff, T. (1974) Osteological development and variation in young tunas, genus *Thunnus* (Pisces, Scombridae), from the Atlantic Ocean. *Fishery Bulletin*, 72(2), 563–588.

Potthoff, T. (1975) Development and structure of the caudal complex, the vertebral column, and the pterygiophores in the blackfin tuna (*Thunnus atlanticus*, Pisces, Scombridae). *Bulletin of Marine Science*, 25(2), 205–231.

Potthoff, T. (1980) Development and structure of fins and fin supports in dolphin fishes *Coryphaena hippurus* and *Coryphaena equiselis* (Coryphaenidae). *Fishery Bulletin*, 78(2), 277–312.

Potthoff, T. & Kelley, S. (1982) Development of the vertebral column, fins and fin supports, branchiostegal rays, and squamation in the swordfish, *Xiphias gladius*. *Fishery Bulletin*, 80(2), 161–186.

Potthoff, T. & Tellock, J.A. (1993) Osteological development of the Snook, *Centropomus undecimalis* (Teleostei, Centropomidae). *Bulletin of Marine Science*, 52(2), 669–716.

Potthoff, T., Richards, W. & Ueyanagi, S. (1980) Development of *Scombrolabrax heterolepis* (Pisces, Scombrolabracidae) and comments on familial relationships. *Bulletin of Marine Science*, 30(2), 329–357.

Potthoff, T., Kelley, S., Moe, M. & Young, F. (1984) Description of porkfish larvae (*Anisotremus virginicus*, Haemulidae) and their osteological development. *Bulletin of Marine Science*, 34(1), 21–59.

Potthoff, T., Kelley, S. & Collins, L.A. (1988) Osteological development of the red snapper, *Lutjanus campechanus* (Lutjanidae). *Bulletin of Marine Science*, 43(1), 1–40.

Rice, A.N. & Bass, A.H. (2009) Novel vocal repertoire and paired swimbladders of the three-spined toadfish, *Batrachomoeus trispinosus*: insights into the diversity of the Batrachoididae. *The Journal of Experimental Biology*, 212, 1377–1391.

Richards, W.J. (Ed.) (2005) Chapter 1 Introduction. In: *Early stages of Atlantic fishes: an identification guide for the western Central North Atlantic*. Boca Raton: CRC Press, pp. 759–767.

Sabaj, M.H. (2019) Standard symbolic codes for institutional resource collections in herpetology and ichthyology: an online reference. Version 7.1 (21 March 2019). Washington: American Downloaded from https://academic.oup.com/zoolinnean/article-abstract/189/1/228/5697420 by guest on 05 May 2020 Society of Ichthyologists and Herpetologists. Available at: http://www.asih.org/

Schnell, N.K. & Hilton, E.J. (2015) Osteology and ontogeny of the wrymouths, genus *Cryptacanthodes* (Cottiformes: Zoarcoidei: Cryptacanthodidae). *Journal of Morphology*, 276, 185–208.

Schultze, H.-P. & Arratia, G. (2013) The caudal skeleton of basal teleosts, its conventions, and some of its major evolutionary novelties in a temporal dimension. In: Arratia, G., Schultze, H.P. & Wilson, M.V.H. (Eds.) *Mesozoic fishes 5 – global diversity and evolution*. München: Dr Friedrich Pfeil, pp. 187–246.

Sereno, P.C. (2007) Logical basis for morphological characters in phylogenetics. *Cladistics*, 23, 565–587.

Taylor, W.R. & Van Dyke, C.C. (1985) Revised procedures for staining and clearing small fishes and other vertebrates for bone and cartilage study. *Cybium*, 9, 107–120.

Vaz, D.F.B. (2020) *Morphology and systematics of Batrachoidiformes (Percomorphacea: Teleostei). Ph.D. dissertation for the Virginia Institute of Marine Science*., p. 437.

Vaz, D.F.B. & Hilton, E.J. (2020) The caudal skeleton of Batrachoidiformes (Teleostei: Percomorphacea): a study of morphological diversity, intraspecific variation, and phylogenetic inferences. *Zoological Journal of the Linnean Society*, 189, 228–286.

Walker, H.J. & Rosenblatt, R.H. (1988) Pacific toadfishes of the genus *Porichthys* (Batrachoididae) with descriptions of three new species. *Copeia*, 4, 887–904.

Warth, P., Hilton, E.J., Naumann, B., Olsson, L. & Konstantinidis, P. (2017) Development of the skull and pectoral girdle in Siberian sturgeon, *Acipenser baerii*, and Russian sturgeon, *Acipenser gueldenstaedtii* (Acipenseriformes: Acipenseridae). *Journal of Morphology*, 278(3), 418–442.

Waterman, T.H. (1948) Studies on deep-sea anglerfishes (Ceratioidea). III. The comparative anatomy of *Gigantactis longicirra* Waterman. *Journal of Morphology*, 82(2), 81–149.

Watson, W. (1996) Batrachoididae: toadfishes, midshipman. In: Moser, H.G. (Ed.) *The early stages of fishes in the California current region. CalCOFI atlas*. Lawrence, KS: Allen Press, Inc. Vol. 33, pp. 546–549.

Wiley, E.O. & Johnson, G.D. (2010) A teleost classification based on monophyletic groups. In: Nelson, J.S., Schultze, H.-P. & Wilson, M.V.H. (Eds.) *Origin and phylogenetic interrelationships of Teleosts*. Munchen: Verlag Dr. Friedrich Pfeil, pp. 123–182.

How to cite this article: Vaz, D.F.B. & Hilton, E.J. (2022) Skeletal ontogeny of the Plainfin Midshipman, *Porichthys notatus* (Percomorphacea: Batrachoidiformes). *Journal of Anatomy*, 00, 1–48. Available from: https://doi.org/10.1111/joa.13794

APPENDIX A

ADDITIONAL MATERIAL EXAMINED

Batrachoidinae

Amphichthys cryptocentrus (4). cleared-and-stained: USNM 144888, aprox 30.0 mm SL; USNM 226515, 126.7 mm SL. CT-scanned: USNM 226515 (2), 151.5 mm SL, 145.7 mm SL.

Batrachoides liberiensis (3). cleared-and-stained: USNM 219393 (2), 90.2 mm SL, 105.8 mm SL. CT-scanned: USNM 219393, 116.4 mm SL.

Batrachoides manglae (2). cleared-and-stained: USNM 226605, 20.4 mm SL. CT-scanned: USNM 226605, 67.0 mm SL.

Batrachoides pacifici (6). cleared-and-stained: UF 227127 (4), 45.7 mm SL, 54.3 mm SL, 61.6 mm SL, 73.5 mm SL; USNM 144886(2), 36.1 mm SL, 46.8 mm SL. CT-scanned: USNM 144886, 98.0 mm SL.

Batrachoides waltersi (3). cleared-and-stained: USNM 367548, 60.2 mm SL; USNM 369505, 47.8 mm SL. CT-scanned: USNM 367548, 150.9 mm SL.

Batrachoides boulengeri (2). cleared-and-stained: USNM 220127, 101.1 mm SL. CT-scanned: USNM 220127, 129.6 mm SL.

Batrachoides gilberti (3). cleared-and-stained: FMNH 84549, 73.0 mm SL; UF 12013, 28.8 mm SL. CT-scanned: FMNH 84549, 80.8 mm SL

Batrachoides goldmani (2). cleared-and-stained: USNM 219383, 72.6 mm SL. CT-scanned: USNM 219383, 116.0 mm SL

Batrachoides surinamensis (3). cleared-and-stained: FMNH 88024, 76.9 mm SL; UF 23108, 113.2 mm SL. CT-scanned: UF 23108, 110.5 mm SL.

Opsanus beta (3). cleared-and-stained: UF89642, 38.1 mm SL; UF 153948, 60.5 mm SL, 75.8 mm SL.

Opsanus pardus (4). UF 153830, 52.1 mm SL; VIMS 38032, 57.4 mm SL; VIMS 38031, 86.6 mm SL. CT-scanned: VIMS 38033, 90.5 mm SL.

Opsanus phobetron. CT-scanned: UF 227128, 123.6 mm SL.

Opsanus tau (14). cleared-and-stained: VIMS 34755, 24.0 mm SL; VIMS 34756, 29.9 mm SL; VIMS 34763, 32.4 mm SL; VIMS 34765, 75.9 mm SL; VIMS 34769, 28.3 mm SL; VIMS 34770, 35.1 mm SL; VIMS 34771, 37.6 mm SL; VIMS 34772, 52.1 mm SL; VIMS 34778, 36.4 mm SL; VIMS 34781, 27.7 mm SL; VIMS 34782, 28.9 mm SL; VIMS 34783, 47.8 mm SL; VIMS 34783, 57.1 mm SL. Dry skeleton. VIMS uncat (approx. 230.0 mm SL).

Potamobatrachus trispinosus. cleared-and-stained: USNM 330064, 49.5 mm SL (paratype).

Sanopus astrifer. CT-scanned: USNM 209720, 246.2 mm SL.

Sanopus barbatus (4). cleared-and-stained: MCZ 44549, 27.5 mm SL; SIO 67-45, 90 mm SL. CT-scanned: MCZ 44550, 36.0 mm SL. X-ray: USNM 211322, 250.0 mm SL.

Sanopus reticulatus. CT-scanned: UF 112976, 205.0 mm SL.

Sanopus greenfieldorum. CT-scanned: USNM 415327, 24.6 mm SL.

Vladichthys gloverensis (5). cleared-and-stained: FMNH 104587, 39.3 mm SL; USNM 218916, 52.0 mm SL, 60.4 mm SL; USNM 267789, 19.2 mm SL. CT-scanned: USNM 267789, 50.0 mm SL

Porichthyinae

Aphos porosus (5). cleared-and-stained: USNM 309738 (4), 152.3 mm SL, 98.6 mm SL, 89.4 mm SL, 77.5 mm SL. CT-scanned: USNM 305005, 151.4 mm SL.

Porichthys bathoiketes. cleared-and-stained: UF 228539, 73.5 mm SL. CT-scanned: UF 12965 (paratype), 93.8 mm SL.

Porichthys greenei (6). cleared-and-stained: UF 226105 (5), 37.1 mm SL, 44.0 mm SL, 50.7 mm SL, 56.2 mm SL, 60.7 mm SL. CT-scanned: UF 226105, 64.9 mm SL

Porichthys margaritatus (11). cleared-and-stained: UF 226009 (5), 70.2 mm SL, 70.3 mm SL, 78.8 mm SL, 89.4 mm SL, 99.2 mm SL; USNM 101730 (5), 19.3 mm SL, 27.9 mm SL, 33.4 mm SL, 39.2 mm SL, 41.3 mm SL. CT-scanned: UF 225009, 121.8 mm SL

Porichthys pauciradiatus (2). cleared-and-stained: UF 226549, 44.6 mm SL. CT-scanned: UF 226549, 50.3 mm SL.

Porichthys cf. *plectrodon*: USNM 302134 (6), 48.7 mm SL, 53.5 mm SL, 56.1 mm SL, 58.6 mm SL, 75.5 mm SL, 77.6 mm SL.

Porichthys plectrodon/porosissimus (5). MZUSP 45398, 35.0 mm SL, 40.0 mm SL; VIMS 1132, 55.7 mm SL, 81.5 mm SL. CT-scanned: MCZ 170729, 150.8 mm SL.

Thalassophryninae

Daector dowi (12). cleared-and-stained: UF 226263 (9), 43.1 mm SL, 47.9 mm SL, 60.0 mm SL, 65.2 mm SL, 73.1 mm SL, 73.7 mm SL, 82.3 mm SL, 84.0 mm SL; 89.6 mm SL; USNM 206532 (2), 59.7 mm SL, 79.1 mm SL. CT-scanned: UF 226263, 105.7 mm SL

Daector reticulata. CT-scanned: UF 225055, 144.0 mm SL.

Thalassophryne amazonica (2). cleared-and-stained: ANSP 178103, 76.8 mm SL. CT-scanned: ANSP 178103, 94.3 mm SL.

Thalassophryne natteri (4). cleared-and-stained: MZUSP 47262, 114.8 mm SL; MZUSP 47283, 70.4 mm SL; USNM 302333, 69.4 mm SL. CT-scanned: USNM 302333, 113.0 mm SL.

Thalassophryne maculosa (5). USNM 199524 (2), 64.4 mm SL, 84.2 mm SL; USNM 200558 (2), 26.0 mm SL, 36.1 mm SL. CT-scanned: USNM 200558, 137.6 mm SL.

Halophryninae

Allenbatrachus grunniens. cleared-and-stained: FMNH 51762, 114.3 mm SL. CT-scanned: LSUMZ-F 14041, 87.3 mm SL.

Allenbatrachus reticulatus (3). cleared-and-stained: FMNH 47420, 94.6 mm SL; USNM 333283, 45.8 mm SL (c&s). CT-scanned: USNM 333283, 61.4 mm SL.

Barchatus cirrhosus. CT-scanned: USNM 221140, 133.9 mm SL.

Barchatus indicus. CT-scanned: USNM 305979, 128.6 mm SL (holotype).

Batrachomoeus dahli. CT-scanned: AMI 13282, 49.2 mm SL.

Batrachomoeus dubius (5). cleared-and-stained: AMI 17793-002, 114.5 mm SL; AMI 20605-009 (2), 119.1 mm SL, 114.9 mm SL; CSIRO CA 1223, 78.9 mm SL. CT-scanned: CSIRO CA-550, 119.5 mm SL.

Batrachomoeus occidentalis. CT-scanned: AMI 18472-002 (paratype), 65.3 mm SL.

Batrachomoeus rubricephalus. CT-scanned: AMI 18473-001 (paratype), 220.8 mm SL.

Batrachomoeus trispinosus (5). cleared-and-stained: AMI 15557-280, 116.1 mm SL; CSIRO A-2185, 33.1 mm SL; USNM 423891, 105.7 mm SL. CT-scanned: LSUMZ-F 16715, 84 mm SL; USNM 423891, 128.5 mm SL.

Batrichthys apiatus (3). cleared-and-stained: SAIAB 12728, 52.8 mm SL; SAIAB 70353, 72.0 mm SL. CT-scanned: SAIAB 12736, 46.3 mm SL.

Bifax lacinia. CT-scanned: CAS 81232 (paratype), 232.1 mm SL.

Chatrabus hendersoni. CT-scanned and cleared-and-stained: SAIAB 70864, 110.9 mm SL.

Chatrabus melanurus (2). cleared-and-stained: SAIAB 13859, 18.3 mm SL. CT-scanned: USNM 325744, 156.4 mm SL.

Colletteichthys dussumieri (2). cleared-and-stained: USNM 226512, 84.5 mm SL. CT-scanned: UF 146291, 101.6 mm SL.

Colletteichthys occidentalis (3). cleared-and-stained: USNM 147914, 45.0 mm SL. CT-scanned: LSUMZ-F 18075, 79.6 mm SL; USNM 147914, 104.4 mm SL.

Halobatrachus didactylus (5). cleared-and-stained: UF 216854, 81.0 mm SL; USNM 205066 (2), 59.5 mm SL, 68.1 mm SL. CT-scanned: CAS 234463, 75.3 mm SL; USNM uncat HAB-st53, 120.0 mm SL.

Halophryne diemensis (5). cleared-and-stained: AMI 6162, 100.0 mm SL; AMI 23930-001, 24.0 mm SL; USNM 174023, 113.8 mm SL; USNM 174024, 55.7 mm SL. CT-scanned: CSIRO H-4155, 86.4 mm SL.

Halophryne hutchinsi. X-ray: USNM 219717, 96.0 mm SL.

Halophryne occellatus (3). cleared-and-stained: H-3253-06, 25.1 mm SL. CT-scanned: CSIRO C2767, 58.7 mm SL, H2784-10, 41.9 mm SL.

Halophryne queenslandiae (2). CT-scanned: AMI 9500, 117.5 mm SL; CSIRO C2824, 178.3 mm SL.

Perulibatrachus aquilonarius. CT-scanned: CAS 231001, 245.0 mm SL.

Perulibatrachus rossignoli (4). CT-scanned: CAS 225368 (2), 154.0 mm SL, 111.4 mm SL; FMNH 117453, 167.4 mm SL; SAIAB 67750, 146.6 mm SL.

Riekertia ellisi. CT-scanned: SAIAB 12739, 233.2 mm SL.

Triathalassothia argentina (2). cleared-and-stained: USNM 214438, 100.0 mm SL. CT-scanned: USNM 214438, 104.6 mm SL

Triathalassotia lambaloti (1). cleared-and-stained: MZUSP 87217, approximately 80 mm SL.